# SEISMIC RISK ANALYSIS OF BRIDGE STRUCTURAL SYSTEMS

by

ABDALLAH MECHAKHCHEKH

A dissertation submitted to the Graduate Faculty in Engineering in partial fulfillment of the requirements for the degree of Doctor of Philosophy, The City University of New York

2008

UMI Number: 3296963





ProQuest Information and Learning Company
300 North Zeeb Road
P.O. Box 1346
Ann Arbor, MI 48106-1346

This manuscript has been read and accepted for the
Graduate Faculty in Engineering in satisfaction of the
dissertation requirement for the degree of Doctor of Philosophy.

Prof. Michel Ghosn

Date

Chair of Examining Committee

Dean Mumtaz Kassir

Date

Executive Officer

Prof. Anil Agrawal

Prof. Huabei Liu

Prof. Feng Bao Lin

Prof. George Tsiatas

Supervision Committee

THE CITY UNIVERSITY OF NEW YORK

# *Acknowledgment*

I would like to express my deepest gratitude to my Thesis Adviser Professor Michel Ghosn for his support and encouragement. His guidance and valuable advice all along my studies at the City College of New York and the Graduate Center of the City University of New York, first as a Master's student and subsequently as a Ph.D. candidate in the Department of Civil Engineering, were extremely helpful for conducting my research and achieving my goals. As a mentor, Professor Michel Ghosn provided me with a great opportunity to learn from him during long discussions of my research work.

My gratitude also goes to Dean Mumtaz Kassir, Executive Officer of the Ph.D. Program in Engineering, for his support and help in administrative matters. Thanks are also due to Professor Feng-Bao Lin, Professor Anil Agrawal, Professor George Tsiatas, and Professor Huabei Liu, for serving on my Ph.D. committee and for their useful comments and advice.

In terms of this work, I would like to express my deepest gratitude to my parents Larbi and Fatima, my brothers Simohamed, Rachid, Mohamad, Karim, my sisters Halima and Rokia. Thank you very much for your patience and supports, I miss you all and see you soon.

# *Abstract*


## *SEISMIC RISK ANLAYSIS OF BRIDGE STRUTCURAL SYSTEMS*

**By Abdallah Mechakhchekh**

**Adviser: Professor Michel Ghosn**

The objective of this Ph.D. Dissertation is to develop a new model for the seismic risk assessment of bridge structural systems. The model is designed to account for the random nature of the seismic input, the variability in the material properties, and also for the modeling uncertainties or systemic uncertainties that reflect our lack of knowledge of all the factors that control the seismic response of bridges and the ability of the bridge structural system to withstand seismic ground motions.

To accommodate the large number of random variables and the various modes of failure that may exist in a bridge system subjected to seismic input, this study develops a new reliability method herein called the Radial Sampling method to calculate the probability of failure of each mode of failure as well the overall system's probability of failure.

The application of the proposed risk analysis methodology to study the reliability of reinforced concrete bridge columns has led to proposing a rational approach for selecting appropriate response modification factors, normally used for the force-based

design of typical bridge configurations in low seismic regions, that would lead to uniform and consistent levels of safety.

The efficiency of the proposed risk analysis approach is tested on a nonlinear finite element analysis model of a typical bridge configuration. The material varaibilities are studied and identified from existing experimental data on the dynamic response of reinforced concrete columns. The resulting material statistical models and the seismic uncertainties defined based on the seismic hazard analysis are introduced into a nonlinear dynamic reliability analysis model that is solved using the proposed Radial Sampling method. The example demonstrates the ability of the Radial sampling method to efficiently handle large numbers random variables and identify the most important failure modes as well as calculate each mode's probability of failure and the failure probability of the complete structural system.

The models developed in this study can be used to set up a preparedness plan, following the occurrence of an earthquake event that speeds up the recovery process by identifying and targeting for repair high seismic risk members of critical bridges. The models can also serve to develop a bridge rehabilitation strategy that rationally uses available resources to optimize the chances of survivability and provide a uniform and acceptable seismic risk.

# *TABLE OF CONTENT*

# *LIST OF TABLES*

# *LIST OF FIGURES*

# *CHAPTER 1*

# *Introduction*

## 1.1 REVIEW OF SEISMIC RISK ANALYSIS OF BRIDGE SYSTEMS

During the last two decades, significant progress has been made in advancing our understanding of the major factors that control the seismic behavior of highway bridges, the development of improved methods for their seismic analysis, and the establishment of seismic design criteria. The new version of seismic ground acceleration maps developed by the U.S Geological Survey (USGS) in 2002 provide contours of peak ground accelerations (PGA) and spectral accelerations (SA) in the contiguous US. These developments in conjunction with Probabilistic Seismic Hazard Analysis methods (Boore; 2002), and the availability of a large amount of information and data collected from several earthquake events have provided a solid scientific foundation for estimating possible ground motion levels throughout the US and the application of risk-based seismic design methods. To take advantage of these developments in seismic predictions, several agencies sponsored a series of studies on the seismic vulnerability assessment of highway bridges that encompassed research on seismic hazard, as well as the structural and soil/foundation seismic response of highway bridges. Some of these studies

addressed the differences in seismicity, bridge type, and typical design details between Eastern and Central U.S. bridges, and those in the Western U.S. (Maragaris & Jennings 1987; Werner 1994; Geol & Chopra 1997; Zhang & Makris 2000,2001) The issue of establishing a common probability of exceedance criterion for ground motion intensities was also examined and a 2% probability of exceedance in 50 years that corresponds to a return period of approximately 2500 years was recommended as the basis for bridge collapse prevention (Friedland 2001). However, some bridge agencies have expressed their concern with regard to the economic costs that would be associated with raising the seismic standards to such levels. For this reason, a recent proposal proposed changing the seismic hazard level for design to 7% probability of exceedance in 75 years.(NCHRP 20-07/Task 193)

Another factor that has been recognized by researchers as being important for the development of seismic design specifications is related to the effect of the uncertainties in the earthquake characteristics on the response of structural systems. This triggered a new research field and design philosophy, which became known as "probabilistic based design approach". The focus of this approach is on studying the randomness in the most critical earthquake characteristics that affect the structural response. Intensive research efforts initiated by Cornell (1968, 1975), McGuire (1995), Bazzuro & Cornell (1999), and Wen & al (2001), have identified the major earthquake parameters that affect the structural response to be: 1) earthquake intensity, 2) moment magnitude, and 3) epicentral distance from the source to the bridge site. Large differences in the response of structural systems were observed due to variations in any of these three seismic parameters. Most of the studies concentrated on the response of structural columns and

little effort was spent on studying other possible failure modes (Kent & Park 1971; Mander, Priestley, & Park 1984; Mander 1984; Lehman & Moehle 1998). The emphasis on column failures was due to observations made on building and on bridge failures during the Imperial Valley earthquake and other major events such as the Kobe earthquake However, more recent earthquakes such as the 1992 Cape Mendocino earthquake and the 1994 Northridge earthquake uncovered another important mode of failure. In fact, in many cases, excess displacements or pounding between the bridge superstructure and abutments resulted in the failure of several girder slab systems (Cooper. J. D; & al 1994). Column failure and superstructure failure are certainly two major modes but not the only ones. The possibilities of bearing failure, abutment failure or pile failure are always present and the occurrence of any one of these is strongly dependent on the detailing of the bridge in question. Furthermore, bridges in the same vicinity having nominally similar configurations and properties have been observed to respond in different manners to the same earthquake input. This has been attributed to the random nature of the material properties that control the response of bridges including the effect of the variability in the soil and foundation properties as well as variations in the abutment and support conditions. These issues, which are deemed less important for buildings, have not been properly examined by previous research on the behavior of bridges under seismic input. Preliminary investigations have indicted that the uncertainties associated with determining the material and structural properties of all the above-mentioned components may be significant for bridge structures and should be included when performing a risk-based seismic analysis of bridges.

The presence of seismic related uncertainties and material related variabilies have certainly a considerable effect on the reliability of bridge structures' seismic integrity and their ability to resist various possible modes of failure. Knowing that the probabilities of bridge failure are typically small, and currently available structural risk analyses are computationally costly, and given the high number of random variables that control the structural response of bridge systems, an efficient computational method is needed to assess the reliability of bridge structures and their probabilities of failure.

Recent improvements in the efficiency of simulation methods for calculating small probabilities of failure in high multivariate structural systems have been made by Koutsourelakis, Schueller & al (2004) and Au & Beck (2001). Although these novel techniques have been demonstrated on single degree of freedom systems controlled by large numbers of random variables, their applicability for studying the reliability of realistic models of structural systems has not been thoroughly evaluated.

Given the above facts, it is clear that efficient models to perform comprehensive bridge risk analyses that account for the uncertainties in material properties and the estimated bridge model parameters, the randomness in the earthquake itself as well as its parameters, should be developed to study the risk of bridge system collapse and identify all the important bridge modes of failure.

## 1.2 RESEARCH OBJECTIVES AND REPORT OUTLINE

The object of this study is to develop a detailed model to perform the seismic risk analysis of bridge structural systems. The main ingredients necessary to develop such a model include: 1) The identification of seismic uncertainties, 2) The identification of

material vaiabilities within the bridge structure, 3) development of a structural reliability analysis model, 4) development of efficient reliability estimation methods. This thesis provides a detailed description of the methodology that is followed to achieve the goals of this study.

Specifically, after the brief introduction provided in this Chapter, Chapter Two reviews the concept of structural reliability and reviews the basic structural reliability simulation methods used to estimate the probability of structural failures.

However, the simulation methods described in Chapter Two of this thesis may fail in the estimation of small probabilities of failure when the complete bridge structural system is considered along with its several possible failure modes. In this case, more advanced reliability techniques need to be used. Chapter Three describes two recently developed Markov Chain-based simulation techniques that have been found to reduce the number of analyses needed to estimate the probability of failure of structural systems. These advanced reliability methods, namely the Subset method (Au & Beck; 2001) and the Stepwise method (Koutsourelakis & al; 2004), are studied and modified to propose a new method herein called the Radial Sampling method.

Chapter four of this dissertation presents an application of the Radial Sampling method to estimate the seismic risk of reinforced concrete bridge columns. The results of this new approach are applied for developing a method for selecting the appropriate Response Modification Factor for bridge column design purposes using a reliability calibration technique, consistent with the method used for developing modern structural design and evaluation codes worldwide.

This approach is further extended in Chapter five of this thesis and applied to a typical bridge system. The Chapter serves to demonstrate the efficiency of the Radial Sampling method in solving problems involving a large number of random variables and multiple possible failure modes. The Radial Sampling method developed in this thesis is not only able to assess the probability of failure of the structural bridge system but it further breaks down the total seismic risk to assess the contributions of each mode to the integrity of the whole system.

Finally, to conclude this Ph.D thesis, Chapter six summarizes the research findings and outlines directions for future research.

# *Chapter2*

# *Review of Structural Reliability*

## 2.1 INTRODUCTION TO STRUCTURAL RELIABILTY

The aim of the theory of structural reliability is to provide the tools necessary to account for the uncertainties encountered while evaluating the safety of structural systems or during the calibration of load and resistance or partial safety factors for structural design codes. The uncertainties associated with predicting the load carrying capacity of a structure, the intensities of the loads expected to be applied, and the effects of these loads may be represented by random variables. The value that a random variable can take is described by a probability distribution function. That is, a random variable may take a specific value with a certain probability and the ensemble of these values and their probabilities are described by the distribution function. The most important characteristics of a random variable are its mean value or average, and the standard deviation that gives a measure of dispersion or a measure of the uncertainty in estimating the variable. The standard deviation of a random variable R with a mean $\overline{R}$ is defined as $\sigma_R$. A dimensionless measure of the uncertainty is the coefficient of variation (COV),

which is the ratio of the standard deviation divided by the mean value. For example the COV of the random variable R is defined as $V_R$ such that:

$$V_R = \frac{\sigma_R}{\overline{R}} \tag{2.1}$$

Codes often specify nominal values for the variables used in design equations. These nominal values are related to the means through bias values. The bias is defined as the ratio of the mean to the nominal value used in design. For example, if R is the member resistance, the mean of R, namely, $\overline{R}$ can be related to the nominal or design value $R_n$ using a bias factor such that:

$$\overline{R} = b_r . R_n \tag{2.2}$$

Where $b_r$ is the resistance bias, and $R_n$ is the nominal value as specified by the design code. For example, A36 steel has a nominal design yield stress of 36 ksi but coupon tests show an actual average value close to 40 ksi. Hence the bias of the yield stress is 40/36 or 1.1.

In structural reliability, safety may be described as the situation where capacity (strength, resistance, fatigue life, or seismic damage) exceeds demand (load, moment, stress ranges, acceptable damage). Probability of failure or the probability that capacity is less than applied load effects, may be formally calculated; however, its accuracy depends upon detailed data on the probability distributions of load and resistance variables. Since such data are often not available, approximate models are often used for calculation.

Let the reserve margin of safety of a bridge component be defined as, Z, such that:

$$Z = R - S \tag{2.3}$$

where R is the resistance or member capacity, S is the total load effect. Probability of failure, $P_f$, is the probability that the resistance R is less than or equal to the total applied load effect S or the probability that Z is less or equal to zero. This is symbolized by the equation:

$$P_f = \Pr[R \le S] \tag{2.4}$$

where Pr[ ] is used to symbolize probability. If R and S follow independent normal distributions then:

$$P_f = \Phi\left(\frac{0-\overline{Z}}{\sigma_Z}\right) = \Phi\left(-\frac{\overline{R}-\overline{S}}{\sqrt{\sigma_R^2+\sigma_S^2}}\right) \tag{2.5}$$

where $\Phi$ is the normal probability function that gives the probability that the normalized random variable is below a given value. $\overline{Z}$ is the mean safety margin and $\sigma_Z$ is the standard deviation of the safety margin. Thus, Equation 2.5 gives the probability that Z is less than 0. The reliability index, $\beta$, is defined such that:

$$P_f = \Phi(-\beta) \tag{2.6}$$

which for the normal distribution case gives:

$$\beta = \frac{\overline{Z}}{\sigma_z} = \frac{\overline{R}-\overline{S}}{\sqrt{\sigma_R^2+\sigma_S^2}} \tag{2.7}$$

Thus, the reliability index, $\beta$, which is often used as a measure of structural safety, gives the number of standard deviations that the mean margin of safety falls on the safe side as illustrated in Figure 2.1.

The reliability index, β, defined in Equations 2.6 and 2.7 provides an exact evaluation of risk (failure probability) if R and S follow normal distributions. Although β was originally developed for normal distributions, similar calculations can be made if R and S are lognormally distributed (i.e. when the logarithms of the basic variables follow normal distributions). Also, "Level II" methods have been developed to obtain the reliability index for the cases when the basic variables are not normal. Level II methods referred to as FORM (First Order Reliability Method) or FOSM (First Order Second Moment) are numerical optimization techniques that search in the multidimensional random variables space for the “design point” which is the point located on the failure surface and is the closest to the point whose coordinates correspond to the means of all the random variables. To calculate the probability of failure, FORM assumes that the boundary of the failure domain is piecewise linear and is tangent to the failure surface at the design point. SORM assumes that the boundary of the failure domain is of second order. The reliability index, β gives the shortest distance between the mean point and the failure surface in the standard normal space and is used as a measure of structural safety even for non-normal distributions. More detailed explanations of the principles discussed in this section can be found in published texts on structural reliability (e.g. Thoft-Christensen & Baker; 1982, Nowak & Collins; 2000, Melchers, 1999).

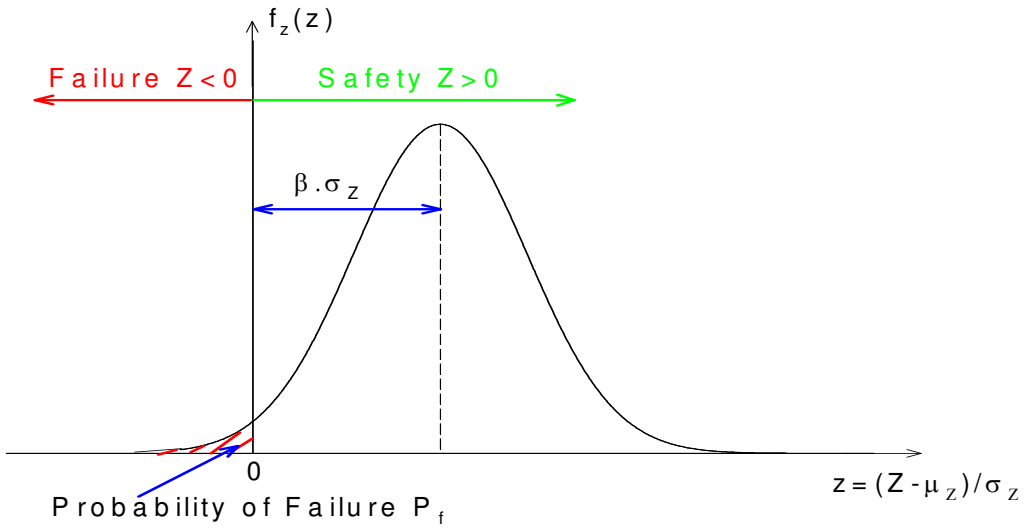


Figure 2.1 Illustration of failure region, safety region, and reliability index

FORM has been widely used to obtain the reliability index by many code writing groups and thus quantify structural risk. β in the range of 2 to 4 is usually specified for different structural applications (e.g. β=3.5 was used for the calibration of the Strength I limit state in AASHTO LRFD Specifications). These values usually correspond to the failure of a single component. If there is adequate redundancy, overall system reliability indices will be higher.

Over the last few years, with the advent of advanced computers with high numerical processing abilities, researchers and engineers shifted back to using traditional and advanced simulation techniques for estimating structural risk as will be explained in the next section.

## 2.2 MONTE CARLO SIMULATION METHOD

Monte Carlo Simulation is one of the simplest simulation methods used to estimate the probability of failure. Monte Carlo simulations are suitable for any random variable distribution type and failure equation. In essence, a Monte Carlo simulation creates a

large number of numerical experiments through the random generation of sets of resistance and load variables. Estimates of the probability of failure are obtained by comparing the number of experiments that produce failure to the total number of generated experiments.

Mathematically speaking, structural reliability problems are defined by a scalar performance function g(X) in an n-dimensional space $R^n$ of random variables assembled in a vector X. The hyper surface by g(X)=0 is called the response surface and it separates the failure domain where g(X)<0 from the safe domain corresponding to g(X)>0. The probability of failure $P_f$ is commonly defined by an integral form in terms of the random vector X and its probability density h(X).

$$P_f = \int_{g(X)<0} h(X)dX \qquad 2.7$$

The Monte Carlo simulation method transforms the integration domain over the failure region as in Equation 2.7 to cover the entire random variable space $R^n$ as expressed in the Following equation;

$$P_f = \int_{R^n} 1_F(X).h(X)dX \qquad 2.8$$

where $1_F$ denotes the indicator function that takes a value of 1 when X belongs to the failure domain and 0 otherwise.

The exact solution of Equation 2.7 or 2.8, which ideally will lead to the unknown parameter $P_f$, is unachievable analytically for most structural reliability problems. In addition to the complexity of the integrand of Equation 2.7 or 2.8, the unavailability of closed form expressions for the performance function g(X) is a main obstacle to determining an analytical solution of the probability of failure. Instead, a numerical

approach appears to be the only valid way to solve structural reliability problems especially with the rapid development of advanced numerical tools in recent decades that try to take advantage of the computational efficiencies of modern-day computers.

An unbiased estimator of Equation 2.8 is formulated in the following expression:

$$\tilde{P}_f = \frac{1}{N}\sum_{i=1}^{N} 1_F(X^{(i)}) \qquad 2.9$$

Based on the above estimator, the Monte Carlo simulation procedure consists of sampling individual samples $X^{(i)}$ from the random variable space according to the density distribution h. The associated indicator function is evaluated by a simple verification of whether the sampled variables fall in the failure or the safe domain. This crude process is repeated until a sufficiently large number of samples, N, is checked. Theoretically, and according to the law of large numbers, the Monte Carlo estimator will ultimately produce the exact solution of probability of failure as the number of samples approaches infinity. However, in practice, the Monte Carlo convergence rate is measured in terms of the coefficient of variation of the probability of failure $P_f$ in the mean square sense. This can be represented by the following expression:

$$\delta_{MC} = \frac{\sqrt{Var\left(\tilde{P}_f\right)}}{P_f} = \sqrt{\frac{\left(1-P_f\right)}{N.P_f}} \qquad 2.10$$

This convergence rate clearly shows the main reason for the inefficiency of Monte Carlo simulations: as $P_f$ becomes very small as is the case when analyzing a structure's probability of failure, the number of samples required to achieve a fixed level of accuracy grows proportionately to $1/P_f$. To overcome this handicap, First Order Reliability Methods were developed as a second generation of numerical techniques that try to

balance the need of accurate estimations of the probability of structural failures and the need to reduce the computational effort necessary to reach acceptable levels of accuracy. Although the first generation of FORM methods required an explicit formulation of the failure function, subsequent modifications led to the development of the Response Surface Method which can be used in conjunction with the results of Finite Element Analyses to obtain estimates of the probability of a structure's failure even when the failure function cannot be obtained in closed form.

## 2.3 RESPONSE SURFACE METHOD

The First Order Reliability Method often referred to as FORM requires the transformation of the original independent random variable space, X, into the standard normal space, x, even when the random variables are not normally distributed as explained by Ang & Tang (1975). In some structural reliability problems, the original random variables may be correlated, which would require their decoupling prior to the standardized transformation. The reduction of dependent random variables into uncorrelated random variable can be easily achieved using the Rosenblatt transformation technique (Melchers1987).

As mentioned earlier, the FORM algorithm revolves around finding the design point, which is defined as the closest point of the failure surface from the origin in the standard normal space (also called Gaussian space). It represents the point of greatest probability density or maximum likelihood. If the design point is denoted by $x^*$, and the failure surface defined by the performance function $g(X)=0$ is approximated by a hyperplane tangent to the failure surface at $x^*$, then the reliability index $\beta$ becomes the distance

between the design point and the point of origin as illustrated in Figure 2.2. This geometrical description of the reliability index can be represented by the following equation:

$$\beta = \min(x^T.x) = x^{*T}.x^* \qquad 2.11$$

where the superscript T indicates the application of the transpose function.

The FORM process is not as simple as it first appears from the above geometrical description. The key step in estimating the probability of failure in the FORM procedure is the localization of the design point on the failure surface in a multidimensional space. Furthermore, the unavailability of a closed form of the performance function, g, creates another level of challenge for FORM.

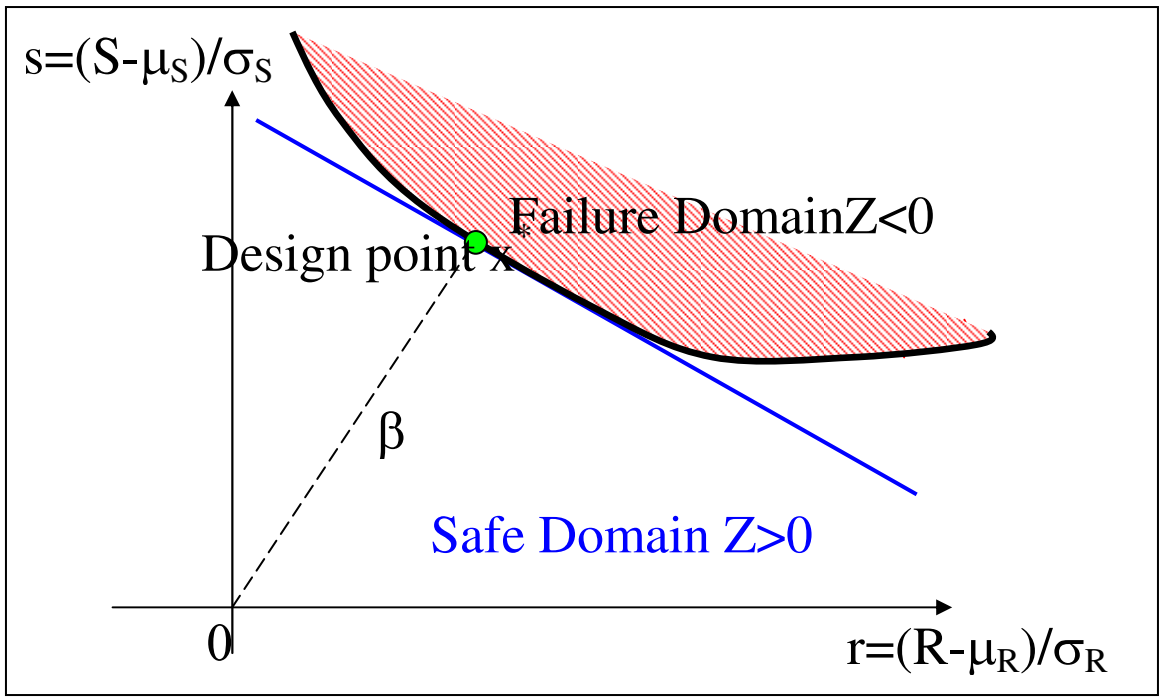


Figure 2.2 Illustration of Design Point concept in two dimension Gaussian space

Rajashekhar & Ellingwood (1993) describe the Response Surface approach that provides a method to approximate the unknown performance function, g, by a polynomial function of order m. The basic procedure involves the identification of the unknown coefficients of an $m^{th}$ order polynomial function $\tilde{g}$ that approximates the exact response limit state function around a design point candidate. The process requires the availability of experimental points near the failure surface which can be obtained by performing several finite element analyses to check the parameters that would lead to structural failure. The search, however, must be done in a systematic manner to ensure the efficiency of the method as described below.

Suppose that the structural response depends on n random variable $x=(x_1, x_2, \ldots, x_n)$. Let's assume that the approximated limit state function $\tilde{g}$ involves m coefficients. It is true up to a certain degree that a higher polynomial improves the accuracy of the approximation at the expense of additional computation (Rajashekhar & Ellingwood 1993). The rate of increase in accuracy reduces with the order of the polynomial but the computational effort increases exponentially since higher order polynomials involve greater numbers of unknown coefficients and require more structural analyses. The degree of $\tilde{g}$ is also upper-bounded by the shape of the exact response surface, g, around the region of interest. A lesser order of $\tilde{g}$ than the actual order of g results in a well-conditioned system of linear equations to solve for the unknown coefficients, while a higher order of $\tilde{g}$ than the actual order of g yields an ill-conditioned system of equations. (Engelund & Rackwitz 1992).

To illustrate the search process for the design point in the Response Surface method, let a second order polynomial function $\tilde{g}$ that excludes the cross terms $x_i x_j$ be given by:

$$\tilde{g}(x_1, x_2, ..., x_n) = a + \sum_{i=1}^{n} b_i x_i + \sum_{i=1}^{n} c_i x_i^2 \qquad 2.12$$

where a, $b_i$, and $c_i$ are the unknown coefficients to be determined, and $x_i$ are the random variables that control the response function. If 2n+1 numerical experiments are conducted, after ensuring the properties of the well-conditioned linear system, then the unknown coefficients are the solution of the following linear system:

$$\begin{pmatrix} g_1 \\ g_2 \\ . \\ . \\ g_{2n+1} \end{pmatrix} = \begin{pmatrix} 1 & x_{1,1} & x_{2,1} & . & . & x_{n,1} & x_{1,1}^2 & x_{2,1}^2 & . & . & x_{n,1}^2 \\ 1 & x_{1,2} & x_{2,2} & . & . & x_{n,2} & x_{1,1}^2 & x_{2,1}^2 & . & . & x_{n,1}^2 \\ . & . & . & . & . & . & . & . & . & . & . \\ . & . & . & . & . & . & . & . & . & . & . \\ 1 & x_{1,(2n+1)} & x_{2,(2n+1)} & . & . & x_{n,(2n+1)} & x_{1,(2n+1)}^2 & x_{2,(2n+1)}^2 & . & . & x_{n,(2n+1)}^2 \end{pmatrix} \begin{pmatrix} a \\ b_1 \\ b_2 \\ . \\ b_n \\ c_1 \\ c_2 \\ . \\ c_n \end{pmatrix}$$

2.13

in which $(g_{1,..,(2n+1)})$ are (2n+1) numerical experiments that correspond to sets of (2n+1) random variable vectors $(x_{i,j})$. The first subscript i of x refers to the rank of the random variable in the vector x between 1 and n, and the second subscript j to the set number of the random vector x.

$(g_{1,..,(2n+1)})$ may be obtained by using the central composite design method proposed by Bucher & Bourgund (1990). This method involves an iterative procedure for the calculation of the response state functions g for a set of random variables located around the center point as illustrated in Figure 2.3. In addition to the center point $x_c$, each two

points are located along each variable axis $x_i = x_{ci} \pm h\sigma_i$ (denoted by stars in Figure 2.3). This process provides 2n+1 values for g that are used to solve for the unknown coefficients of Equation 2.12. In the absence of any prior information about the response function, the prescribed procedure can be started at the mean value of the random variables. The next step consists of determining the minimum norm point $x_D$ located on the approximated failure surface. Finding the norm involves the use of minimization techniques such as the decent method to define the minimum distance measured in the normalized space.

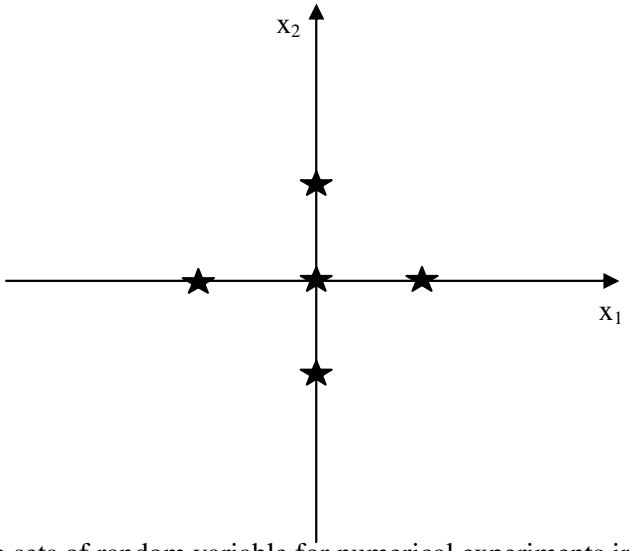


Figure 2.3 Five sets of random variable for numerical experiments in two random variables problem

Once $x_D$ is located, an additional numerical experiment is performed to evaluate $g(x_D)$ and a new center point $x_M$ is chosen by interpolating on a straight line between the previous center point $x_C$ and $x_D$ conditional on $g(x_M)=0$, using:

$$x_M = x_C + (x_D - x_C)\frac{g(x_C)}{g(x_C) - g(x_D)} \qquad 2.14$$

The iteration process shown in Figure 2.4 is carried out using the new center point until convergence is reached and the design point is identified. Many criteria can be used here to stop the iteration; steady values of β or identical $x_C$ and $x_D$ are good criteria for convergence among others.

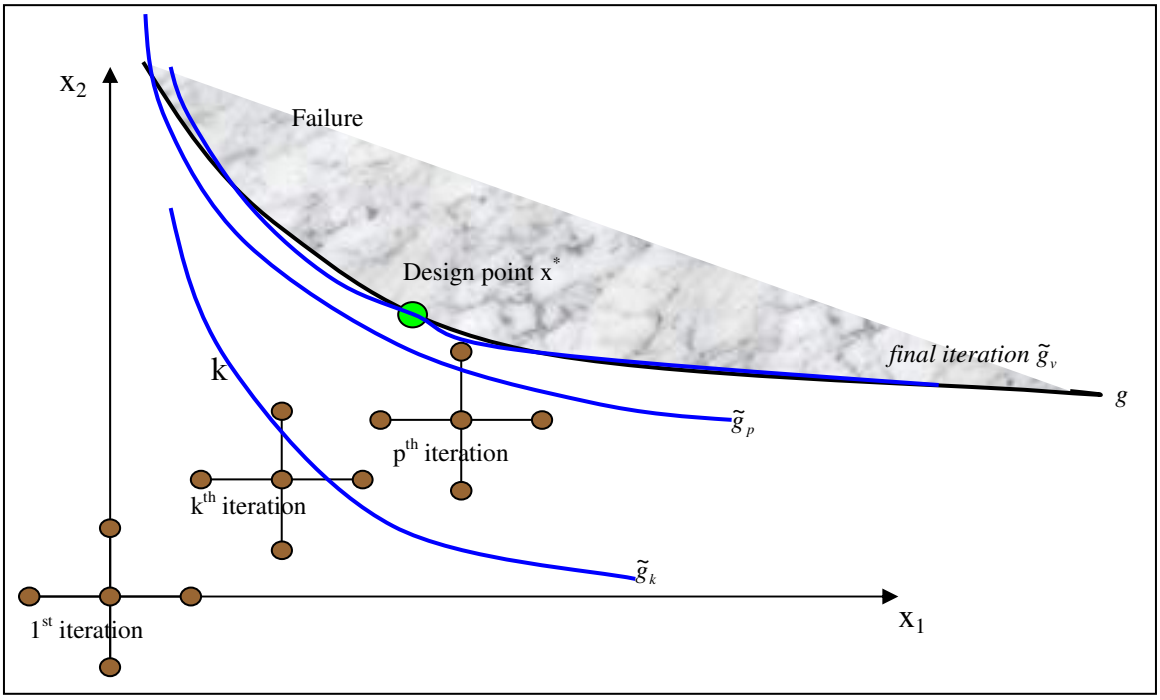


Figure 2.4 Illustration of search process for the design point

As an illustrative example taken from Rajashekhar & Ellingwood (1993), a cantilever beam with a rectangular cross section subjected to a uniformly distributed loading is considered. Assuming a limit state of serviceability with respect to maximum deflection at the free end of *l/325* is given by:

$$g = -\frac{wbL^4}{8EI} + \frac{L}{325}$$

where *w, b, L, E* and *I* are respectively the load per unit area, width, span, modulus of elasticity and moment of inertia of the cross section. *E,* and *L* are assumed deterministic quantities equal to $2.6 \times 10^4$ Mpa and 6 m respectively, while the load per unit area and the

depth of the cross section are random variables which are normally distributed with mean values of 1000N/m$^2$ and 250mm, and coefficients of variation of 0.2 and 0.15 respectively. After plugging the numerical value of deterministic parameters, the limit state equation is reduced to:

$$g(X) = 1846154 - 7.476923 \times 10^{10} \frac{X_1}{X_2} = 0$$

The response surface is approximated by a polynomial of second order without the cross terms, which includes five unknown coefficients. After carrying out the Bucher's algorithm, the approximated response surfaces at the limit state at each iteration are plotted in Figure 2.5. The error for the distance from the center point to the design point as well as the design points locations are listed in Table 2.1.

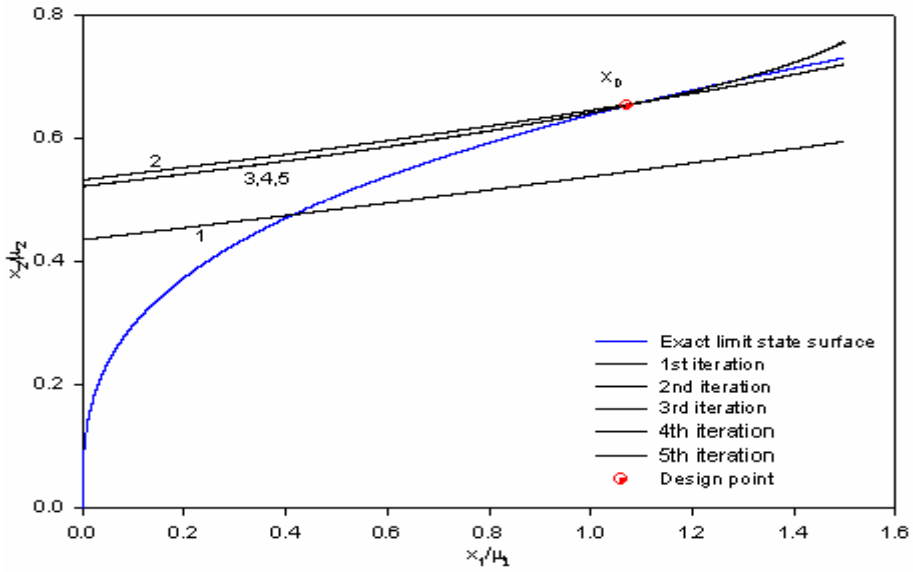


Figure 2.5 Approximation of exact limit state surface

Table 2.1 convergence of design point

| Iteration | error | $X_{1D}(N/m^2)$ | $X_{2D}(mm)$ |
|---|---|---|---|
| 1 | 3.0523 | 1089.6 | 136.7778 |
| 2 | 0.7880 | 1073.5 | 163.6843 |
| 3 | 0.0040 | 1073.9 | 163.2045 |
| 4 | $1.3987.10^{-6}$ | 1073.9 | 163.2321 |
| 5 | 0 | 1073.9 | 163.2321 |

The final value of the reliability index β is 2.3431 which corresponds to a probability of failure of $9.5615x10^{-3}$. The estimated probability of failure is very close to the exact value of $9.6071x10^{-3}$.

The illustrative example shows that the search for the design point was achieved in five iterations and yielded a good estimation of the probability of failure. This speed of convergence is generally the case when dealing with a smooth failure surface that has only one optimum design point. But, if the same response surface has two design points as shown in Figure 2.6, then the FORM will considerably underestimate the probability of failure.

Furthermore, the illustrative example involves two random variables. The actual number of random variables in most structural reliability problems is obviously much higher than 2 which would require higher number of FORM iterations and also a large number of structural analyses for each iteration. The determination of the design point that is the crucial step in the success of FORM is based entirely on the optimization technique. These techniques become completely inefficient in the case of a large number of random variables or unsmooth failure surfaces. The Genetic Algorithm can overcome these problems and is capable of detecting or at least pointing out the general directions

of all possible design points when the failure domain is a combination of different modes of failure.

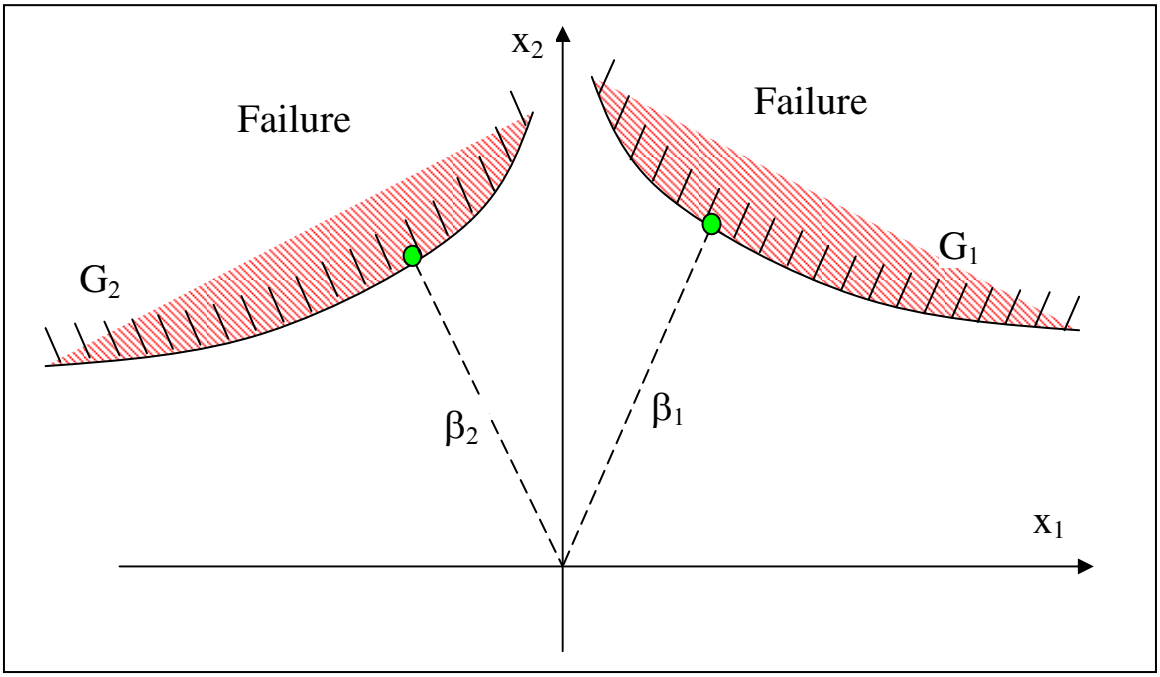


Figure 2.6 Presence of multiple design points in structural reliability problem

## 2.4 GENETIC ALGORITHM METHOD

The reliability analysis of complex structural systems like bridges may involve a large number of random variables with multiple failure modes. The identification of the modes of failure is very difficult with classical simulation methods such as Monte-Carlo simulation or the First Order Reliability Method. To overcome this challenge, many advanced techniques have been developed over the last few years. Among these methods, the Genetic Algorithm (GA) proved to be a useful technique for its ability to both reduce the computational effort and detect critical modes of failure. The Genetic Algorithm approach as proposed by Shao & Morutsu (1999) is based on the observation that any given mode of failure ($g_i$) of a structural system in the independent standard normalized space of random variables can be reached by following a failure path in a preset direction

$I_i$. Particularly, if this direction is chosen at $45^o$ angles from the standard random variable axes as illustrated in Figure 2.7, the components of the unit direction vectors will belong to the set (-1,0,1). The proposed coding of search directions in $45^o$ angles is similar to the coding in the natural genetic field, and therefore the unit direction vectors are called the chromosomes while each of their components represents a gene that can take any digit number of -1, 0, or 1. The fitness of a chromosome that measures its performance is defined as the speed by which the failure point is reached along the direction corresponding to the gene. Therefore, in reliability terms, the most fit chromosomes are those that produce low Norms the smallest of which would become reliability index values for the dominant modes.

The incorporation of other techniques in the GA such as linkage learning methods improves substantially the robustness and the versatility as well as the efficiency of GA in finding the global maximum. But, this would occur at the expense of the GA's ability of detecting local maxima. The linkage- Shredding Genetic Algorithm developed by Deng (2000) as one of the linkage-learning methods is based on shredding the chromosome. Through a progressive learning process, the fitness is updated and possibly modified based on acquired information about the performance of a number of gene sets. As the search goes on, only the best combinations of genes are allowed to travel together while the weak combinations are eliminated and prohibited from returning into the process. Deng's (2000) algorithm contributed to considerably improving the efficiency of the Genetic Algorithm by reducing the number of structural analyses necessary to reach the failure surface in the critical directions.

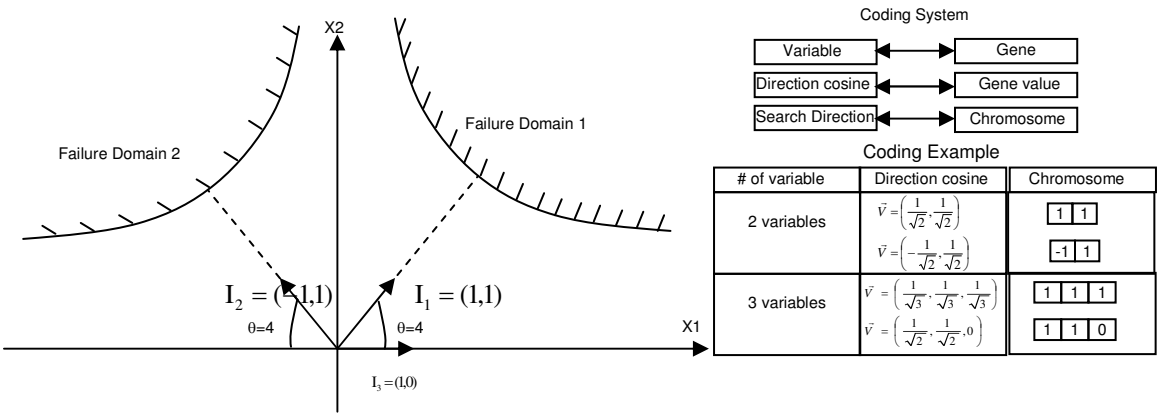


Figure 2.7 Genetic coding of search directions of 45° intervals in normalized space.

Another technique known as Data Mining was also found to be suitable for exploring relations and linkages between the important search directions. The Apriori algorithm as one of the Data Minig algorithms has been shown to be a powerful tool for reducing the list of possible search directions to focus on the most important ones. However, its ability to identify the search directions is compromised by its failure in the case of skewed, biased, or too narrow data sets. The combination of the Linkage-Shredding Genetic Algorithm and the Data-Mining technique proved to be efficient when applied to structural reliability problems (Wang & Ghosn 2003). A detailed description of these methods can be found in Wang & Ghosn(2003).

## 2.5 CONCLUSION

This Chapter described the application of structural reliability techniques for the safety assessment of structural systems. New generation of structural design codes have been developed based on structural reliability concepts whereby uncertainties in estimating structural capacity and applied loads are incorporated into the code provisions by ensuring that new designs meet a target reliability index which reflects the structural risk that the society can tolerates. One of the first methods used for the assessment of

probability of failure is the Monte Carlo simulation. Although this method can be utilized for any random variable distribution, its slow convergence in terms of number of experiments necessary to achieve an acceptable level of accuracy makes it unsuitable for solving problems with large numbers of random variables especially when the probability of failure is small. Due to the low efficiency of Monte Carlo Simulations, the FORM algorithm along with the Response Surface Methods became common tools for solving structural reliability problems. The FORM approach exploited the rotational symmetry of the Gaussian space by transforming random variables following different types of probability distributions into equivalent standardized Gaussian variables. The advantages of FORM can be severely compromised by the presence of multiple design points which reflect different failure modes frequently observed in structural systems. Therefore, some researchers have proposed the application of other techniques such as the Genetic Algorithm. The traditional Genetic Algorithm's inefficiencies required its supplementation with additional methods to improve its convergence efficiency. These modifications produced a complex process which is hard to implement in practice on a regular basis.

To overcome these difficulties, a new generation of numerical simulation methods has been recently explored. These methods are designed to reduce the computational effort and ameliorate the accuracy of the estimates of the probability of failure. Examples of such methods include the Line Sampling, Subset and Stepwise methods [Koutsourelakis & al (2004); Au & al (2001)]. These were found to be efficient for solving real size structural reliability problems with high number of random variables and small probabilities of failure. The next chapter of this Thesis will review the concepts behind

these three methods and will also propose a new similar approach for estimating small probability of failures in multivariate random space. The proposed method builds on the concepts of the line sampling method and the ability of the Genetic Algorithm to detect the approximate directions of the most important failure regions and will lead to accurate estimates of the probability of failure.

# *CHAPTER 3*

# *Estimation of Probability of Failure in High Multivariate Structural Systems*

## 3.1 INTRODUCTION

Chapter 2 of this thesis reviewed the background of structural reliability and described two classical methods for the assessment of probability of failure. Despite its ability to include any type of density distribution, The Monte Carlo simulation is found to have a slow convergence rate and requires a large number of experiments when estimating a small probability of failure. On the other hand, the First Order Reliability Method (FORM) was found to improve the efficiency compared to Monte Carlo simulation when the reliability problem has only one design point. However, FORM may considerably underestimate the probability of failure when estimating probability of failure with multiple design points. Moreover, the methods described in Chapter 2 are known to be inefficient when it comes to analyzing complex structural systems such as typical bridge structures that could have several important failure modes controlled by a large number of random variables and associated with low probabilities of failure. For this reason, the reliability analysis that is proposed in this study will require the application of advanced

structural reliability techniques that have been recently developed. For example, the Genetic Algorithm developed by Wang (2003) and Deng (2000) and described in Chapter 2 of this thesis has been found to be superior to other methods such as the various versions of the Response Surface Method as described by Engelund & Rackwitz (1992) and Rajashekhar & Ellingwood (1993) for determining structural modes of failure or finding the most important directions that lead to the points on the failure surface which are the closest to the mean point of the random variables in the Gaussian normalized space. The information acquired by the Genetic Algorithm, which consists of the direction cosines that approximately point in the direction of the most important failure points, can be exploited to estimate with good accuracy the probability of system failure. One way of achieving this objective is by applying the line sampling method proposed by Schueller & al (2003) to the directions identified by the Genetic Algorithm. However, although the line sampling method has been shown to be superior to the crude Monte Carlo simulation, it still requires a significant number of samples to produce accurate estimates of the probability of failure for large-scale structural systems. On other hand, the recent introduction of Markov Chain methods into the structural reliability analysis process has led to several new approaches to reduce the number of samples needed in Monte Carlo type simulations while maintaining a high order of precision in estimating the probability of failure particularly when the latter is very small and the number of random variables is high. The benefit of using Markov Chains during the simulation sampling process stems from their ability to use conditional sampling from a transition probability distribution (Tierney ;1994). It can be shown that as the length of the Markov Chain increases, samples drawn from the transition distribution tend to perfectly fit the

desired distribution (Tierney; 1994). Taking advantage of this concept, Au & Beck (2001) developed the Subset method that proved to be efficient when dealing with a very small probability of failure in a high dimension space. The Stepwise method recently developed by Koutsourelakis & al (2004) uses also Markov chains and its efficiency is found to be similar to that of the Subset method for assessing small probabilities of failure. In this Chapter, the theory of Markov Chains is laid out along with its application in the Metropolis-Hasting algorithm (Metropolis & al; 1953, and Hastings;1970) that forms the basis of the Subset and Stepwise methods. In addition, this Chapter develops a new method herein called the Radial Sampling method that builds on the Line Sampling method. The proposed Radial Sampling method is described and its accuracy and efficiency are compared to those of the Subset and Stepwise methods through the solution of multivariate single degree of freedom dynamic problems subjected to white noise excitation.

## 3.2 MARKOV CHAIN THEORY

A Markov Chain is a stochastic process that is based on three elements, 1) a random variable X that changes over time, 2) the state space describing the states that the random variable can be in, 3) the transition probability matrix that describes how the variable's states change. Let $X_t$ denote the value of the random variable at time t, the state space $s_i$ refers to the range of possible values of X at time t. A random variable is said to form a Markov process if the probability that X takes a certain value $s_j$ at time t+1 depends only on the current state $s_i$ of X at time t and is independent of previous states that X may have taken before time t. This can be expressed as:

$$\Pr(X_{t+1} = s_j \mid X_0 = s_k, ...., X_t = s_i) = \Pr(X_{t+1} = s_j \mid X_t = s_i) \quad 3.1$$

Therefore, in a Markov process, the only information needed to predict the next state of a random variable is its current state and the transition probability, which does not depend on the earlier states. The sequence of random variables ($X_0$, $X_1$, … $X_n$) is hence a Markov Chain generated by a Markov process characterized by its transition probabilities assembled in the transition matrix that is also called the transition kernel, P (i,j) = P(j $\rightarrow$ i), which defines the probability that the process at state space $s_j$, moves to state $s_i$ in one step as depicted by the following:

$$P(i, j) = P(j \rightarrow i) = \Pr\left(X_{t+1} = s_i \mid X_t = s_j\right) \quad 3.2$$

Let $\pi_j(t)$ denote the probability that the variable X is at state j at time t; Pr ($X_t$=$s_j$). Let us assemble in a column vector $\pi(t)$ all the state probabilities at time t. The Markov chain is initiated at a starting vector $\pi(0)$ whose elements are often zeros except for one element which has the value 1. As the chain progresses, the probability values spread out over all the possible states. Using the Chapman-Kolomogrov equation, the probability that the chain has a state value $s_i$ at time t+1 is obtained by summing over all the probabilities of being at state j at the current time and the transition probability from state j to state i:

$$\pi_i(t+1) = \Pr(X_{t+1} = s_i) = \sum_{states\ i} \Pr(X_{t+1} = s_i \mid X_t = s_j).\Pr(X_t = s_j)$$
$$\pi_i(t+1) = \sum_{states\ j} P(j \rightarrow i).\pi_j(t) = \sum_{states\ j} P(i, j).\pi_j(t)$$

3.3

Defining the probability transition matrix P as the matrix whose (i,j) element is the probability $\Pr(j \to i)$ of moving from state j to state i, Equation 3.3 can be written in the following matrix form:

$$\pi(t+1) = P.\pi(t) \qquad 3.4$$

Thus, if a Markov chain starts at a state probability vector $\pi(0)$ at time 0, n steps later, the state probability vector $\pi(t)$ will be:

$$\pi(t) = P^n.\pi(0) \qquad 3.5$$

As an illustration of the Markov chain process, let's suppose that the state space for weather at a given point of time can be classified as (Rainy, Sunny, Cloudy), and the weather follows a Markov process, which simply means that tomorrow's weather depends only on today's weather. Suppose furthermore that the probability transition matrix is given by:

$$P = \begin{pmatrix} 0.5 & 0.5 & 0.25 \\ 0.25 & 0 & 0.25 \\ 0.25 & 0.5 & 0.5 \end{pmatrix}$$

whose entries (i,j) reflect that the weather will be tomorrow at state i given that today's weather is at state j. As an example:

Pr(Sunny tomorrow| Rain today)=P(2,1)=0.25

Seeking to know the probabilities of the weather states after 4 days, 7 days, and 10 days respectively, given that the weather today is sunny, $\pi(0) = \begin{pmatrix} 0 \\ 1 \\ 0 \end{pmatrix}$, Equation 3.5 yields:

$$\pi(4) = P^4.\pi(0) = \begin{pmatrix} 0.375 \\ 0.25 \\ 0.375 \end{pmatrix}$$

$$\pi(7) = P^7.\pi(0) = \begin{pmatrix} 0.4 \\ 0.2 \\ 0.4 \end{pmatrix}$$

$$\pi(10) = P^{10}.\pi(0) = \begin{pmatrix} 0.4 \\ 0.2 \\ 0.4 \end{pmatrix}$$

It is noted that in this example the Markov chain has reached a stationary distribution $\pi^*$ after 7 days that is independent of the initial starting point. The stationary distribution satisfies:

$$\pi^* = \mathrm{P}.\pi^* \qquad 3.6$$

A sufficient condition for a unique stationary distribution is that the detailed balance equation holds true, that is:

$$P(i, j).\pi_j = P(j, i).\pi_i \qquad 3.7$$

The application of the Markov chain theory for sampling from complex probability distributions was first introduced by the Metropolis-Hastings algorithm, which is detailed in the next section of this Chapter.

## 3.3 METROPOLIS-HASTINGS ALGORITHM

Based on the Markov chain theory, the Metropolis-Hastings algorithm (Metropolis & Ulam; 1949, Metropolis & al; 1953, Hastings; 1970) provides an efficient way to sample from probability distributions from which it is difficult to sample directly. This property proved to be a powerful tool to overcome a main challenge in simulation-based reliability methods, which is the need to reduce the number of analyses required to solve large scale problems with low probabilities of failure. Using a proposal or candidate generating conditional distribution, p, the Metropolis-Hastings algorithm generates a sequence of draws from the original distribution also known as the target distribution, q, following these steps:

1. Define a proposal conditional distribution $p(\theta_i \mid \theta_j)$ so that it provides probabilities close to those of q in the vicinity of point $\theta_j$. It is noted here, that the closer is the approximation to q, the faster will be the convergence to the stationary results although any distribution will eventually lead to accurate results if enough iterations are applied.
2. Set i=0 and start with an initial value $\theta_0$ that satisfies $q(\theta_0)>0$.
3. Using the current $\theta_i$ value, sample a new candidate $\theta^*$ from the proposal distribution $p(\theta^*|\theta_i)$.
4. Calculate the density ratio or the Hastings ratio of the new candidate given by: $\alpha = \min\left(1, \frac{q(\theta^*).p(\theta_i \mid \theta^*)}{q(\theta_i).p(\theta^* \mid \theta_i)}\right)$

5. If the jump increases the density i.e $\alpha=1$, then accept the candidate point; $\theta_{i+1}=\theta^*$. In the other case where $\alpha<1$, the candidate is accepted with a probability $\alpha$, and rejected with a probability $1-\alpha$.
6. Set i=i+1 and repeat steps 3 to 5 until the desired number of samples is generated.

It can be easily proven that the Metropolis-Hastings Algorithm sequences constitute a Markov chain and satisfy the Detailed Balance equation that ensures the convergence to the target distribution as the stationary distribution (Au ;2004). Since the sampling accuracy gets better as the number of sequences increases, it is recommended to only retain the samples generated after a certain burn-in number. This is a key issue in the implementation of the Metropolis-Hastings algorithm and it has been recommended that the burn-in number be on the order of 1000 to 5000 elements. However, it should be noted that the burn in number depends largely on the initial value that initiates the Markov chain, and the proposal candidate. The closer are the initial values and the proposal distribution to the mode value and the target distribution respectively, the smaller is the length of the burn-in period. The advantages of the Metropolis-Hastings algorithm have been extensively exploited recently in new reliability analysis methods by sampling from conditional failure distributions. This approach has been found to substantially reduce the number of simulations required to reach a particular coefficient of variation on the probability of failure compared to the crude Monte Carlo simulation (Koutsourelakis &al; 2004).

## 3.4 SUBSET METHOD

The subset method is a simulation-based reliability method recently developed by Au & Beck (2001) to estimate small probabilities of failure of high dimension dynamic systems. In this method, the failure domain, F, is subdivided into a decreasing nested sequence of failure regions $\{F_{1<i<m}\}$ such that:

$$F = F_m \subset F_{m-1} \subset ... \subset F_2 \subset F_1 \tag{3.8}$$

This idea is possible to implement in structural dynamic systems where the response surface function defines failure as the domain where the structural response exceeds a capacity C. For instance, if m increasing values of C are set such that $C_1<C_2<\ldots<C_m$, then a subset of failure domains can be defined as $F_i = \{\theta \mid D(\theta) > C_i\}$ which clearly satisfy Equation 3.8. $D(\theta)$ is the structural demand calculated for each point $\theta$ by a structural dynamic analysis. Therefore, through subsequent steps and using the conditional probability definition, the probability of failure can be calculated from:

$$\begin{aligned} P(F) &= P(F_m) = P(\bigcap_{i=1}^{m} F_i) = P(F_m \mid \bigcap_{i=1}^{m-1} F_i).P(\bigcap_{i=1}^{m-1} F_i) \\ P(F) &= P(F_m \mid F_{m-1}).P(F_{m-1} \mid \bigcap_{i=1}^{m-2} F_i).P(\bigcap_{i=1}^{m-3} F_i) = ... \\ P(F) &= P(F_1).\prod_{i=1}^{m-1} P(F_{i+1} \mid F_i) \end{aligned} \tag{3.9}$$

According to Equation 3.9, the estimation of the probability of failure reduces to the product of $P(F_1)$ and $P(F_{i+1}|F_i)_{1<i<m-1}$. In order to calculate these quantities, Au & Beck (2001) suggested that the standard Monte Carlo simulation be used for finding $P(F_1)$. The

samples generated can also be used for estimating the probability of failure $P(F_2|F_1)$ by considering the samples that fall within the two domains $F_1$ and $F_2$. The process can also be followed for finding $P(F_{i+1}|F_i)$ by sampling from $F_i$. Finding $F_1$ from the crude Monte Carlo simulation is relatively very efficient given the size of the domain. However, as the domain size decreases, it was found that the calculation of $P(F_i)$ is more efficiently executed using the Markov chain as shown by Au & Beck (2001) who proposed a modified version of the Metropolis-Hastings algorithm for multidimensional sampling. The initial point needed to start the process can be selected from the previous sampling executed over $F_{i-1}$ as long as the point also falls in $F_i$.

The application of the modified Metropolis algorithm consists essentially of two levels of acceptance-rejection phases, which ensure that a well-mixed sampling is obtained and eliminate the correlation between subsequent drawings. Assuming that an n dimensional drawing from the failure region $F_i$ is needed, starting from an initial point $\theta_0 = (\theta_0^1, \theta_0^2, ..., \theta_0^n)$ that falls in $F_i$ and also in $F_{i-1}$, the following steps can be used to generate samples from $F_i$ that follow the original distribution q:

1. Set k=0 and choose a starting point $\theta_0 = \theta_k = (\theta_k^1, \theta_k^2, ..., \theta_k^n)$ in the n-dimensional space that falls within the failure domain $F_i$.
2. Generate an n-dimensional candidate point $\xi_{k+1}$ such that the $j^{th}$ component $\xi_{k+1}^j$ is simulated from a proposal distribution $p(\xi_{k+1}^j | \theta_k^j)$.
3. Calculate the density ratio of the $j^{th}$ component from: $\alpha = \min(1, \frac{q(\xi_{k+1}^j).p(\theta_k^j | \xi_{k+1}^j)}{q(\theta_k^j).p(\xi_{k+1}^j | \theta_k^j)})$.

4. Set $\tilde{\theta}_{k+1}^{j} = \xi_{k+1}^{j}$ with probability $\alpha$ and $\tilde{\theta}_{k+1}^{j} = \theta_{k}^{j}$ with probability 1-$\alpha$.
5. Repeat steps 2 through 4 until the simulation of all the components of $\tilde{\theta}_{k+1}$ is complete.
6. Check the new candidate $\tilde{\theta}_{k+1}$. If it falls in $F_i$, then accept this candidate as the next sample i.e set $\theta_{k+1} = \tilde{\theta}_{k+1}$, otherwise the candidate is rejected and the next sample is the previous sample, i.e $\theta_{k+1} = \theta_k$.
7. Set k=k+1 and repeat Steps 2 through 6 until enough samples are simulated.

From these samples, the conditional probability of failure is calculated from the following:

$$P(F_{i+1} \mid F_i) \approx \tilde{P}_{i+1} = \frac{1}{N}\sum_{i=1}^{N} I_{F_{i+1}}(\theta_i) \qquad 3.10$$

Where $I_{F_{i+1}}$ is 1 if $\theta_i$ falls in the failure domain and is 0 otherwise.

Combining Equations 3.9 and 3.10, the probability of failure can be estimated from the following expression:

$$\tilde{P}_F = \prod_{i=1}^{m} \tilde{P}_i \qquad 3.11$$

It is clear that the Subset method converges because of the properties of the Markov chain process. However, the efficiency of this method is critically affected by the choice of the intermediate values of $C_i$ that define the boundaries of the $F_i$ domains. Au & Beck

(2001) recommend that these $C_i$ values be selected in such a way that the intermediate probabilities $\tilde{P}_i$ are all close to 0.1.

## 3.5 LINE SAMPLING METHOD

The Line sampling method is detailed in this section because it is the basis of the Stepwise method and the proposed Radial Sampling method. Let's assume that an n-dimensional vector of random variables $\theta$ is distributed so that its components follow independent standard Gaussian distributions. This can be expressed as:

$$h(\theta) = \prod_{i=1}^{n} \phi(\theta_i) \qquad 3.12$$

Where $\phi$ is the Standard Gaussian distribution. $\theta_i$ denotes the $i^{th}$ component of the random vector $\theta$.

The line sampling method requires the identification of an important direction $\theta_1$, which we suggest in this study can be obtained using the Genetic algorithm. In fact the Genetic Algorithm has been shown to have the ability to identify all the important directions corresponding to all the failure surfaces and design points. The failure domain can be represented by:

$$F = \left\{\theta \in R^n \mid \theta_1 \in F_1(\theta_2, ..., \theta_n)\right\} \qquad 3.13$$

Where $F_1$ is the set containing the values of $\theta_1$ that would lead to failure for a given subset of values ($\theta_2$, $\theta_3$ ...$\theta_n$) also designated as the set ($\theta_{-1}$). Based on this alternate definition of the failure domain, the probability of failure can be written as:

$$P_f = \int_n \int\int I_F(\theta).\prod_{i=1}^{n}\phi(\theta_i)d\theta = \int_{n-1}\int\int\left(\int_1 I_{F_1}(\theta_{-1}).\phi(\theta_1).d\theta_1\right).\prod_{i=2}^{n}\phi(\theta_i)d\theta_{-1}$$

$$P_f = \int_{n-1}\int\int \Phi(F_1(\theta_{-1}))\prod_{i=2}^{n}\phi(\theta_i)d\theta_{-1} \qquad 3.14$$

$$P_f = E_{\theta_{-1}}\left[\Phi(F_1(\theta_{-1}))\right]$$

where $\theta_{-1}$ denotes the subspace of random variables $(\theta_2,...,\theta_n)$. $\phi$ and $\Phi$ are respectively the probability density and the cumulative functions of the standard normal distribution. $I_F$=1 when failure occurs and is 0 otherwise. E[…] is the expectation function.

The estimation of the probability of failure of Equation 3.14 can be carried out using the Monte Carlo estimator which requires sampling from the (n-1) dimensional subspace $\theta_{-1}$ and solving for $F_1(\theta_{-1})$:

$$\tilde{P}_f = \frac{1}{N}\sum_{i=1}^{N}\Phi(F_1(\theta_{-1}^i)) \qquad 3.15$$

The Line sampling method as illustrated in Figure 3.1 reduces the computational effort compared to the direct Monte Carlo simulation but was found to be less efficient than the Subset method (Koutsourelakis & al; 2004). The Stepwise method described in the next section is a further step in improving the line sampling method.

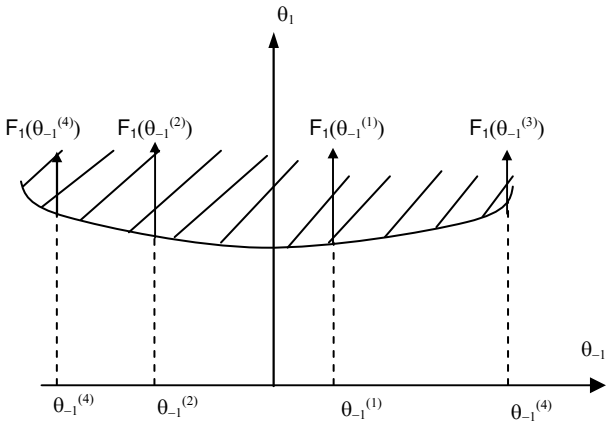


Figure 3.1 Illustration of the line sampling method

## 3.6 STEPWISE METHOD

The Stepwise method proposed by Koutsourelakis & al (2004) was designed to accelerate the rate of convergence of the line sampling method by benefiting from the Metropolis-Hastings algorithm. The main idea is to define a new random variable $u=\Phi(F_1(\theta_{-1}))$ whose distribution density $f(u)$ and cumulative distribution $F(u)=Pr(x<u)$ are not available in an explicit form. However, by generating samples $\theta_{-1}$ whose probability density function is $h(\theta_{-1}) = \prod_{i=2}^{n} \phi(\theta_i)$, samples of the random variable u distributed according to $f$ can be obtained by solving for $u=\Phi(F_1(\theta_{-1}))$ for each simulated set $\theta_{-1}$. This obviously requires finding the point on the failure surface through an iterative scheme and a number of dynamic analyses to locate the value β that corresponds to $\theta_1$ for a given set of $\theta_{-1}$. A schematic description of this task is given in Figure 3.2.

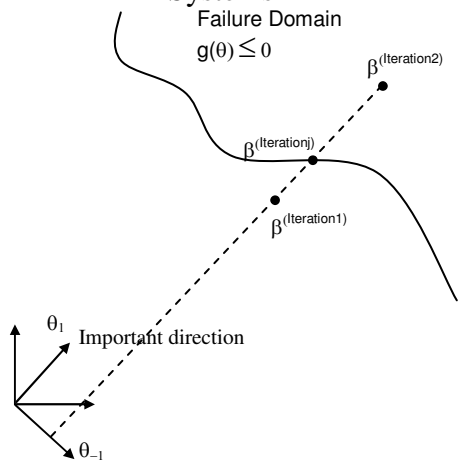


Figure 3.2 Schematic description of the scheme to generate samples of u

Since values of the random variable $u=\Phi(F_1(\theta_{-1}))$ are within the range [0,1], the probability of failure can be expressed as:

$$P_f = \int_0^1 uf(u).du = \int_0^1 u.dF(u) = \int_0^1 F_c(u).du \qquad 3.16$$

where $F_c(u)=1-F(u)=Pr(x>u)$. By breaking the interval [0,1] into m suitable increments, $u_i$, the probability of failure is approximated as:

$$\tilde{P}_f = \sum_{i=1}^{m} p_i$$
$$p_i = \int_{u_{i-1}}^{u_i} F_c(u).du \qquad 3.17$$

The estimation of the quantities $p_i$ necessitates an estimate of $F_c(u)$ which is achievable by the following Monte Carlo estimator that uses the Heaviside function denoted H:

$$\tilde{F}_c(u) = \frac{1}{N}\sum_{i=1}^{N} H(x_i - u) \qquad 3.18$$

By substituting Equation 3.18 in Equation 3.17, the first term $p_1$ can be approximated by:

$$\tilde{p}_1 = \tilde{q}_1.F_c(u_0 = 0) = \tilde{q}_1.1 = \frac{1}{N}\sum_{i=1}^{N}\min(x_i, u_1) \qquad 3.19$$

The other terms are determined subsequently by rewriting them in the following form:

$$p_i = \int_{u_{i-1}}^{u_i} F_c(u).du = F_c(u_{i-1}).\int_{u_{i-1}}^{u_i}\frac{F_c(u)}{F_c(u_{i-1})}du = F_c(u_{i-1}).q_i \qquad 3.20$$

where $q_i = \int_{u_{i-1}}^{u_i} r(u_{i-1}, u).du$ and $r(u_{i-1}, u) = \frac{F_c(u)}{F_c(u_{i-1})}$

This alternate equation is applied to take advantage of the previous sampling and avoid the need of repeating simulations over the same interval. The term $r(u_{i-1}, u)$ in the integrant of Equation 3.20 can be estimated using Equation 3.18 given that the samples are distributed according to $f(u|u>u_{i-1})$:

$$\tilde{r}(u_{i-1}, u) = \frac{1}{N}\sum_{i=1}^{N} H(x_i - u) \qquad 3.21$$

This challenging step of simulating $x_i$ is possible to overcome and can be accomplished using the Metropolis-Hasting algorithm discussed in section 3.3 of this Chapter. The version of this algorithm proposed by Au & Beck (2001 & 2003) can be used efficiently because it increases the possibility of acceptance and reduces the

correlation between two successive samples. The estimation of the quantity $F_c(u_i)$ is given by:

$$F_c(u_i) = F_c(u_{i-1}).\prod_{j=1}^{i-1} r(u_{j-1}, u_j) \qquad 3.22$$

The second term $q_2$ is approximated by the following estimator:

$$\tilde{q}_2 = \frac{1}{N}\sum_{i=1}^{N}(\min(x_i, u_2) - u_1)$$

The samples $x_i$ are generated according to $f(u|u>u_1)$ while $F_c(u_1)$ is estimated in the previous step and $r(u_1, u)$ is estimated by:

$$\tilde{r}(u_1, u) = \frac{1}{N}\sum_{i=1}^{N} H(x_i - u)$$

$F_c(u_2)$ can be calculated using Equation 3.21 as follows :

$$F_c(u_2) = F_c(u_1).\frac{F_c(u_2)}{F_c(u_1)} = F_c(u_1).r(u_1, u) \approx \tilde{F}_c(u_1).\tilde{r}(u_1, u)$$

Following the same procedure described above in quantifying the other terms, the probability of failure $P_f$ is estimated as:

$$P_f = \sum_{i=1}^{m} \tilde{F}_c(u_{i-1}).\tilde{q}_i \qquad 3.23$$

The efficiency of the estimator of Equation 3.23 and hence the stepwise method depends on the intermediate values of $u_i$. An appropriate selection of these values is

possible by selecting the corresponding conditional probability $r(u_{i-1}, u_i)$ large enough. Koutsourelakis & al (2004) recommended that $r(u_{i-1}, u_i)$ be on the order of 0.1.

The methods listed up to this point are efficient in calculating small probabilities in high multivariate structural dynamic systems. The next section of this Chapter introduces the new method called herein Radial Sampling method. The proposed method is based on the radial distribution. This method is designed to accelerate the rate of convergence of the Markov chain, and considerably reduce the computational sampling effort in the Metropolis-Hastings algorithm.

## 3.7 RADIAL SAMPLING METHOD

### 3.7.1 Density Function of Radial Distribution

Let $(\theta_1,...,\theta_n)$ be independent standard normal random variables. If we define $x = \sum_{i=1}^{n} \theta_i^2$, then the random variable x follows a Chi-square probability distribution, with a probability density function given by:

$$f_{\chi,n}(x) = \frac{x^{n/2-1}.\exp\left(-\frac{x}{2}\right)}{2^{n/2}.\Gamma\left(\frac{n}{2}\right)} \qquad 3.24$$

Where $\Gamma$ stands for the Gamma function.

The radius ρ defines the norm of the vector θ. Given that the radius $\rho$ is defined by $\rho = \sqrt{x} = \sqrt{\sum_{i=1}^{n} \theta_i^2}$, its probability distribution is related to the Chi-square distribution by the following expression:

$$f_{\rho,n}(\rho).d\rho = f_{\chi,n}(x).dx \quad \Rightarrow f_{\rho,n}(\rho) = f_{\chi,n}(x).\frac{dx}{d\rho} \quad \Rightarrow f_{\rho,n}(\rho) = f_{\chi,n}\left(\rho^2\right).2.\rho$$

$$f_{\rho,n}(\rho) = \frac{\rho^{n-1}.\exp\left(-\frac{\rho^2}{2}\right)}{2^{n/2-1}.\Gamma\left(\frac{n}{2}\right)} \qquad 3.25$$

The radius follows the distribution given by Equation 3.25 in n dimensional Gaussian space. The mean value of the radius is given by:

$$\mu_{\rho,n}(\rho) = \int_0^{+\infty} \rho.f_{\rho,n}(\rho).d\rho = \int_0^{+\infty} \left[\frac{\rho^n.\exp\left(-\frac{\rho^2}{2}\right)}{2^{n/2-1}.\Gamma\left(\frac{n}{2}\right)}\right].d\rho$$

$$= \frac{2^{(n+1)/2-1}.\Gamma\left(\frac{n+1}{2}\right)}{2^{n/2-1}.\Gamma\left(\frac{n}{2}\right)} . \int_0^{+\infty} \left[\frac{\rho^n.\exp\left(-\frac{\rho^2}{2}\right)}{2^{(n+1)/2-1}.\Gamma\left(\frac{n+1}{2}\right)}\right].d\rho$$

$$= \sqrt{2}.\frac{\Gamma\left(\frac{n+1}{2}\right)}{\Gamma\left(\frac{n}{2}\right)} . \int_0^{+\infty} f_{\rho,n+1}(\rho).d\rho$$

$$= \sqrt{2}.\frac{\Gamma\left(\frac{n+1}{2}\right)}{\Gamma\left(\frac{n}{2}\right)} \qquad 3.26$$

It can be shown that the expression of the mean given by Equation 3.26 can be approximated by $\sqrt{n-\frac{1}{2}}$ as n approaches infinity. The variance of the radius is given by:

$$\sigma^2_{\rho,n} = E\left[\left(\rho-\mu_{\rho,n}\right)^2\right] = E\left[\rho^2\right] - \mu^2_{\rho,n} = \int_0^{+\infty} \frac{\rho^{n+1}.\exp\left(-\frac{\rho^2}{2}\right)}{2^{n/2-1}.\Gamma\left(\frac{n}{2}\right)}.d\rho \quad - \quad \mu^2_{\rho,n}$$

$$= \frac{2^{(n+2)/2-1}.\Gamma\left(\frac{n+2}{2}\right)}{2^{n/2-1}.\Gamma\left(\frac{n}{2}\right)}.\int_0^{+\infty} \frac{\rho^{n+1}.\exp\left(-\frac{\rho^2}{2}\right)}{2^{(n+2)/2-1}.\Gamma\left(\frac{n+2}{2}\right)}.d\rho \quad - \quad \mu^2_{\rho,n}$$

$$= 2.\frac{\Gamma\left(\frac{n+2}{2}\right)}{\Gamma\left(\frac{n}{2}\right)}.\int_0^{+\infty} f_{\rho,n+2}(\rho) \quad - \quad \mu^2_{\rho,n} = 2.\frac{\Gamma\left(\frac{n+2}{2}\right)}{\Gamma\left(\frac{n}{2}\right)} \quad - \quad \mu^2_{\rho,n} \qquad 3.27$$

$$= n \quad - \quad \mu^2_{\rho,n}$$

Figure 3.3 shows the typical shape of the radial distribution for different values of the integer n.

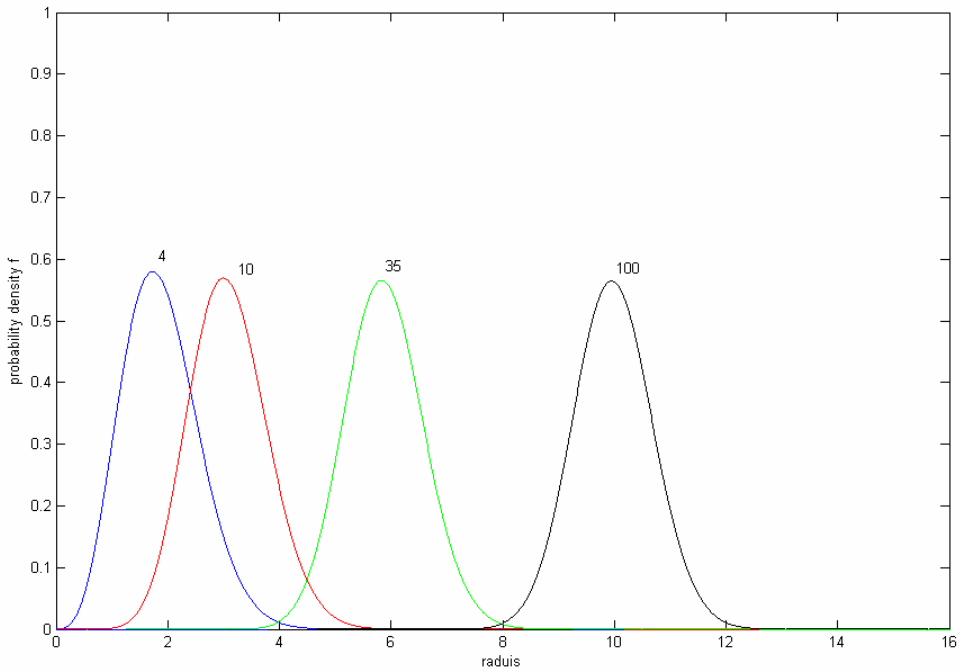


Figure 3.3. Typical shape of the radial distribution for different number of n

### 3.7.2 Cumulative Function of Radial Distribution

The Cumulative function of the Radial distribution is given by the following expression:

$$G(\rho) = \int_0^{\rho} f(x).dx \qquad 3.28$$

By a recursive proof, it can be shown that the cumulative function G is given by the expression:

$$G(\rho) = 1 - \exp\left(-\frac{\rho^2}{2}\right).\left[1 + \sum_{\substack{i=1 \\ step2}}^{n-3} \frac{2^{i/2}.\Gamma\left(\frac{i}{2}\right)}{\Gamma(i+1)}\right] \qquad 3.29$$

### 3.7.3 Radial Sampling method procedure

The proposed Radial Sampling method is based on dividing the Gaussian space into m separate regions $H_{1\le i\le m}$ based on the radius probability distribution to cover the total probability space S such that:

$$\bigcup_{i=1}^{m} H_i = S \qquad H_i \bigcap_{i\neq j} H_j = 0 \tag{3.30}$$

If a sequence of increasing values $\rho_{1\le i\le m+1}$ are selected, $H_{1\le i\le m}$ can be defined by:

$$\begin{aligned} H_1 &= \{\theta / \rho(\theta) \le \rho_1\} \\ H_i &= \{\theta / \rho_{i-1} < \rho(\theta) \le \rho_i\} \\ H_m &= \{\theta / \rho(\theta) > \rho_m\} \end{aligned} \tag{3.31}$$

Where $\theta=\theta_{-1}=(\theta^{(2)},\theta^{(2)},..,\theta^{(n)})$ is a vector of standard normal random variables of length n-1, and $\rho(\theta) = \sqrt{\sum_{j=2}^{n}\left(\theta^{(j)}\right)^2}$ . Based on the observation made in section 3.5 that described the line sampling method, the vector $\theta$ of equation 3.31 will be the random vector of the subspace $\theta_{-1}$ which is perpendicular to the important direction $\theta_1$ that should be identified before the simulation process is initiated. Therefore, the probability of failure can be expressed as:

$$\Pr(F) = \Pr(F \mid \bigcup_{i=1}^{m} H_i = S) = \sum_{i=1}^{m} \Pr(F \mid H_i).\Pr(H_i) \tag{3.32}$$

The evaluation of $Pr(H_i)$ can be executed directly from the cumulative function of the Radial distribution given by Equations 3.2 by taking:

$$\Pr(H_i) = G(\rho_i) - G(\rho_{i-1}) \tag{3.33}$$

The estimation of the terms $Pr(F|H_i)$ can be performed following the approach of the line sampling method given that the sampled random vector θ falls in the $H_i$ region in the subspace $\theta_{-1}$ perpendicular to the important direction $\theta_1$. $Pr(F|H_i)$ can be obtained using the Metropolis-Hastings algorithm. To accomplish this step, an approach is adopted in this method, which reduces the sampling effort n times. It is proposed herein to generate a number N of unit vectors in $\theta_{-1}$ subspace from their true distribution in the Gaussian space and use them to create new directions. Once the unit vectors are generated in the first step, the only variable that will need to be generated in subsequent steps is the radius $\rho$. This can be achieved by means of the Metropolis-Hastings algorithm. Thus, for each interval $[\rho_{i-1},\rho_i[$, a number N of radiuses $\rho$ equal to the number of directional vectors are simulated according to the radius distribution developed in section 7.1 and given by Equation 3.25. The proposal distribution of the Metropolis-Hastings algorithm used in this approach is the normal distribution which is centered at the previous sample. These generated samples of the radius $\rho$ are used to obtain samples from $H_i$ by simply multiplying each of the N directional unit vectors by a sampled radius value at random without replacement.

Therefore, $Pr(F|H_i)$ will be estimated using the following expression:

$$\Pr(F \mid H_i) = E_{H_i}\left[\Phi\left(F_1(\theta_{-1})\right)\right] \approx \tilde{P}_f^i = \frac{1}{N}\sum_{i=1}^{N}\Phi\left(F_1(\theta_{-1})\right) \qquad 3.34$$

Finally by plugging Equations 3.33 and 3.34 back in Equation 3.32, the probability of failure can be estimated by:

$$\tilde{P}_f = \sum_{i=1}^{m}\tilde{P}_f^i.\left(G(\rho_i) - G(\rho_{i-1}\right) \qquad 3.35$$

In the proposed method, two key elements control the efficiency of the procedure. The first element is the number of generated directional unit vectors whose number should be large enough to cover most of the subspace directions and depends on the dimension n or the number of independent variables in the subspace. In this Ph.D study, the following sets of $H_i$ are considered

$$\begin{aligned} H_1 &= ]\ 0\ ,\ \rho_1[ \quad \text{such that} \quad G(H_1) = 0.40 \\ H_2 &= ]\ \rho_1\ ,\ \rho_2\ [ \quad \text{such that} \quad G(H_2) = 0.40 \\ H_3 &= ]\ \rho_2\ \ ,\ \rho_3[ \quad \text{suchthat} \quad G(H_3) = 0.10 \\ H_4 &= ]\ \rho_3\ ,\ +\infty[ \quad \text{suchthat} \quad G(H_4) = 0.10 \end{aligned} \qquad 3.36$$

In the Radial Sampling method, the intermediate values of the radius can be selected at the onset of the simulation. Furthermore, instead of generating all the vector samples by the Metropolis-Hastings algorithm, the proposed method requires the generation of the radius only which reduces considerably the computational effort in the sample generation phase. In the next section, the efficiency of the radial method is tested and compared to the other methods.

## 3.8 NUMERICAL EXAMPLES

### 3.8.1 Example 1

This numerical example is similar to the one considered by Au & Beck (2001) and Koutsoulakis & al (2004). It consists of a single degree of freedom linear oscillator with natural frequency $\omega$=2π rad/sec and damping ration ξ=2% subjected to a Gaussian white noise excitation with variance equal to 2π. The governing equation of this system initially at rest in terms of the SDOF response X is given by:

$$\ddot{X}(t) + 2.\xi.\omega.\dot{X}(t) + \omega^2.X(t) = W(t) \qquad t \in [0, 2.5\,\text{sec}] \qquad 3.37$$

If the time duration 2.5sec is discretized into 50 intervals of Δt=0.05sec width, the Gaussian white noise excitation at time $t_k$=(k-1).Δt will be $W(t_k) = \sqrt{2\pi/\Delta t}.\theta_k$, where $\theta_k$ is a standard Gaussian random variable. A typical representation of the Gaussian white noise is illustrated in Figure 3.4.

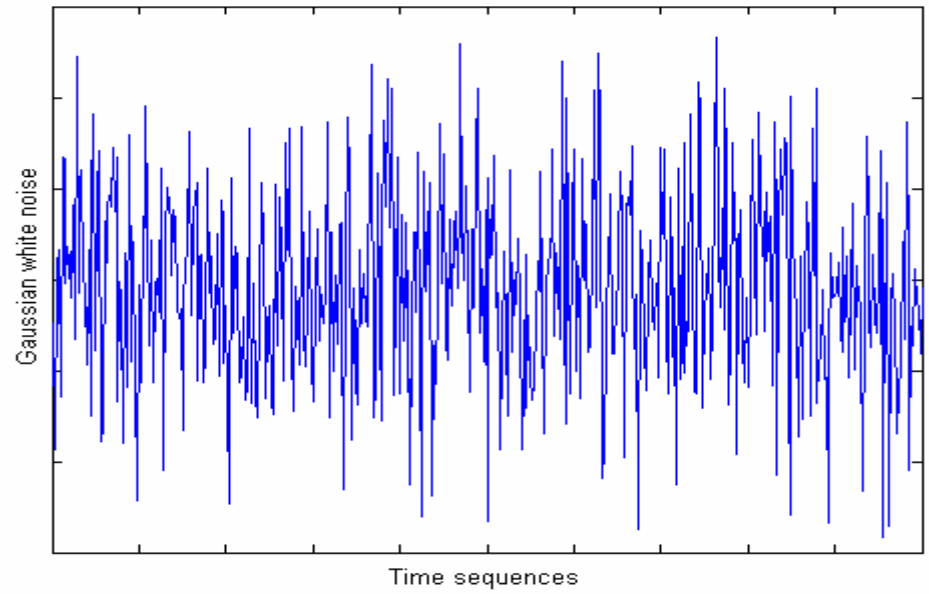


Figure 3.4 Typical Gaussian white noise

The system failure for this example is assumed to occur when the SDOF response X exceeds a threshold value b=1.5. The simulation methods described earlier in this Chapter are used to calculate the probability of failure. The Radial Sampling method and the Stepwise method require the identification of the important directions pointing to the design points on the failure surface. This can be accomplished using the Genetic Algorithm described briefly in chapter Two. The resultant dominant chromosome associated with the important direction is plotted in Figure 3.5 and shows that the frequency of this direction is close to the natural frequency of the single degree of freedom $w=2\pi$.

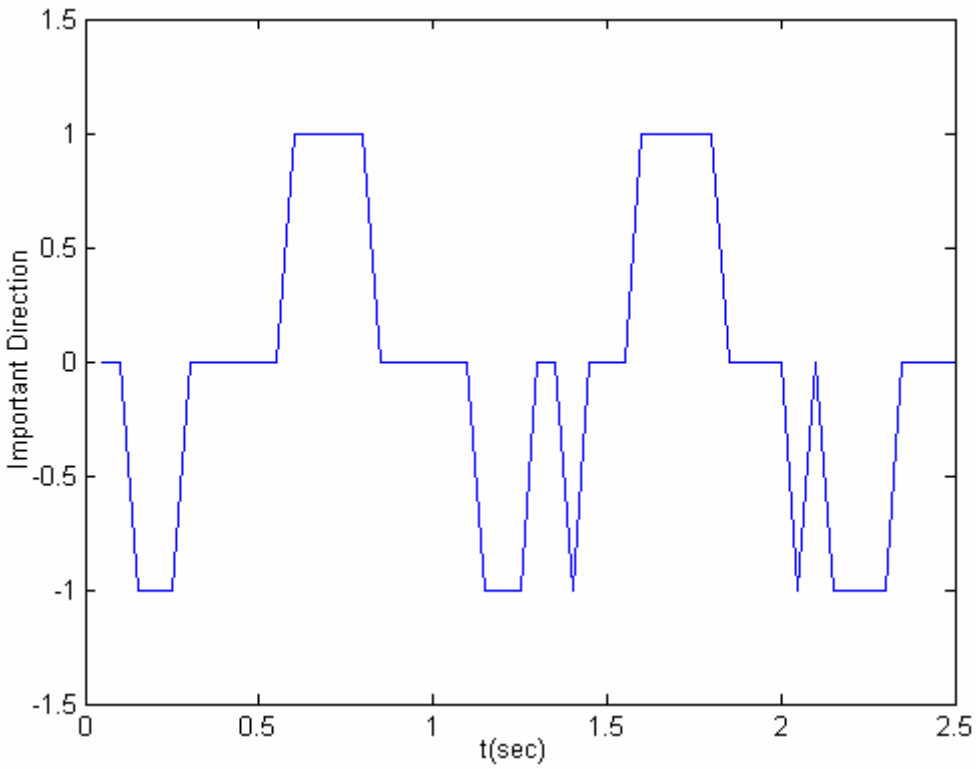


Figure 3.5. Dominant chromosome obtained by Genetic Algorithm

The unit vector in the dominant direction is represented by $\theta_1$. The subspace $\theta_{-1}$ perpendicular to $\theta_1$ can be constructed which is now the sampling space for the Stepwise

method and the Radial method. The proposal distribution needed for the application of the original and the modified Metropolis-Hastings algorithm in association with the Stepwise method is the standard normal distribution. The one dimensional Metropolis-Hastings algorithm is used to provide the sample of radiuses for the Radial simulation method. Ten thousand unit vectors are used in the Radial Sampling method at each of the four steps while fifty and forty thousand simulations are generated for the Stepwise method and the Subset method respectively. For comparison purposes, we perform 50 runs in order to calculate the coefficient of variation in the probability of failure for each method. The results tabulated in Table 3.1 show that the Radial sampling method is efficient for this example. In the next example, the Radial Sampling method is tested for different probabilities of failures.

***Table 3.1***. Mean and C.O.V values obtained by each method

| Probability of Failure $P_f$ | Subset method | Stepwise method | Radial method (Proposed method) |
|---|---|---|---|
| Mean value $\mu(P_f)$ | $2.445\ 10^{-4}$ | $2.466\ 10^{-4}$ | $2.447\ 10^{-4}$ |
| C.O.V $\delta(P_f)$ | 8.84 | 12.13 | 8.27 |
| # of structural Analysis | 40000 | 40000 | 40000 |

### 3.8.2 Example 2

In the first example, the different methods presented in this chapter were compared for 50 random variables and a probability of failure on the order of $10^{-4}$. The results are comparable when using a large number of samples in the Gaussian space. In this following example, 400 random variables are considered for the same stochastic problem described in Equation 3.37. The threshold value b is varied between 2 and 2.8 to produce

different orders of probability of failure. In this example, the number of samples used in each step is taken equal to 500 samples. In order to calculate the accuracy of each method, one thousand independent simulations are performed and the coefficient of variation is calculated based on the one thousand estimates of the probability of failure calculated from the independent runs. Furthermore, the calculated coefficient of variation is multiplied by the square root of the number of simulations averaged over the total number of runs.

Table 3.2. Comparison of different methods

| | b-value | 2 | 2.2 | 2.4 | 2.5 | 2.8 |
|---|---|---|---|---|---|---|
| | **Pf** | 1.30E-02 | 3.40E-03 | 8.30E-04 | 3.62E-04 | 3.20E-05 |
| | **MC** | 8.63 | 16.81 | 35 | 50.50 | 201.61 |
| | **L Sampling** | 5.98 | 11.06 | 23.74 | 32.43 | 106.82 |
| **cov** | **Stepwise** | 7.54 | 11.48 | 17.10 | 20.41 | 34.40 |
| | **Subset** | 7.84 | 12.40 | 16.88 | 21.06 | 30.78 |
| | **Radial** | 6.31 | 11.80 | 22.38 | 31.41 | 84.82 |

Table 3.2 shows the performance of each method based on the coefficient of variation. The results clearly indicate that all the methods outperform the Monte Carlo simulation as the probability of failure gets smaller. As it was shown in chapter 2, the coefficient of variation of the Monte Carlo Simulation is inversely proportional to the probability of failure which explains why the performance of the Monte Carlo Simulation decreases rapidly from 8.63 for a probability of failure of 1.34E-02 to 35 for a probability of failure of 8.70E-4 and jumps to 202 when the probability of failure is 3.04E-5.

For threshold values b of 2 and 2.2 which correspond to probabilities of failure of 1.34E-02 and 3.60E-03, the Radial Sampling method and the Line Sampling method provide better results than those of the Stepwise method and Subset method. This observation can be explained by the correlation introduced by the Markov Chain between

successive candidates especially when the initial burnout samples are not excluded and a multidirectional sampling is used. The use of a one directional Markov chain in the Radial sampling method reduces the correlation between the samples.

However, as the probability of failure gets smaller, the effect of the correlation between successive samples introduced by Markov Chain seems to be overshadowed by the effect of the very small probability of failure. Therefore, the Subset method and the Stepwise method become more efficient than the Radial and the Line sampling methods.

## 3.9 CONCLUSION

The results of the examples described in this chapter show that the Radial Sampling method is as efficient as the most recently developed advanced simulation techniques when the probability of failure is in the range of $10^{-1}$ to $10^{-4}$. In particular, the fluctuation in the probability of failure produced by the Radial Sampling method is found to be similar to those of the Subset method and the Stepwise method. One advantage of the Radial Sampling method over the other methods is in the considerable reduction in the effort of the Markov chain sampling. In fact, the Radial Method requires Markov Chain sampling in a single degree of freedom rather than the multidimensional approach used in the Subset and Stepwise method. Furthermore, the one directional Markov Chain Sampling employed by the Radial Sampling method reduces the correlation between successive samples compared to the multidirectional Markov Chain sampling used in the Subset and the Stepwise methods.

Another advantage of the Radial Sampling method lies in its ability to estimate the probabilities of failure for each failure mode of the structural system in addition to

finding the total probability of failure of the system as will be further demonstrated in Chapter 5 of this thesis. The issue of finding individual modes of failure was not addressed in either the stepwise method or the subset method.

In the next chapters, the Radial Sampling method will be used to calculate the structural probability of failure typically in the range of $10^{-1}$ to $10^{-4}$ where its performance is found to be most efficient. Specifically, in the next Chapter of this Thesis, the Radial Sampling method will be used to develop a nonlinear dynamic reliability analysis model to appropriately calibrate the response modification factor for the force based seismic design procedure for reinforced concrete columns. The proposed reliability analysis model will be subsequently applied in Chapter 5 to analyze the seismic risk of a typical bridge system associated with different possible modes of failure where the system behavior is controlled by the interaction of all the bridge's components including the columns, bearings, superstructure, foundations, and abutments.

# *Chapter4*

# *Calibration of Response Modification Factor for Seismic Design of Bridge Columns*

## 4.1 INTRODUCTION

The design of simple highway bridges subjected to seismic input relies on the use of the response modification factors, $R_\mu$, that account for the nonlinear behavior of the members. Nominal values for the response modification factors for bridge columns are provided in the AASHTO bridge design specifications. These have been empirically determined based on the experience of bridge engineers, experimental investigations conducted on laboratory models of bridge columns under cyclic dynamic forces, and various time history analyses of elasto-plastic single degree of freedom systems. To account for the variations observed in the actual response of bridge columns as compared to analytically derived responses, code writers have relied on their experience and judgment to recommend conservative values of $R_\mu$. Analytical investigations have shown large variations in $R_\mu$ for members that have the same material and geometric properties when subjected to various earthquake records having similar characteristics. This large

variability is caused by the variations in the time histories of earthquakes that nominally have the same characteristics including the same magnitudes, and epicentral distances. However, these variations have not been properly analyzed and recent recommendations for new sets of response modification factors for adoption in the AASHTO LRFD Design Specifications have focused on matching the average nonlinear response of bridge columns without accounting for the large variability around these average values.

LRFD codes are normally designed to apply appropriate load and resistance safety factors that explicitly account for the uncertainties associated with estimating the loads to be applied on the structure, the response of the structure to these loads, and the ability of the structure to sustain the load effects. The goal of LRFD codes is to recommend a consistent procedure that leads to the design of structures providing an acceptable and uniform level of risk. Thus, using average values for the response modification factors is inconsistent with the basic LRFD methodology as this may lead to the design of some over-conservative structures while others would be under-designed. It is noted that the risk of bridge failure can be drastically reduced, even for bridges designed with un-conservative values of $R_\mu$, by applying high safety factors on other design parameters such as selecting long return periods for the seismic input. However, such an approach would still be inconsistent with the LRFD methodology, as it would unfairly penalize designs in situations where the dynamic input is better defined as compared to other regions where seismic studies suffer from the paucity of data, or for the cases where the seismic input is less destructive.

A rational approach for calibrating LRFD design criteria that take into consideration the uncertainties in each of the design parameters as well as the random nature of the

seismic input and the bridge response is based on the application of structural reliability concepts. Thus, the objective of this chapter is to propose a nonlinear dynamic reliability-based analysis method to calibrate a set of Response Modification factors that will lead to the design of typical highway bridge columns with uniform and consistent levels of safety for bridges situated in different regions of the U.S. including the East Coast, West Coast, or Mid-America.

## 4.2 OBJECTIVE

The objective of this chapter is to develop a reliability-based method to calibrate a rational set of seismic design specifications that will lead to the design of typical highway bridge columns that will have uniform and consistent levels of safety. In particular, the calibration procedure will take into consideration the uncertainties associated with estimating the magnitude of the seismic input in different regions and sites, the variability in the seismic time histories as well as the uncertainties associated with estimating the corresponding structural response of bridge columns and estimating the structural damage. The goal of the calibration process is to provide uniform and consistent levels of reliability for bridges situated in different regions of the U.S. including the East and West Coasts as well as Mid-America. To achieve these objectives, the following tasks should be completed. 1) Identify the seismic hazards at different typical sites; 2) develop a suite of earthquake records that represent the seismic hazard for each of the selected sites; 3) develop probabilistic models for analyzing the response and assessing the damage of bridge columns subjected to seismic input; 4) develop a methodology to estimate the reliability of bridge columns accounting for the uncertainties in the seismic

input and the structural response; 5) apply the models and the structural reliability methodology to a range of typical bridge configurations and estimate the reliability levels inherent in bridges designed to satisfy current seismic design specifications; 6) propose a set of response modification factors that would meet target reliability levels extracted based on the performance of acceptable existing designs and study the sensitivity of these factors for changes in the target reliability levels. The proposed approach would lead to a rational set of response modification factors that would be compatible with the LRFD methodology and account for the uncertainties associated with estimating both the structural response as well as the seismic hazard.

The technical background needed to achieve the objectives of this study is described in Sections 4.3 through 4.12 of this part of this Chapter. In particular, Section 4.3 overviews the approach normally followed to calibrate LRFD codes. Section 4.4 provides a definition of the response modification factor and its implication in the current code provisions. Section 4.5 discusses how the variability in the seismic input characteristics affects the variability in the calculated response modification factors. Section 4.6 reviews the seismic hazard analysis procedure recommended by USGS. Section 4.7 studies the effects of cyclic loading on the performance of RC bridge column. Sections 4.8 and 4.9 describe a method to assess the seismic damage to bridge columns taking into consideration the uncertainties in the column stiffness, strength, mass, and ductility, as well as the energy dissipated during cyclic seismic loading. In section 4.10, uncertainties related modeling errors in the hysteresis Model are studied and identified. Sections 4.11 and 4.12 outline how the models described in the previous sections can be used in a comprehensive reliability analysis of bridge columns subjected to seismic

excitations to calibrate nominal response modification factors for the seismic design of bridge columns.

To achieve the objectives of this study, the tools developed in sections 4.3 through 12 are applied in section 4.13 on hypothetical bridge columns located in the San Francisco area to come up with a set of $R_\mu$ and the associated probability of failure. Section 4.14 of this chapter studied the sensitivities of the Response Modification Factor to material variabilities inherent in bridge columns. The results obtained from the analysis of San Francisco examples can be generalized as demonstrated in section 4.15 for selected sites for the application to other regions of the US located in West Cost, Mid-America, as well as East Cost.

## 4.3 RELIABILITY-BASED CODE CALIBRATION

The reliability index, $\beta$, discussed in chapters 2 and 3 is not used in practice for making decisions regarding the safety of a design or existing structure but it is rather used by code writing groups for recommending appropriate load and resistance safety factors for new structural design or evaluation specifications. The most accepted calibration approach for developing design equations is based on the principle that each type of structure should have uniform or consistent reliability levels over the full range of applications. For example, load and resistance factors should be chosen to produce similar $\beta$ values for bridges of different span lengths, number of lanes, simple or continuous spans, roadway categories, designed in different regions of the U.S. Thus, a single target $\beta$ must be achieved for all applications. Some engineers and researchers on the other hand are suggesting that higher values of $\beta$ should be used for more important

structures such as bridges with longer spans, bridges that carry more traffic, or bridges that, according to AASHTO, are classified as critical for "social/survival or security/defense requirements". Since higher β levels would require higher construction costs, the justification should be based on a cost-benefit analysis whereby target β values are chosen to provide a balance between cost and risk (Aktas, Moses and Ghosn, 2001).

In many code calibration efforts, appropriate target β values are deduced based on the performance of existing designs. That is, if the safety performance of bridges designed according to current standards has generally been found satisfactory, then the reliability index obtained from current designs is used as the target that any new design should satisfy. The aim of the calibration procedure is to minimize designs that deviate from the target reliability index. Such calibration with past performance also helps to minimize any inadequacies in the database as has been previously reported by Ghosn & Moses (1985). It was found that load and resistance factors obtained following a calibration based on "safe existing designs" are relatively insensitive to errors in the statistical database as long as the same statistical data and criteria are used to find the target reliability index and to calculate the load and resistance factors for the new code. In fact, a change in the load and resistance statistical properties (e.g. in the coefficients of variation) would affect the computed β values for all the bridges in the selected sample population of existing bridges and consequently their average β value. Assuming that the performance history of these bridges is satisfactory, then the target reliability index would be changed to the new "average" and the calibrated load and resistance factors that would be used for new designs would remain approximately the same.

The code calibration effort is usually executed by code groups as follows:

- Statistical models are assembled for all the parameters that describe the loads expected to be applied on a structure within its design life.
- Statistical models are also assembled for all the parameters that control the strength and the response of the structure when subjected to the loads identified in the first step. These statistical models should account for both the alleatory as well the epistemic uncertainties that respectively would describe the random nature of the parameters as well as our ability to model the response of the structure even when all the input parameters are exactly defined.
- A reliability analysis is performed and the reliability indices are calculated for a representative samples of bridge configurations that satisfy current code design criteria deemed to produce satisfactory performance. The calculation is based on statistical information about the randomness of the strength and stiffness of members, the statistics of load intensities and time histories, and their effects on the structures.
- In general, there will be considerable scatter in such computed reliability indices. If the existing code is believed to provide an average satisfactory performance, a target $\beta$ can then be directly extracted. This is done by examining the performance of a selected representative sample of bridges and averaging their $\beta$ values.
- For the development of new design codes, load and resistance factors as well as nominal design loads and return periods are selected by trial and error to

satisfy the target β as closely as possible for the whole range of applications including different bridge sites, geometries, dimensions and configurations.

To execute the calculation of the reliability index, one needs to obtain the statistical data for all the random variables that affect the safety margin Z of Equation 2.3 including all the uncertainties in estimating the variables that describe the member resistances and the load effects.

Although, this reliability methodology has been successfully applied for calibrating design codes for gravity loads, most bridge seismic design specifications have concentrated on identifying the seismic hazards while ignoring the uncertainties associated with the other parameters that are critical for ensuring that the code provides a uniform and balanced level of risk for all the regions of the U.S. The sections that follow will review models that can be used for evaluating the reliability of bridge columns subjected to seismic input and will propose a method to use these models to calibrate response modification factors that will provide a uniform level of risk taking into consideration the seismic hazard as well as the uncertainties associated with estimating the damage of bridge columns subjected to earthquake input

## 4.4 RESPONSE MODIFICATION FACTOR

### 4.4.1 Definition

The purpose of seismic design is to allow a structure to sustain a given ground motion so that the corresponding ductility response is smaller than the structure's ductility capacity. Therefore, an estimation of the lateral strength is needed during the design

process in order to limit the displacement demand at that strength level to a certain pre-determined value.

Under a given ground motion, the inelastic deformation experienced by a system is typically expressed in term of the ductility ratio μ, which is defined as the ratio of the maximum displacement to the yield displacement, $u_y$:

$$\mu = \frac{\max|u(t)|}{u_y} \tag{4.1}$$

For a single degree of freedom system, the time history of the displacement u(t), is obtained by solving the following differential equation:

$$m\ddot{u}(t) + c\dot{u}(t) + F(t) = -m\ddot{u}_g(t) \tag{4.2}$$

Where m, c and F(t) are respectively the mass, damping coefficient and restoring force of the system. $u(t)$ and $\ddot{u}_g(t)$ are the relative displacement of the system and the ground acceleration respectively as a function of time. According to Newmark and Hall(1973), the strength reduction factor is defined as the ratio of the elastic strength demand to the inelastic strength demand as shown in Figure 4.1.

$$R_\mu = \frac{F_y(\mu = 1)}{F_y(\mu = \mu_T)} \tag{4.3}$$

Where $F_y(\mu = 1)$ is the lateral yielding strength required to keep the system in the elastic range, and $F_y(\mu = \mu_T)$ is the lateral yielding strength required to maintain the displacement ductility demand μ,less than or equal to a ductility target $\mu_T$. The period of the system is given as:

$$T = 2\pi\left[\frac{m}{k}\right]^{1/2} = 2\pi\left[\frac{mu_y}{F_y}\right]^{1/2} \quad 4.4$$

Where m and k are respectively the mass and stiffness of the SDOF.

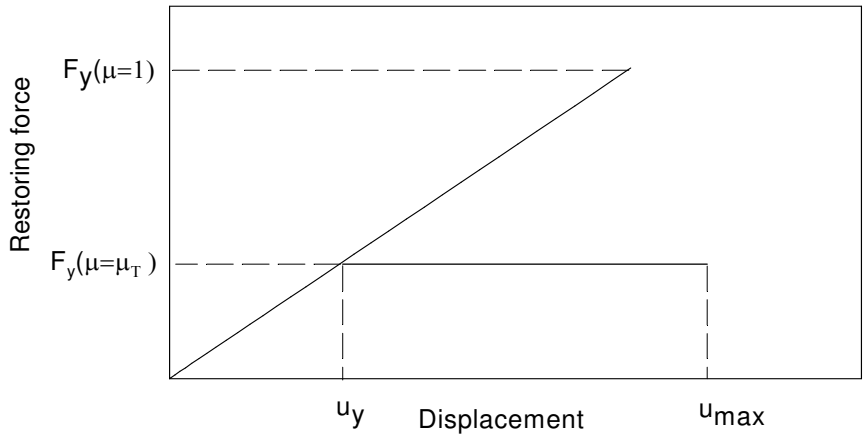


Figure 4.1 Idealized elastic strength and inelastic strength for ductility target $\mu_T$

### 4.4.2 Response Modification Factor in Seismic Design Provisions

It has been recognized that it is uneconomical to design bridges to sustain large earthquakes elastically. Therefore, the conventional ductile design approach was first introduced by Caltrans in 1973 as a consequence of the 1971 San Fernando earthquake. This design approach was nationally adopted after further refinement through the 1981 AASHTO Guide Specification for Seismic Design of Highway Bridges (ATC, 1981). These provisions were adopted by AASHTO in 1991 as their Standard Seismic Provisions. The design strength is obtained from an elastic analysis of the bridge using spectra for the appropriate earthquake design event. Component design strength such as column moment is obtained by dividing the demanded elastic moment by a Response Modification Factor specified based on the damage performance objectives. An $R_\mu$-Factor less than 1.5 is used for minor damage requirement where the bridge column is

expected to remain essentially elastic when it is subjected to an earthquake ground motion. For an $R_\mu$-Factor between 1.5 and 3, the bridge column will produce repairable damage, while if the $R_\mu$-Factor is higher than 3, the column may experience significant plastic hinging such that the induced damage may not be repairable. Based on this classification, AASHTO seismic specification requires $R_\mu$ values of 1.5, 2.0, and 3.0 for critical, essential and other structures respectively.

Recently, NCHRP 12-49 report recommended an approach to determine appropriate response modification factors. Friedland et al (2001) recommended the implementation of a relationship between $R_\mu$ and the structure period for the selection of the appropriate $R_\mu$-factors for bridge column design. This relationship was based on the work of Miranda & Bertero (1996), Nasser & Krawinkler(1991), and Chang & Mander(1994). The proposed simplified equation is a bilinear piecewise equation defined as:

$$R_\mu = 1 + (R_B - 1)\frac{T}{T^*} \le R_B \qquad 4.5$$

The values of $R_B$ and $T^*$ to be used in Equation 4.5 were proposed in NCHRP 12-49 report based on an evaluation of existing test data of structural components such as ductility capacity, axial load, and longitudinal and confinement reinforcement.

The approach proposed by Friedland(2001) still lacks a rational aspect that would account for uncertainties in seismic and material parameters. Indeed, the study of Mechakhchekh & Ghosn(2005) investigated the scatter of the $R_\mu$ factor and revealed that the use of average value is inappropriate due to the large variation in this factor that results from the random nature of earthquakes and the uncertainty in their prediction.

## 4.5 VARIABILITY IN RESPONSE MODIFICATION FACTOR

The use of the response modification factor, Rμ, in seismic design allows for performing a linear elastic analysis of a system and then proportioning the member for an ultimate capacity corresponding to the ratio of the required elastic capacity divided by Rμ. A recent study by Mechakhchekh & Ghosn (2005) investigated the scatter in the Rμ factor and revealed the presence of extremely large variations due to the random nature of the earthquake time histories even when the primary earthquake characteristics are accounted for. For example, typical results obtained for a set of earthquakes having similar magnitudes and epicentral distances are plotted in Figure 4.2. These observations lead to the conclusion that recent proposals to use the mean value of Rμ in design specifications may result in some bridges being overly designed while others will have high levels of risk. To reduce the level of risk, seismic design specifications have relied on using earthquake design spectra corresponding to high return periods, which currently are on the order of 500 to 2500 years. This approach of lumping all the safety factors into the use of long return periods is inconsistent with the LRFD methodology that requires that the safety factors be explicitly applied to each design parameter separately to reflect the uncertainties associated with estimating this particular parameter's variability and level of randomness.

Given the fundamental requirement of the LRFD methodology, it is herein proposed to use an alternative to the approach proposed in the NCHRP12-49 recommendations that lumped together all the safety factors by requiring very high return periods. Instead, it is recommended to calibrate safety factors that would be directly applied to the response modification factor. The safety factors to be applied on Rμ must reflect the variability in

the seismic response of typical bridge configurations and should be calibrated using a reliability analysis that accounts for both the seismic hazard and material variability.

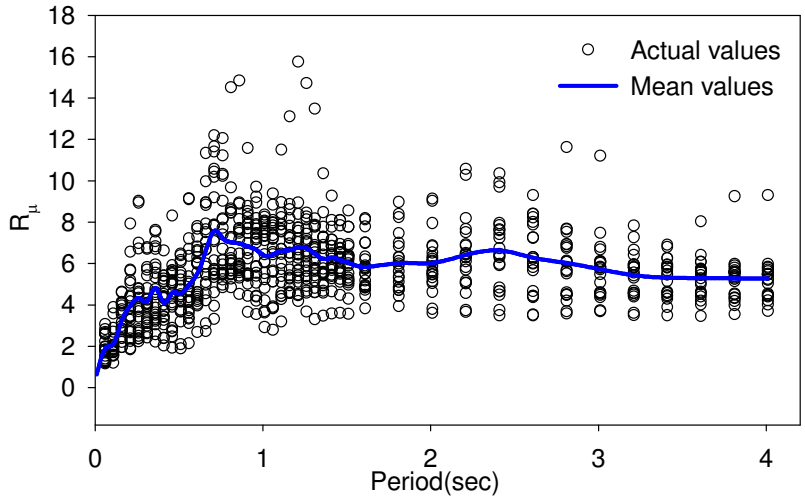


Figure 4.2. Typical large scatter in $R_\mu$ (A.Mechakhchekh & M. Ghosn 2005)

## 4.6 SEISMIC HAZARD ANALYSIS

Methods to perform a Probabilistic Seismic Hazard Analysis (PHSA) were first introduced by Cornell (1971), and refined by several other researchers since then (A. Mechakhchekh & M. Ghosn 2005). The main idea behind PSHA is to provide estimates of the strong ground motions expected to occur at a selected site from different sources. This approach implemented by USGS provides sets of earthquake magnitudes and epicentral distances for a specified site using as input the number of EQ occurrences in a period of time from different types of seismic sources, the epicentral distances of the earthquake sources to the specified site, R, and variations in moment magnitude, $M_w$. The effect of other random parameters related to the size and geometry of the rupture surface, stress drop, and slip variation are to a certain extent absorbed in the attenuation equations used during the analysis.

From the broad wide ranges of $M_w$ and R values of all possible earthquakes, a deaggregation technique is used to narrow the selection of ground motions for structural analysis purposes to a number of ($M_w$,R) pairs associated with different weights which are equal to their contributions to the total seismic hazard. These weights reflect the probability of occurrence of an earthquake of magnitude $M_w$ and source to site distance R that exceeds a prescribed ground motion amplitude. The flowchart of Figure 4.3 describes the process of potential seismic threat identification. Once the potential seismic threats are identified, the dominant modes along with their percentage contributions to the total hazard are exploited to produce ground motions that represent the seismic activity at each site. The sets of ground motions thus extracted can be used as input excitations that implicitly incorporate the variations in the moment magnitudes, epicenter distances, earthquake intensities, and the random nature of the ground motion history for each selected site. Following the probabilistic modeling of the seismic input at a site, the next step consists of developing a probabilistic model for estimating the response of bridge columns under seismic input. This could be achieved following the approach described in the next sections.

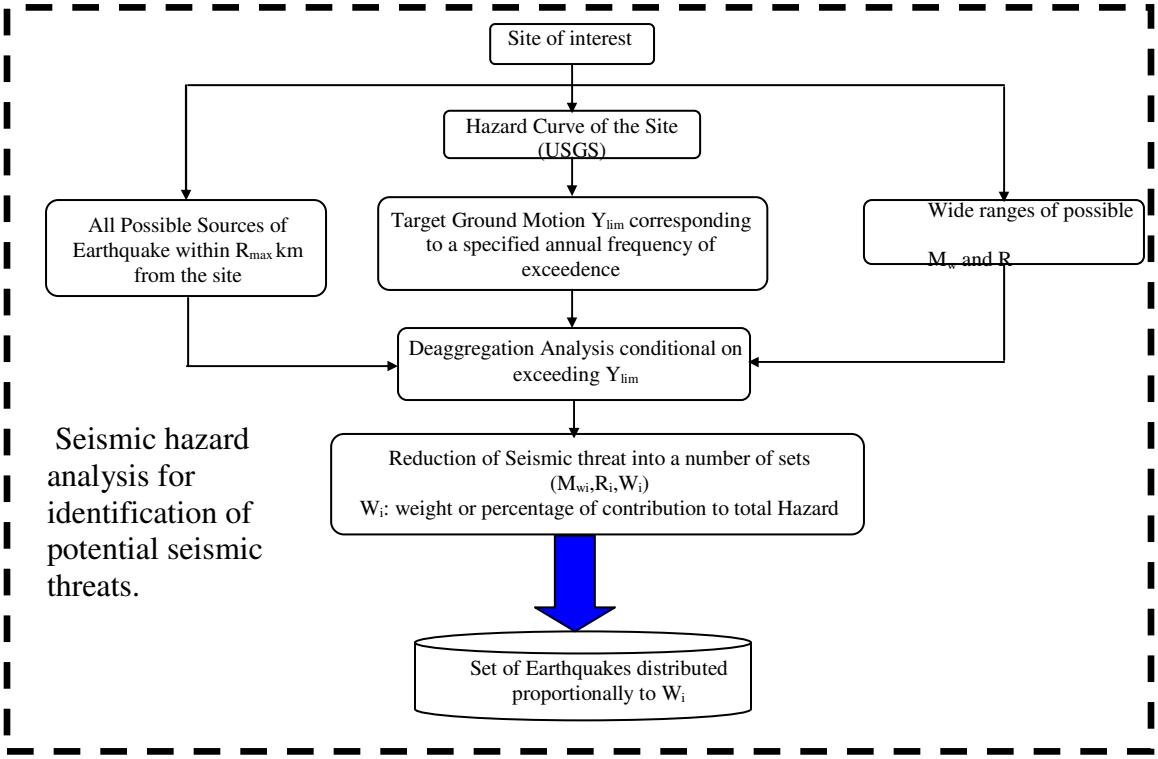


Figure 4.3 Flowchart for selection of earthquake records based on PSHA.

## 4.7 EFFECT OF CYCLIC LOADING

In order to establish the proposed reliability based calibration model for response modification factor, a limit state or performance function described in Chapter Two of this thesis needs to be defined. In the case of monotonic loading, the failure limit state can be defined based on the monotonic displacement ductility at the failure point when the loaded column collapses. However, this limit state measure cannot be applied when dealing with seismic loading because of the effect of cyclic loading effect on the column response. To better understand the cyclic loading effects, three actual columns tested under cyclic loading by different researchers are considered and their associated monotonic displacement ductility is estimated using a monotonic analysis developed by the Author (see Appendix A).

These columns are selected from the database available on the web site of the University of Washington (http://www.ce.washington.edu/~peera1). The Web page provides valuable information about the cyclic loading of reinforced concrete columns tested by different researchers. It includes each column's material properties, its geometry and reinforcement details. The web page also provides the test results including the failure mode, force-deflection histories, axial loads and the observed damage.

The first two columns considered in this study were tested by Lehman & Moehle (1998). The column specimens **815** and **1015** having the same circular cross section with 2 ft in diameter are 16 ft and 20 ft in height respectively. Both columns were subjected to the same constant axial force of 654 kN applied at the top of the specimens. The third column is a full-scale flexure specimen tested by Cheok et al (1986) for the National Institute of Standards and Technology (NIST). This specimen of 5 ft cross sectional diameter and 30 ft height was subjected to a constant axial force of 4450 kN. Table 4.1 provides additional information about these three columns.

Table 4.1 Geometries of columns

| **Column** | Length(ft) | Diameter(ft) | Concrete Cover(in) | $f_c^{'}$ (Mpa) at 28 days | Axial Force P(kN) | $\frac{P}{A_g \cdot f_c^{'}}$ |
|---|---|---|---|---|---|---|
| **Lehman Spec 815** | 16 | 2 | 22.3 | 31 | 654 | 0.07 |
| **Lehman Spec 1015** | 20 | 2 | 22.3 | 31 | 654 | 0.07 |
| **NIST(1986)** | 30 | 5 | 58.70 | 35.80 | 4450 | 0.07 |

Specimens 815 and 1015 were reinforced in the longitudinal direction by twenty-two No. 14 bars. In the transverse direction, these two columns were reinforced with a spiral size No. 2 spaced at 1.25". The NIST specimen was reinforced with 25 bars of 43 mm

diameter and transverse spiral reinforcement spaced at 89 mm. Table 4.2 summarizes the reinforcement properties for the three columns.

Table 4.2 Reinforcement properties of the columns

| | **Longitudinal reinforcement** | | | | **Transverse reinforcement** | | | |
|---|---|---|---|---|---|---|---|---|
| **Columns** | $\rho_l$ | D(mm) | # bars | $f_y$(Mpa) | $\rho_v$ | D(mm) | S(mm) | $f_y$(Mpa) |
| **Lehman Spec 815** | 1.49% | 15.875 | 22 | 462 | 0.70% | 6.4 | 31.75 | 606.76 |
| **Lehman Spec 1015** | 1.49% | 15.875 | 22 | 462 | 0.70% | 6.4 | 31.75 | 606.76 |
| **NIST(1986)** | 2% | 43 | 25 | 475 | 0.63% | 15.9 | 89 | 493 |

Results of the monotonic analyses of these three columns are graphed in Figures 4.4, 4.5, and 4.6 with the actual cyclic force displacement curves obtained from the experiments. The axial effects known as the P-Δ effects are subtracted from the monotonic forces. Therefore, the restoring force will account only for the horizontally applied force.

To assess the ultimate monotonic displacement, a failure limit state is needed at this stage. Kowalsky (2000) defined a damage control limit state when the concrete compression strain reaches 0.018 and the damage is assumed to be repairable. This assessment is a function of the transverse reinforcement details. The energy balance method developed by Mander (1988) can be utilized to estimate the maximum compression strain of the confined concrete. The comparison of this ultimate strain with the actual experimental results shows that this method can be more than 50% conservative (Priestley el al 1996). Thus, this study will adopt a failure limit state corresponding to an ultimate compression strain of 0.027, which is consistent with actual experimental observations reported by Priestley et al (1996).

The yield displacement that corresponds to the yield of the first longitudinal bars is generally low and doesn't lead to a curve consistent with the bilinear Takeda model used in the nonlinear dynamic analysis. This issue was well discussed by Zahn, Park and Priestly (1986) when defining the yield displacement for the experimental curve. In this study, the monotonic curve is first approximated by a bilinear curve with a post yielding stiffness ratio to the initial stiffness of 3%, where the initial stiffness is calculated for the cracked section. The yield displacement is the displacement measured at the intersection of the two portions.

Once the yield and the maximum monotonic displacements are identified, the monotonic displacement ductility can be calculated as the ratio of the maximum to the yielding displacements. Table 4.3 summarizes the results of the monotonic and cyclic loading of the three columns considered in this study.

Table 4.3 Yielding and maximum displacements and displacement ductility

| **Columns** | Yielding displacement | Max. displacement | | Displacement ductility | |
|---|---|---|---|---|---|
| | | Monotonic | Cyclic test | Monotonic | Cyclic test |
| **Lehman Spec 815** | 78.5mm | 635mm | 446mm | 8.09 | 5.68 |
| **Lehman Spec 1015** | 110mm | 955mm | 636mm | 8.68 | 5.78 |
| **NIST(1986)** | 93.8mm | 746mm | 593mm | 7.95 | 6.32 |

Results of Table 4.3 show that the monotonic displacement ductilities of Lehman specimens 815, 1015, and the NIST specimen are respectively 8.09, 8.68, 7.95. For the same specimens, cyclic displacement ductilities extracted from the testing data indicate values of 5.68, 5.78, and 6.32. This simple comparison yields the conclusion that the cyclic displacement ductility is considerably lower than that produced by the monotonic loading. Therefore, the use of monotonic displacement ductility as a failure limit state

will certainly over estimate the column capacity. Many studies such as Park & Ang (1985) suggested that the difference in displacement ductility is due to energy dissipation under cyclic loading. The calibration of this energy based on a large number of test data showed that it is proportionally equal to the area under the hysteresis loops of the load displacement curve (Park & Ang; 1985). These observations led Ang & Park(1985) to propose a damage model that incorporates the dissipated energy into a damage index as a measure of damage and to define the failure limit state.

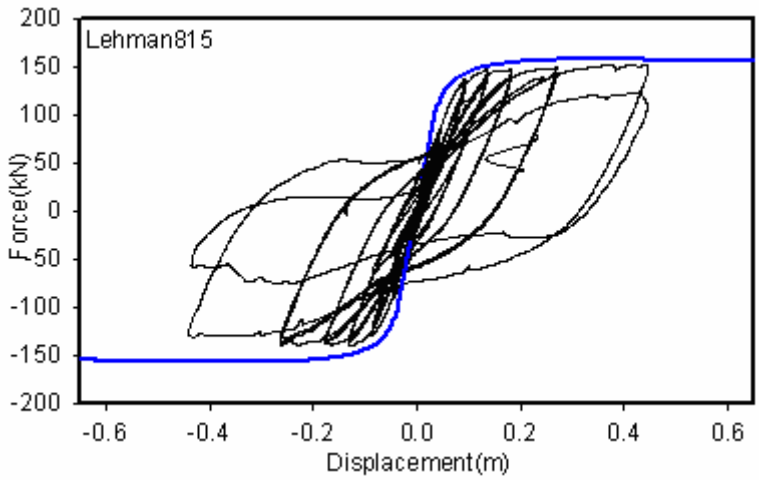


Figure 4.4 Monotonic and Cyclic loading results of the specimen 815(Lehmen 1998)

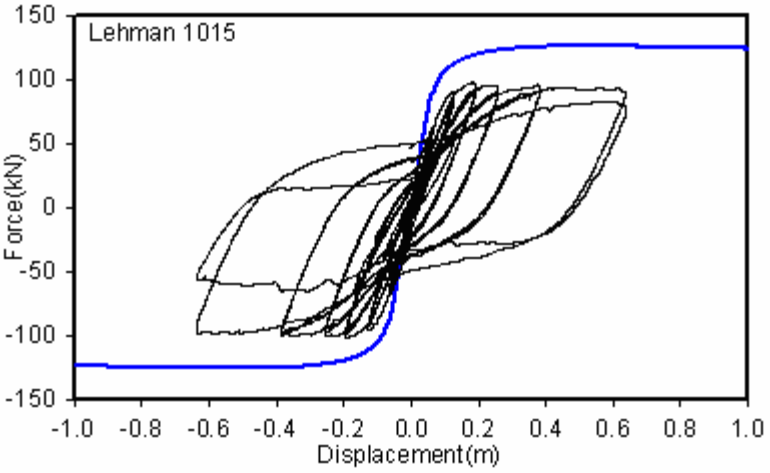


Figure 4.5 Monotonic and Cyclic loading results of the specimen 1015 (Lehmen 1998)

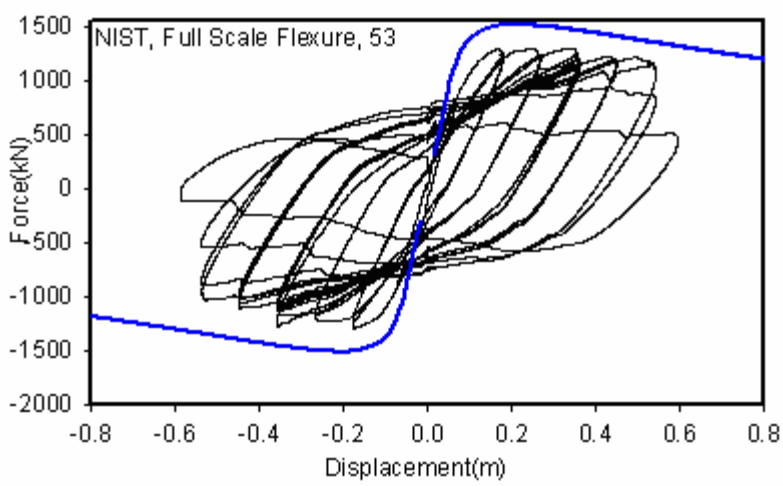


Figure 4.6 Monotonic and Cyclic loading results of the NIST specimen ( Cheok 1998)

## 4.8 PARK & ANG DAMAGE MODEL

Park & Ang (1985) proposed a model for evaluating the structural damage induced by the dynamic loading of reinforced concrete members. This model is expressed as a linear combination of the damage caused by plastic deformations and the dissipated energy enclosed under the cyclic loops of the load deformation curve. This is represented in terms of a damage index by the following expression:

$$DI = \frac{1}{\mu_{mon}}\left(\mu + En\right) \quad ; \quad E_n = \beta_{DI}\frac{\int dE}{F_y.u_y} \qquad 4.6$$

where μ is the displacement ductility under dynamic loading. $\mu_{mon}$ is the displacement ductility under monotonic loading. $F_y$ and $u_y$ are the yielding strength and displacement respectively. $dE$ is the hysteretic energy which is equal to the area under the force-displacement loops. $\beta_{DI}$ is a factor that account for the percentage contribution of the hysteretic energy to total damage. Park & Ang (1985) found that columns that collapsed under dynamic loading have on the average a mean damage index value equal to 1.00 and

a standard deviation of 0.535. However, when evaluating the variation of failure damage index $DI_{lim}$ of a large number of reinforced concrete columns, Park & Ang implicitly lumped the uncertainties associated with the monotonic ductility $\mu_{mon}$ and the energy coefficient $\beta_{DI}$ into the variation in $DI_{lim}$. Therefore, values of $\mu_{mon}$ and $\beta_{DI}$ used in the estimation of the damage index are the mean values proposed by Park & Ang(1985) and given by the following equations:

$$\mu_{mon} = \left(\frac{\varepsilon_p}{\varepsilon_o}\right)^{0.218\rho_w - 2.15} Exp[0.654\rho_w + 0.38] \quad 4.7$$

$$\beta_{DI} = 0.7^{\rho_w}.\left[-0.447 + 0.073\frac{l}{d} + 0.24n_o + 0.314\rho_t\right] \quad 4.8$$

Where $\rho_w$ represents the confinement ratio with maximum value of 2% if it is larger than 2%. $\varepsilon_p$ is the principal strain of the extreme compression bar at yielding of the first bar in tension and $\varepsilon_o$ is the strain at ultimate stress of the concrete. l/d is the span ratio and $n_o = N/(f_c^{'}A_g)$ is the axial force, $N$ divided by the concrete strength, $f_c^{'}$, and the gross area, $A_g$.

Park & Ang Damage Index of a bridge column subjected to seismic loading is evaluated after the completion of a nonlinear dynamic analysis of the column assumed as a single degree of freedom system. This analysis requires the column yield strength and the initial stiffness in addition to the hysteresis model. These properties are certainly sources of uncertainties that have to be identified and introduced to the reliability based-calibration model. Sections 9 and 10 of this chapter are devoted to identify these uncertainties.

## 4.9 MATERIAL UNCERTAINTIES IN R-C BRIDGE COLUMNS

### 4.9.1 Uncertainties in estimating initial stiffness

The uncertainties in estimating the initial stiffness of a column are primarily due to the randomness in material properties and boundary conditions that are usually assumed as perfectly fixed or free ignoring possible partial rotations. To investigate the statistical properties of the stiffness, this study compares the ratio of the actual stiffness to the estimated stiffness obtained based on the gross column area for about 60 cantilever circular columns extracted from the database of the University of Washington (http://www.ce.washington.edu/~peera1). The stiffness of cantilever column is estimated by the following:

$$k_{estimated} = 3\frac{E_c.I_g}{L^3} \tag{4.9}$$

Where $E_c(MPa)$ is the concrete elastic modulus calculated in terms of concrete strength $f_c^{'}$ by $4700\sqrt{f_c^{'}(MPa)}$. $I_g$ and $L$ are the moment of inertia of the gross section and column length respectively. On the other hand, the extraction of the actual stiffness $k_{actual}$ from data of cyclic loading necessitates first the identification of the onset of the yield point. This point corresponds to the yield of the first longitudinal bar and is determined by monotonic analysis of the column in question. By means of linear regression involving all experiments data points prior to the onset of the identified yield point, the slope which represents the actual stiffness is then extracted. Since the considered columns represent a population with different geometric and reinforcement properties, their effects on the ratio of the actual to the estimated stiffnesses is inspected

and found to be partially correlated to the transverse steel ratio, span ratio, and the axial force ratio. Thus, the variations observed in this ratio are a function of transverse steel ratio $\rho_w$ in percentage, span ratio *L/d*, and axial force ratio $n_o$ in percentage and expressed by the following equation:

$$\frac{k_{actual}}{k_{estimated}} = \chi_k + \left(0.071 + 0.00703.n_o + 0.0973.\rho_w + 0.0372.\frac{L}{d}\right) \qquad 4.10$$

As illustrated in Figure 4.7, the random variable $\chi_k$ is found to be normally distributed with a mean value of 0 and a standard deviation of 0.0977. It is worth mentioning that the effect of the longitudinal steel ratio on the stiffness is negligible. The mean ratio of Equation 4.10 predicts the stiffness ratio with relatively uniform scatter as shown in Figure 4.8. These conclusions are valid for axial ratio between 0 and 42%, transverse steel ratio ranging from 0 to 6% although most data are below 2%, and span ratio between 1.5 and 10. The actual design features of typical bridge columns and limitations as proposed by design code specifications fall within the range of the data. Priestley & al (1996) and many other researchers suggested the use of $0.5E_c.I_g$ as effective section stiffness to account for the concrete cracking which is found to be conservative for most practical cases compared to the proposed estimator of Equation 4.10. Indeed, for $n_o$=15%, $\rho_w$=2%, and span ratio of 7, Equation 4.10 yields a ration of 0.63 which is higher than the 0.5 as proposed by Priestley & al (1996). It is worth noting that the proposed statistical model for stiffness ratio can also be applied for rectangular columns or for columns with end fixity other than cantilever assuming that the estimating stiffness model contains the same level and type of error and the randomness in the material properties and the fixity modeling are the same.

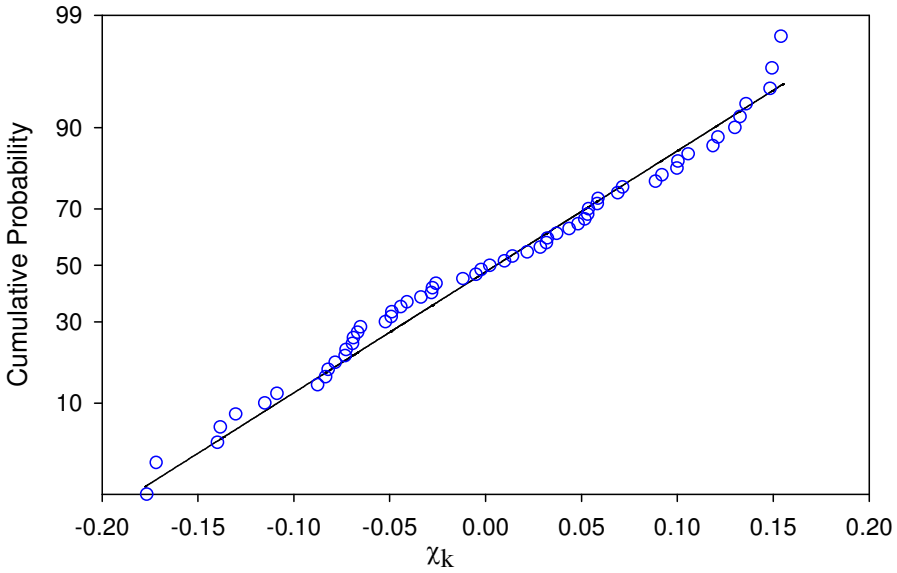


Figure 4.7. Normal probability paper test for $\chi_k$

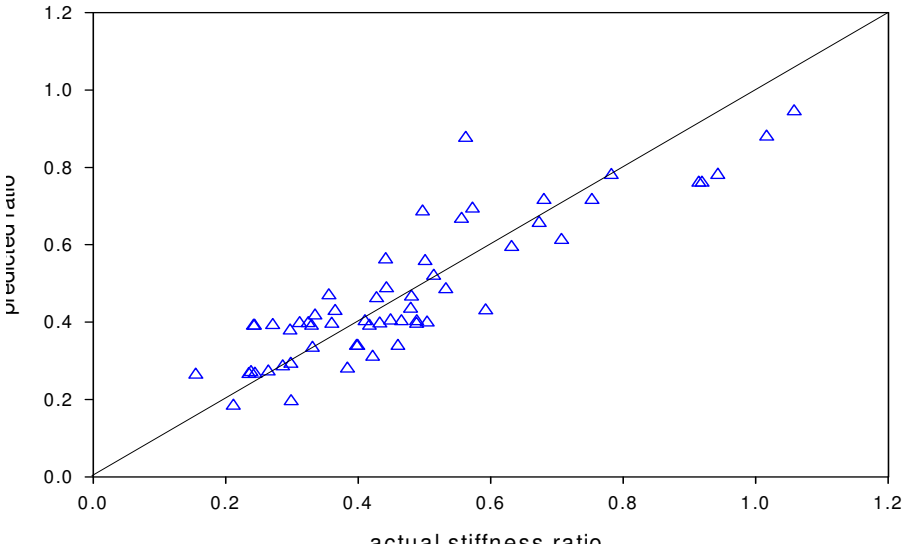


Figure 4.8. Scatter of the actual stiffness ratio to mean predicted value by Equation 4.10

### 4.9.2 Uncertainties in estimating column strength

The uncertainties associated with the estimation of the ultimate strength of reinforced concrete columns can be attributed to the randomness in material properties and the error introduced by model used to estimate the column strength. The estimation of the ultimate strength is obtained from the monotonic analysis performed on each column using the constitutive material law of both concrete and steel. A full description of the analysis is

detailed in Appendix A. The ratio of the actual strength over the estimated strength is calculated for 86 circular reinforced concrete columns as a function of the axial force ratio, $n_o$ as expressed in the following equation:

$$\frac{F_{actual}}{F_{estimated}} = \chi_F .(-0.0048.n_o + 1.0259) \qquad 4.11$$

The normal probability paper test illustrated in Figure 4.9 shows that the random variable $\chi_F$ is normally distributed with mean value of 1 and standard deviation of 0.116.

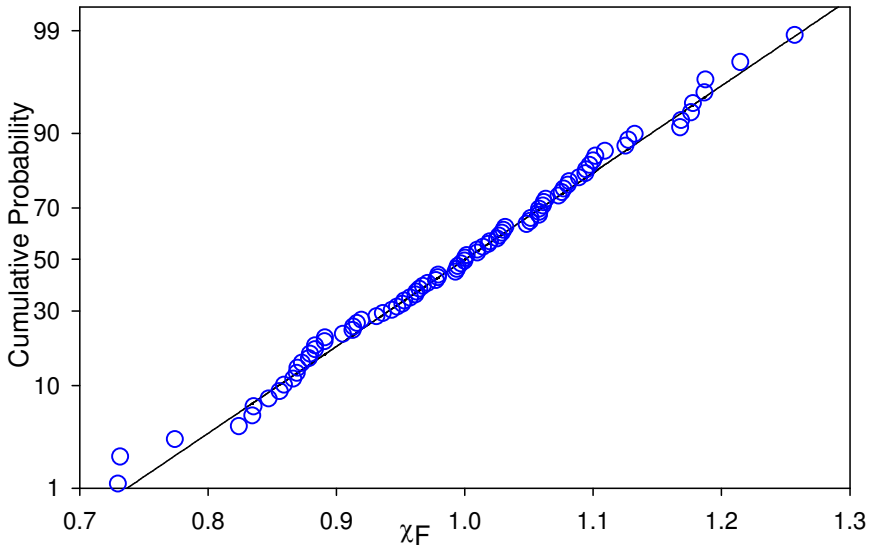


Figure 4.9. Normal probability paper plot for $\chi_F$

## 4.10 UNCERTAINTIES IN HYSTERESIS MODEL

### 4.10.1 Takeda Model

The calculation of the dissipated energy under a given earthquake record requires the execution of a hysteretic analysis that would properly account for the degradation of the stiffness and strength as well as account for pinching behavior. In this study, the Takeda model (Takeda(1970)) for reinforced concrete bridge columns is used to describe the

dynamic behavior because of its simplicity and acceptable level of accuracy. The model illustrated in Figure 4.10 is governed by the following rules:

Rule 1: Before experiencing any inelastic deformations, the initial stiffness is always equal to $k_o$.

Rule 2: In the plastic region the stiffness is equal to $r.k_o$

Rule 3: During the unloading phase, the degraded stiffness is given by:

$$K_{un} = K_o \left( \frac{X_Y}{X_{\max}} \right)^{\alpha} \tag{4.12}$$

where $X_y$ and $X_{max}$ are the yielding and maximum displacements.

Rule 4: In the reloading phase, the load displacement curve heads to the point ($X_j$, $F_j$) defined as:

$$X_j = X_{\max} - \beta_H . X_p \tag{4.13a}$$

$$F_j = k_o X_y + r.k_o .(X_j - X_y) \tag{4.13b}$$

where $X_p$ is the total plastic displacement as defined in Figure 4.10 and $\alpha$ and $\beta_H$ are characteristics of the structure hysteresis.

Determination of Takeda model parameters namely $\alpha$, $\beta_H$, and r as well as their uncertainties are also incorporated in reliability based model calibration. Their probability distributions are obtained in the next section of this chapter based on experimental data.

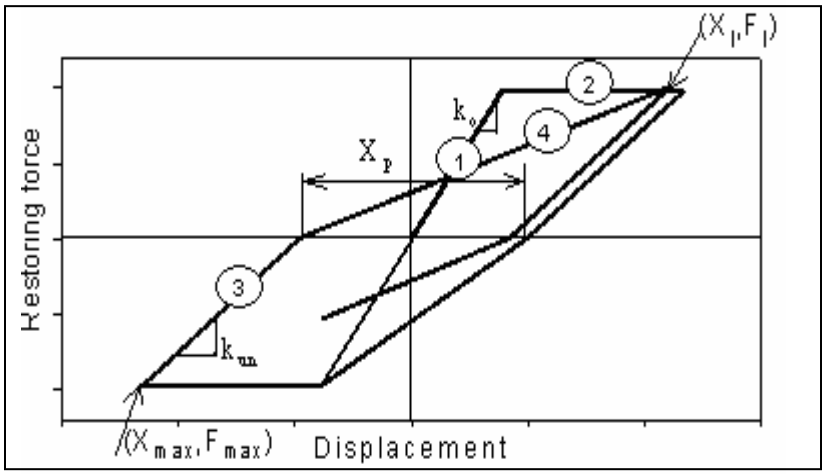


Figure 4.10. Takeda hysteresis model for reinforced concrete columns

### 4.10.2 Uncertainties in Takeda model parameters

Takeda model parameters that control the rate of strength degradation under cyclic loading may highly differ from column to column depending on each column's material and geometric properties given a loading path. Parameters that provide best behavior modeling of columns are not currently available. Many researchers have recommended values for these parameters that generally yield conservative results applicable for design. A first attempt is made herein to define the scale of scatter of these parameters by using an optimization technique based on minimizing the square of the error between the estimated and the measured response. The approach is illustrated in Figure 4.11.

For this purpose, we extract load-displacement histories for twenty reinforced concrete columns tested by previous researchers. The data was assembled from the database of the University of Washington (http://www.ce.washington.edu/~peera1). By means of an optimization technique, the parameters $\alpha$, $\beta_H$, and r, of the Takeda model that provide the best fit for each column's test results are identified. It was observed that Takeda's

model with the optimized parameters traces with reasonable accuracy the hysteretic behavior of the reinforced concrete columns as shown in Figure 4.12 for one of these columns. The optimized parameters are listed in Table 4.4 for each column along with their means, standard deviations, and coefficients of variation. The three parameters are found to follow normal distributions when plotted on normal probability paper as illustrated in Figures 4.13, 4.14, and 4.15 with mean values of 0.26, 0.49, and 0.02 and standard deviations of 0.13, 0.15, and 0.02 for $\alpha$, $\beta_H$, and r respectively.

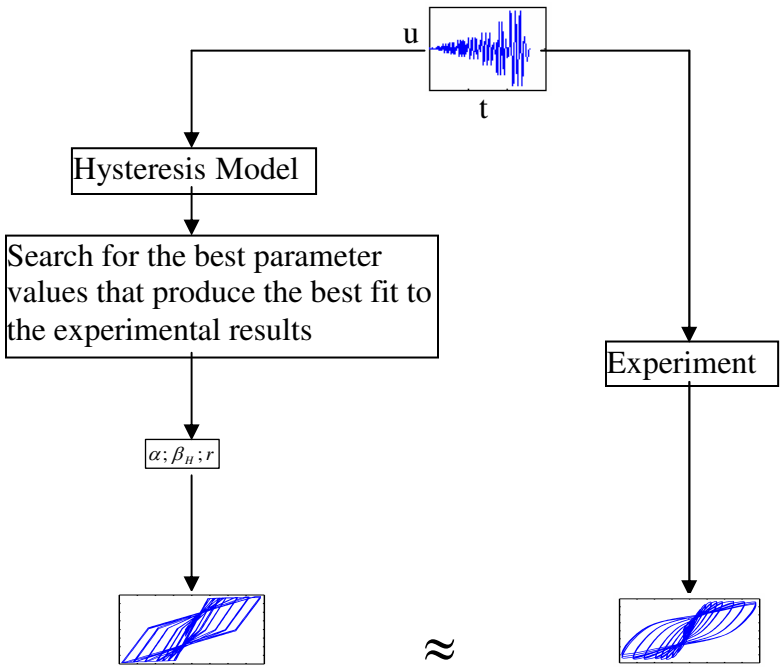


Figure 4.11 Identification problem for hysteretic models

Table 4.4 Result of parameters identification of Takeda model

| **Columns** | **$\alpha$** | **$\beta_H$** | **r** |
|---|---|---|---|
| Ang et al. 1981, No. 1 | 0.25 | 0.59 | 0.005 |
| Davey 1975, No. 2 | 0.55 | 0.29 | -0.051 |
| Hamilton 2002, UCI-2 | 0.02 | 0.78 | 0.056 |
| Hamilton 2002, UCI-1 | 0.22 | 0.4 | 0.03 |
| Kowalsky & Moyer, | 0.19 | 0.65 | -0.011 |
| Kunnath et al. 1997, A2 | 0.25 | 0.53 | 0.021 |
| Calderone et al. 2000, 328 | 0.21 | 0.27 | 0.017 |
| Calderone et al. | 0.15 | 0.59 | 0.051 |
| Calderone et al. 2000, 828 | 0.05 | 0.27 | 0.031 |
| Lehman et al. 1998, 430 | 0.24 | 0.48 | 0.024 |
| Munro et al. 1976, No. 1 | 0.08 | 0.76 | 0.024 |
| Potangaroa et al. 1979, | 0.31 | 0.47 | 0.019 |
| Potangaroa et al. 1979, | 0.4 | 0.40 | 0.028 |
| Potangaroa et al. 1979, | 0.4 | 0.34 | 0.02 |
| Saatcioglu & Baingo | 0.31 | 0.47 | 0.031 |
| Soderstrom 2001,C2 | 0.34 | 0.48 | 0.006 |
| Vu et al. 1998, NH1 | 0.47 | 0.37 | 0.021 |
| Vu et al. 1998, NH3 | 0.31 | 0.47 | 0.037 |
| Vu et al. 1998, NH4 | 0.27 | 0.57 | 0.039 |
| Vu et al. 1998, NH6 | 0.26 | 0.52 | 0.034 |
| **Mean** | **0.26** | **0.49** | **0.02** |
| **Standard Deviation** | **0.13** | **0.15** | **0.02** |

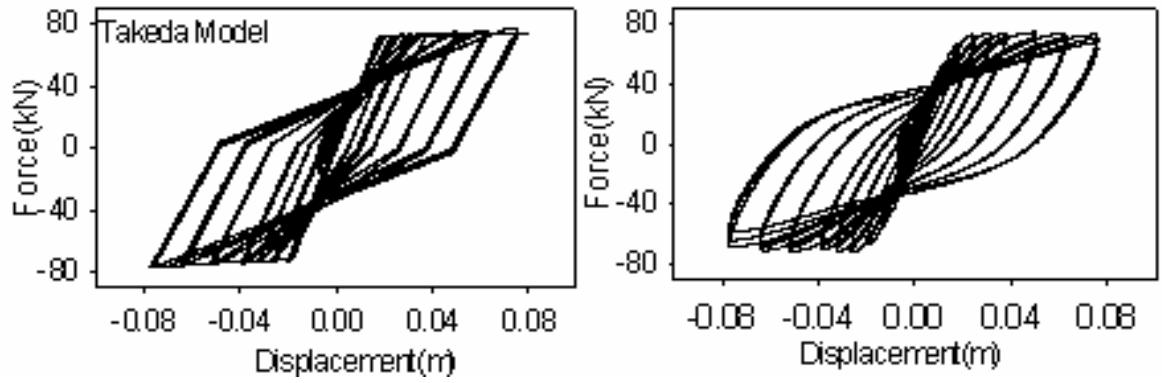


Figure 4.12 Model and experimental hysteresis for specimen A2 (Kunnath 1997)

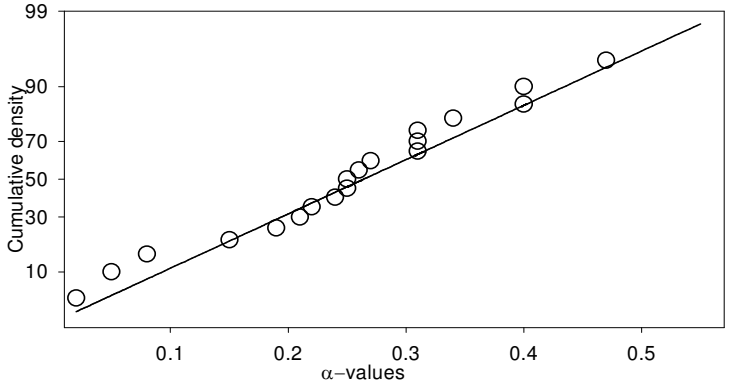


Figure 4.13 Normal distribution plot for α−values

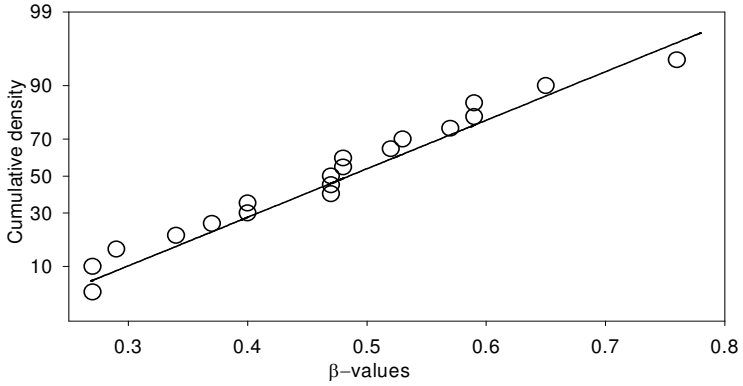


Figure 4.14 Normal distribution plot for $\beta_H$−values

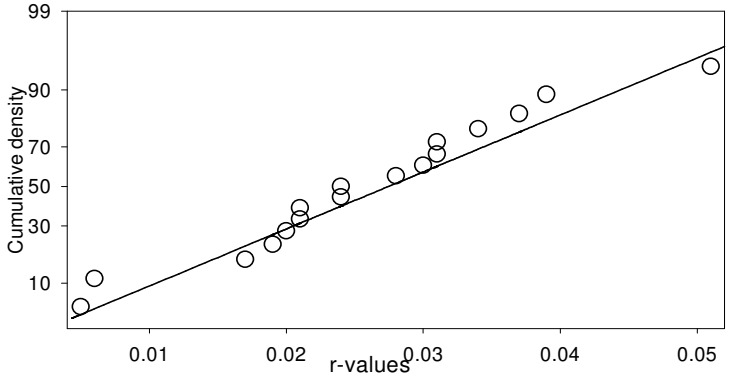


Figure 4.15 Normal distribution plot for r-values

Up to this point of the reliability based calibration model for the Response Modification Factor, the randomness in seismic inputs are discussed in section 4.6 of this chapter. The set of earthquake excitations generated based on the seismic hazard analysis results will include the uncertainties in moment magnitude $M_w$, epicentral distance R, and

record to record variations. On the other hand, the uncertainties related to material randomness as well as the modeling errors are established and identified in sections 4.9 and 4.10 of this chapter. The next sections will detail the methodology of the proposed model that combines the prescribed uncertainties to estimate the probability of failure in conjunction with the Radial Sampling method developed in Chapter 3 of this thesis.

## 4.11 RELIABILITY ANALYSIS METHODOLOGY

The estimation of the failure probability for reinforced concrete bridge columns taking into consideration the seismic uncertainties, material variability, as well as the modeling uncertainties was performed using an advanced reliability simulation procedure known as the Radial Sampling method which is based on the line sampling method of Shueller (2004) detailed in Chapter 3. In this reliability analysis, the failure of a bridge column is assumed to occur when the damage index DI(X) which is calculated in function of the column's material properties and seismic input exceeds an acceptable damage limit $DI_{lim}$. Thus, the limit state function is defined as:

$$Z(X) = DI_{lim} - DI(X) \qquad 4.14$$

where X is a vector that represents the random variables $X_i$ that control the response of the column and the variability in the seismic input. Based on the work of Park & Ang (1985), $DI_{lim}$ is a random variable that follows a lognormal distribution with a coefficient of variation equal to 0.53 (Park & Ang 1985). Its mean value is equal 0.5 for a limit state corresponding to avoiding damage beyond repair (Kunnath et al 1997) and the mean is 1.0 if the limit state consists of avoiding column collapse (Park & Ang 1985).

Since a closed form expression for Equation 4.14 is not available, the calculation of the reliability index, β, and the probability of failure are executed using the Radial Sampling method in conjunction with a nonlinear dynamic analysis based on step-by-step integration method (Clough & Penzien (1975). The reliability analysis is performed separately for each earthquake mode or ($M_w$, R) pair identified earlier in the seismic hazard analysis. The reliability analysis determines the corresponding probability of failure $P_{fi}$ for the collapse limit state and damage beyond repair limit state.

The unconditional probability of failure, $P_f$ is calculated assuming a Poisson probability model for the occurrence of an earthquake *P(EQ)* during an exposure or design period, T, so that:

$$P_f = P(EQ) \times \frac{\sum_{i=1}^{Nm} w_i P_{fi}}{\sum_{i=1}^{Nm} w_i} \quad ; \quad P(EQ) = \int_0^{\infty} \left[1 - \exp(-\nu.T)\right] . f_{\nu}(\nu) . d\nu \qquad 4.15$$

where $N_m$ and $w_i$ are respectively the total number of ($M_W$, R) pairs and the corresponding percentage contribution of each pair to the total hazard. $\nu$ is the rate of earthquake occurrences for the ($M_w$, R) pairs that are considered in the reliability analysis. This rate $\nu$ is assumed to be a random variable that follows a lognormal distribution with a probability density function $f_{\nu}(\nu)$. The log standard deviation of the rate $\nu$ is estimated to be 0.5 for a San Francisco site (Jalayer & Cornell; 2003).

The probability of failure $P_{fi}$ associated with each earthquake mode ,i, is estimated from the radial sampling procedure which requires the identification of the most important random variable which is the Peak Ground Acceleration, PGA, that is used during the deaggregation analysis to select the ($M_W$,R) pairs. This PGA is lognormally

distributed and the probability that it will exceed the cut-off value $Y_{lim}$, can be calculated given that its log mean and standard deviation for the San Francisco area are given by Boore-Joyner model(1993) for firm rock sites as:

$$\log_{10}(PGA) = b_1 + b_2.(M_w - 6) + b_3.(M_w - 6)^2 + b_4.\sqrt{R^2 + h^2} + b_5.\log_{10}(\sqrt{R^2 + h^2})$$
$$\sigma_{\log_{10}} = 0.23$$

4.16

The subspace that is perpendicular to the specified important direction PGA includes all the random variables identified earlier which represent the material variability, seismic uncertainties, and modeling uncertainties.

## 4.12 CALIBRATION OF NOMINAL RESPONSE MODIFICATION FACTORS FOR DESIGN

The algorithm used to obtain an appropriate set of Response Modification Factors based on a reliability calibration is described in the flowchart of Figure 4.16. The algorithm follows the classical approach for reliability-based calibrations of structural design codes as described in Section 4.3 of this Paper. The process begins by analyzing a number of bridges whose columns have shown adequate levels of performance under previous earthquakes. A number of representative sites are selected and typical bridge columns are designed to satisfy current criteria for each site using the Response Modification factors specified in current codes. The PSHA is executed to create a set of N representative earthquake records for each mode and for each site. The reliability indexes are calculated for all the bridge sites and bridge configurations selected for analysis. These reliability index values are compared to the target reliability index. If the reliability index calculated does not match the target value, a new set of response

modification factors will be tried and the process repeated until convergence. Thus, the final set of response modification factors will reflect the variations expected in the time histories for different regions of the U.S. due to the different nature of earthquake sources and characteristics. The application of the methodology described in this section using as input the models described in this paper is illustrated in the next section.

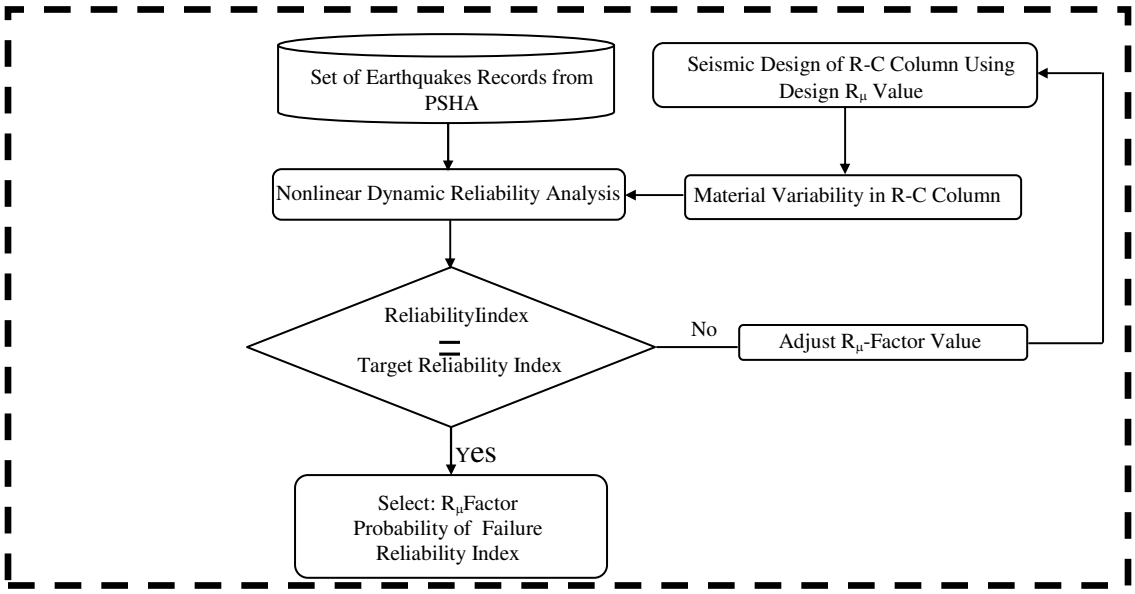


Figure 4.16 Reliability-based calibration of Response Modification factors

## 4.13 APPLICATION

### 4.13.1 Seismic Column Design

Most current design codes that use the force based design method require that the elastic strength of structural elements be determined from spectral acceleration hazard curves. The hazard corresponding to a specified value of the ground motion intensity is defined as the probability that the intensity of future ground motion events will be greater or equal to this specified value. These curves are available on the USGS web site, which provides the mean annual frequency of exceeding a particular spectral acceleration for a

given period and damping ratio. The structural designer must decide based on code requirements or owner recommendations how much seismic risk can be tolerated. For example, Figure 4.17 shows the Hazard curve for the San Francisco area obtained for a natural period of 1.0 sec and a damping ratio of 5%. Specifically, the corresponding spectral acceleration for an annual mean frequency of exceedance equal to 1/2475 (2% PE in 50 years) is 1.4508g for a period of 1.0 sec in the San Francisco area ($37^o$46'N,$122^o$26'W). For the same spot and the same period, the annual mean frequency of exceeding a spectral acceleration of 0.6911g is 1/475 (10% PE in 50 years).

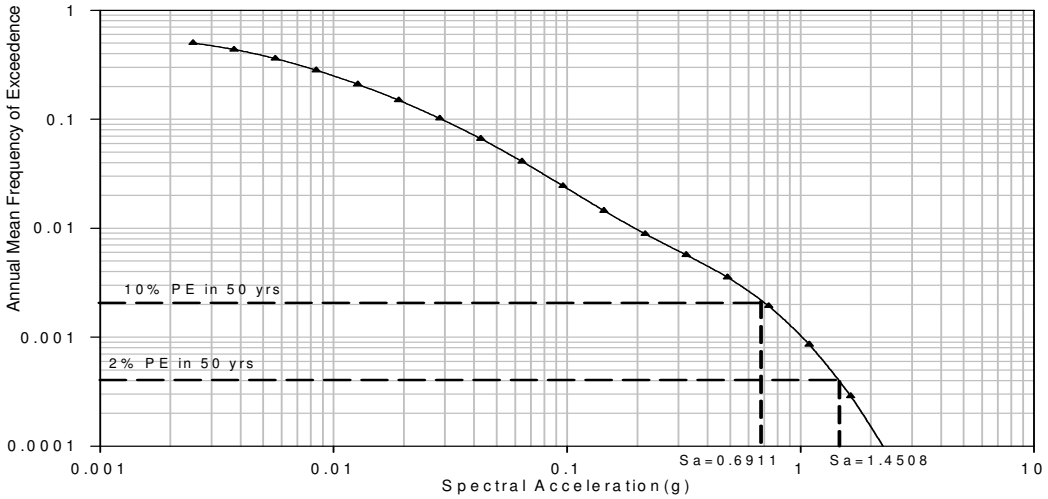


Figure 4.17 SA hazard curve for San Fransisco area ($37^o$46'N, $122^o$26'W.)

Assuming a bridge founded on bedrock is located in the San Francisco area at $37^o$46'N latitude and $122^o$26'W longitude, the design spectrum acceleration for a 2475-yr return period can be constructed following the procedure proposed by the National Earthquake Hazard Reduction Program (NEHRP) for firm rock sites as shown in Figure 4.18 for a 2475-year return period. The design spectral accelerations include the 2/3 adjustment factor that is specified for building design in the NEHRP specifications.

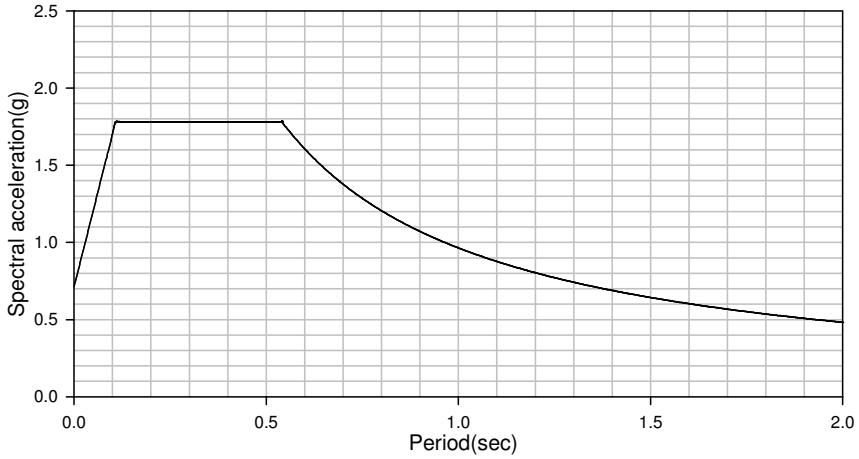


Figure 4.18 Design Spectrum for San Francisco (37°46'N,122°26'W).

Figure 4.18 is then used to determine the elastic strength requirements of several hypothetical columns having different natural periods ranging between 0.5, 1.0, and 2 sec. The nonlinear ultimate strength requirements are calculated by dividing the required elastic strength by the Response Modification Factor $R_\mu$. A wide range of $R_\mu$ values are used from which the appropriate values will be selected.

To illustrate the proposed procedure, a set of typical bridge columns are designed for a site in San Francisco at latitude of 37°46'N and a longitude of 122°26'W. The columns considered herein are assumed to have a span ratio *L/d*=7, transverse and longitudinal steel reinforcements of 1.2% and 2%, and axial load ratio of 15%. The strain factor $\varepsilon_p/\varepsilon_o$ is assumed to be 0.5 leading to an expected value for the monotonic ductility capacity of about $\mu_{mon}$=12 and a $\beta_{DI}$ = 0.10 calculated according to equations 4.7 and 4.8. The mass that is carried by the column is assumed to be normally distributed with a standard deviation of 0.10 (Nowak 1993).

### 4.13.2 Identification of Seismic Threat

The PSHA is performed to generate earthquake records that have spectral accelerations with a 20% probability of exceedence in 50years. This cut off is intended to cover all earthquake magnitudes that are likely to produce significant structural damage. A sample of the ($M_W$, R) pairs for these earthquakes are listed in Table 4.5 along with their percentage contributions to the total hazard.

Four hundred synthetic earthquake records are generated for each mode using the program SMSIM-version 2.3 developed by Boore (2002) and the input parameters of a single-corner frequency coastal California model (WR032496.dat (Frankel & al 1996)) to represent rock sites. The seismic inputs along with the material random properties are introduced into the nonlinear dynamic reliability analysis and the total probability of failure is calculated using Eq. 4.15.

Table 4.5: Summary of earthquake deaggregation at 20% PE in 50 years for San Francisco (damping ratio=5%)

| Modal Earthquakes | Distance (km) | Magnitude ($M_w$) | Contribution to total Hazard(%) |
|---|---|---|---|
| Mode # 1 | 3.4 | 7.84 | 32.883 |
| Mode # 2 | 3.2 | 7.98 | 15.13 |
| Mode # 3 | 3.3 | 7.44 | 12.167 |
| Mode # 4 | 3.3 | 7.26 | 7.742 |
| Mode # 5 | 3.7 | 7.05 | 4.852 |
| Mode # 6 | 3.3 | 7.69 | 4.232 |
| Mode #7 | 4.3 | 6.65 | 4.162 |
| Mode #8 | 4.5 | 6.84 | 2.704 |
| Mode #9 | 5 | 6.44 | 2.516 |
| Mode #10 | 17.6 | 7.26 | 1.44 |
| Mode#11 | 17.6 | 7.44 | 1.42 |
| Mode#12 | 6.6 | 6.2 | 0.945 |
| | | | Total Contribution 90.20% |

### 4.13.3 Reliability Analysis of Hypothetical R-C Bridge Column

As an example of the analysis results, Figure 4.19 and 4.20 illustrate respectively the probability of failure and the associated reliability index obtained for various values of the response modification factor, $R_\mu$ for columns having a natural period of 1sec and $\mu_{mon}$=12 and for a return period of 75 years. It is noted that the 75-year return period selected for this analysis is the expected design life of a bridge as specified in the AASHTO LRFD.

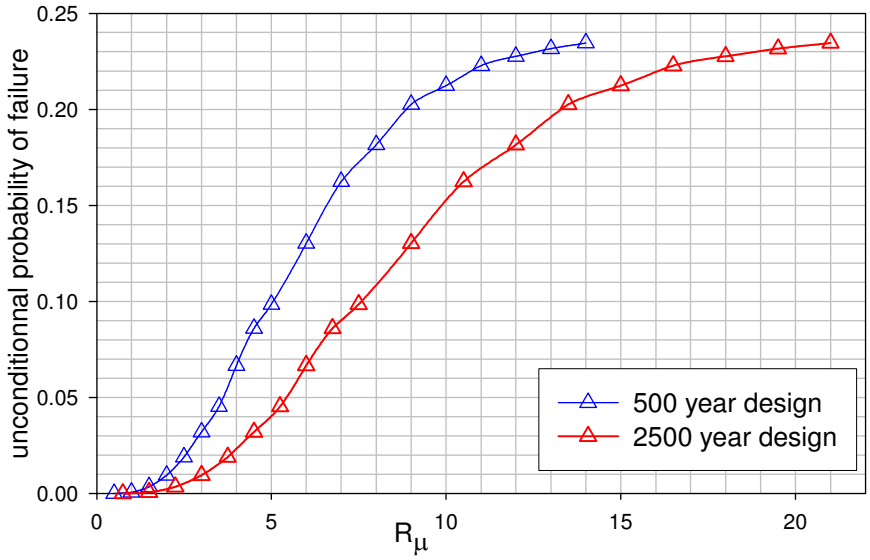


Figure 4.19. Unconditional probability of failure for period of 1 sec for various $R_\mu$ values

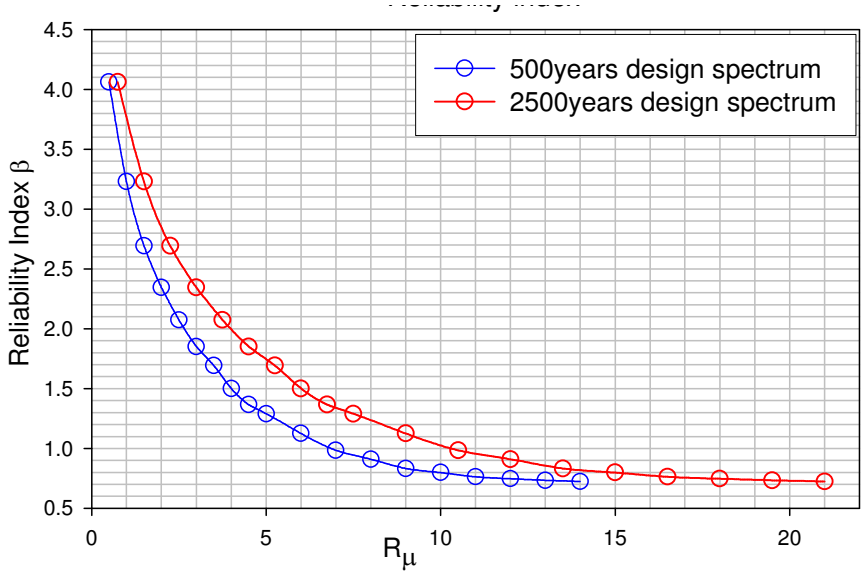


Figure 4.20. Reliability Index, β, versus $R_\mu$ for two different design spectra for period of 1sec

The results of the reliability analysis for different natural periods and return periods are assembled in Table 4.6 for both damage beyond repair and the collapse limit states. Table 4.6 can then be used to select the appropriate design values for $R_\mu$ to satisfy a predetermined target reliability index value. For example, assuming that a R-C bridge column of natural period $T_p$=1sec has to survive with repairable damage the seismic excitations expected in a 75-yr design life with a reliability β=2.0. Then, by interpolation, the appropriate $R_\mu$ factor to be used during the design process should be $R_\mu$=1.82. If the bridge column should avoid collapse in a 75-yr design life with the same reliability index β=2.0, then the adequate response modification factor should be $R_\mu$=2.66. For comparison, the AASHTO standard specifications for seismic design require $R_\mu$ values of 1.5, 2.0, and 3.0 for critical, essential and other structures, which compare favorably with the 1.82 and 2.66 values obtained in these calculations. On the other hand, for the range of natural periods $T_p$ considered, typical nonlinear analyses show that the average value for $R_\mu$ will be approximately $R_\mu$=μ where μ is the dynamic ductility factor which gives

the ratio of the dynamic deformation of the nonlinear system to the yielding deformation. Although the dynamic ductility factor $\mu$ should be less than the expected monotonic ductility $\mu \leq \mu_{mon}$, it is observed that the $R_\mu$ values of 1.82 and 2.66 calculated herein for the San Francisco site are significantly lower than $\mu_{mon}=12$ implying that the use of the monotonic ductility as a criterion for selecting $R_\mu$ is not appropriate.

Table 4.6: Reliability index for damage beyond repair (D.B.R) and Collapse limit state.

| **Period (sec)** | | **0.5** | | | | **1.0** | | | | **2.0** | | | |
|---|---|---|---|---|---|---|---|---|---|---|---|---|---|
| **$R_\mu$** | | **1.5** | **2** | **2.5** | **3** | **1.5** | **2** | **2.5** | **3** | **1.5** | **2** | **2.5** | **3** |
| **1yr** | **D.B.R** | 3.69 | 3.40 | 3.25 | 3.11 | 3.51 | 3.31 | 3.13 | 3.02 | 3.37 | 3.16 | 3.05 | 2.95 |
| | **Collapse** | 4.03 | 3.73 | 3.54 | 3.40 | 3.86 | 3.61 | 3.42 | 3.28 | 3.72 | 3.47 | 3.32 | 3.19 |
| **20yrs** | **D.B.R** | 2.86 | 2.50 | 2.29 | 2.10 | 2.63 | 2.37 | 2.13 | 1.98 | 2.45 | 2.18 | 2.02 | 1.87 |
| | **Collapse** | 3.28 | 2.91 | 2.67 | 2.49 | 3.06 | 2.76 | 2.52 | 2.33 | 2.89 | 2.58 | 2.38 | 2.21 |
| **50yrs** | **D.B.R** | 2.58 | 2.18 | 1.95 | 1.74 | 2.33 | 2.04 | 1.77 | 1.60 | 2.13 | 1.82 | 1.65 | 1.47 |
| | **Collapse** | 3.03 | 2.64 | 2.37 | 2.18 | 2.80 | 2.47 | 2.21 | 2.00 | 2.62 | 2.28 | 2.05 | 1.87 |
| **75yrs** | **D.B.R** | 2.46 | 2.05 | 1.80 | 1.57 | 2.20 | 1.89 | 1.61 | 1.43 | 1.99 | 1.67 | 1.47 | 1.28 |
| | **Collapse** | 2.93 | 2.52 | 2.24 | 2.04 | 2.69 | 2.34 | 2.07 | 1.85 | 2.50 | 2.14 | 1.91 | 1.71 |
| **100yrs** | **D.B.R** | 2.38 | 1.95 | 1.69 | 1.46 | 2.10 | 1.79 | 1.50 | 1.30 | 1.89 | 1.55 | 1.35 | 1.15 |
| | **Collapse** | 2.86 | 2.44 | 2.15 | 1.95 | 2.62 | 2.26 | 1.98 | 1.75 | 2.42 | 2.05 | 1.81 | 1.60 |

## 4.14 SENSITIVITY ANALYSIS OF MATERIAL UNCERTAINTIES

### 4.14.1 Sensitivity Analysis Methodology

Sensitivity analysis is introduced to structural reliability as a measure of the importance of random variables to the safety of the structural system. In other words, how crucial is a given random variable to the outcome that this system may encounter? Supposing that a random variable deviates slightly from its mean value, will this variation lead to a different outcome than it was expected?. Explicitly, let's assume a design of a structure is made based on nominal values of its capacities and the risk is assessed and found to be satisfying the design safety objectives. Then, if a slight change from those nominal values is inherent to the actual capacities for some reasons, then does this

deviation compromise the safety of the structure and therefore present an additional risk that is uncounted for?.

Knowing the sensitivity of the design to its random variables can be beneficial in a sense that those crucial elements can be influenced or changed in a direction that improves the chance of survival of the system. To achieve this objective, a sensitivity measure needs to be established.

One way of measuring the sensitivity is by using the partial differentials of the performance function by respect to the random variable (Melchers; 1987). But in order for this measure to be comparable between the independent random variables, the differentials of performance function have to be normalized by dividing them by the standard deviations of the variables. That is straight forward calculation if the performance function is explicitly known in closed form.

A comparable and valid measure can be drawn for this sensitivity measure for reliability problems that lack a closed form of performance function. Indeed, the normalized differentials of performance function are the components of unit vector perpendicular to the failure surface in the Gaussian random space. But the question that remains to be solved is where in the failure surface those differentials should be calculated i.e what is the suitable point for calculating a meaningful sensitivity measure? The first and the obvious answer that comes to mind is the important region that contributes the most to the total probability of failure. Recalling from chapter Two of this thesis, that the design point used to calculate the probability of failure using the FORM method represents the important region or maximum likelihood and therefore the perfect choice to calculate the sensitivity coefficients. The use of the response surface method

discussed in chapter Two can provide the design points $x^*$ whose components are $(x^*_1,\ldots,x^*_n)$ as well as the reliability index β which represents the distance from the Gaussian space origin to the design point and can be calculated as:

$$\beta = \sqrt{(x_1^*)^2 + \cdots (x_n^*)^2} \qquad 4.17$$

The sensitivity of variable $x_i$ can then be calculated as the following:

$$s(xi) = \frac{(x_i^*)^2}{\beta^2} \qquad 4.18$$

### 4.14.2 Sensitivity of $R_\mu$ to Material Uncertainties

To measure the sensitivity of the Response Modification factor to material uncertainties in reinforced concrete columns, a suite of hundred synthetic earthquakes are generated for the San Francisco site that reflect the earthquake population and its uncertainties based on the seismic hazard identified in section 4.13.2 of this Chapter. For each earthquake, the FORM algorithm is performed to identify the design point on failure surface as well as the associated reliability index β. Equation 4.18 is then used to calculate the sensitivity of each material random variable for that particular earthquake. This process is repeated for the hundred earthquakes and the final sensitivity coefficient associated with each variable is then obtained by averaging over the hundred coefficients estimated earlier. Table 4.7 shows the results for columns with natural periods of 0.5, 1, and 2sec for collapse limit state and values of response modification factor of 1.5, 2, 2.5, and 3. the Material random variables considered in this table are the damage limit index

$DI_{lim}$; Takeda model parameters, $\alpha$, $\beta$, and r; the initial stiffness k; the yield strength $f_y$; and the mass m;

Table 4.7: Sensitivity Analysis of material uncertainties for collapse limit state.

| **Period (sec)** | **0.5** | | | | **1.0** | | | | **2.0** | | | |
|---|---|---|---|---|---|---|---|---|---|---|---|---|
| **$R_\mu$** | **1.5** | **2** | **2.5** | **3** | **1.5** | **2** | **2.5** | **3** | **1.5** | **2** | **2.5** | **3** |
| **$DI_{lim}$** | 0.954 | 0.913 | 0.853 | 0.801 | 0.928 | 0.888 | 0.820 | 0.800 | 0.936 | 0.896 | 0.843 | 0.781 |
| **$\alpha$** | $4.10^{-4}$ | $9.10^{-4}$ | 0.004 | 0.003 | 0.001 | 0.001 | 0.005 | 0.003 | $5.10^{-4}$ | 0.001 | 0.004 | 0.003 |
| **$\beta$** | $9.10^{-5}$ | $4.10^{-4}$ | 0.004 | 0.012 | $7.10^{-4}$ | 0.002 | 0.001 | 0.008 | $3.10^{-4}$ | $2.10^{-4}$ | $3.10^{-4}$ | 0.002 |
| **r** | $2.10^{-5}$ | $2.10^{-4}$ | 0.006 | 0.015 | $1.10^{-4}$ | $9.10^{-4}$ | 0.009 | 0.026 | 0.026 | 0.041 | 0.058 | 0.109 |
| **k** | $3.10^{-3}$ | 0.005 | 0.020 | 0.019 | 0.007 | 0.014 | 0.031 | 0.030 | 0.005 | 0.010 | 0.024 | 0.021 |
| **$f_y$** | 0.037 | 0.070 | 0.097 | 0.121 | 0.054 | 0.08 | 0.111 | 0.105 | 0.028 | 0.044 | 0.058 | 0.070 |
| **m** | 0.005 | 0.009 | 0.017 | 0.028 | 0.008 | 0.013 | 0.020 | 0.026 | 0.004 | 0.006 | 0.012 | 0.013 |

It is clear from the results of Table 4.7 that the damage limit index is dominant over the remaining variables. Its sensitivity coefficient ranges from 78% to 95%. This is can be partially explained by the fact that this variable has a higher standard deviation of 53% which includes the variabilities related to the monotonic ductility, and the damage index coefficient $\beta_{DI}$. The structural risk of the reinforced concrete column is also sensitive to the yield strength to a much lower degree than that of the damage limit index. It can also be concluded that the results of the response modification factor obtained using the radial method are insensitive to the hysteresis modeling parameter which is consistent with observations made by earlier researchers ( Nassar & Krawinkler (1991), and Miranda & Bertero (1994)). The sensitivities of the bridge column to the initial stiffness and mass are found to be on the same order of 2%.

The Results of Table 4.7 also show that the sensitivity to the damage limit index decreases while the remaining random variable sensitivities increase as $R_\mu$ increases. The decrease in $R_\mu$ induces a higher safety margin to the bridge column. That can be translated in Gaussian space by the design point that moves away from the mean values. Therefore, only strong variables, in this case the Damage limit index, can reach faster the design point. This means that the damage limit index influence the safety of the column globally in the Gaussian space. As $R_\mu$ increases, the probability of failure becomes bigger and the design point becomes closer to the mean point. This closeness to the mean point gives more chance to the remaining random variables to affect the outcome locally.

### 4.14.3 Sensitivity of $R_\mu$ to Monotonic Displacement Ductility

Unlike the material and modeling random variables whose sensitivity coefficients are calculated in the previous section. The uncertainty in monotonic displacement ductility was implicitly accounted for by lumping its variability to the damage limit index $DI_{lim}$ as it was discussed in section 4.8 of this Chapter. The procedure for sensitivity analysis developed in the previous section is not applicable to the monotonic displacement ductility. However, by varying the mean value of this variable, we can provide useful information about how this variable can affect the reliability of a bridge column in a seismic event.

Therefore, to assess the sensitivity of response modification factor to the monotonic displacement ductility $\mu_{mon}$, values of $R_\mu$ are calculated for three $\mu_{mon}$ values of 8, 10, 12 to meet a reliability target of 2 for a 75 year return period for three different columns of natural periods respectively of 0.5, 1, and 2sec. The results are plotted in Figure 4.21 and

clearly indicate that all three columns show the same degree of sensitivity to monotonic displacement ductility.

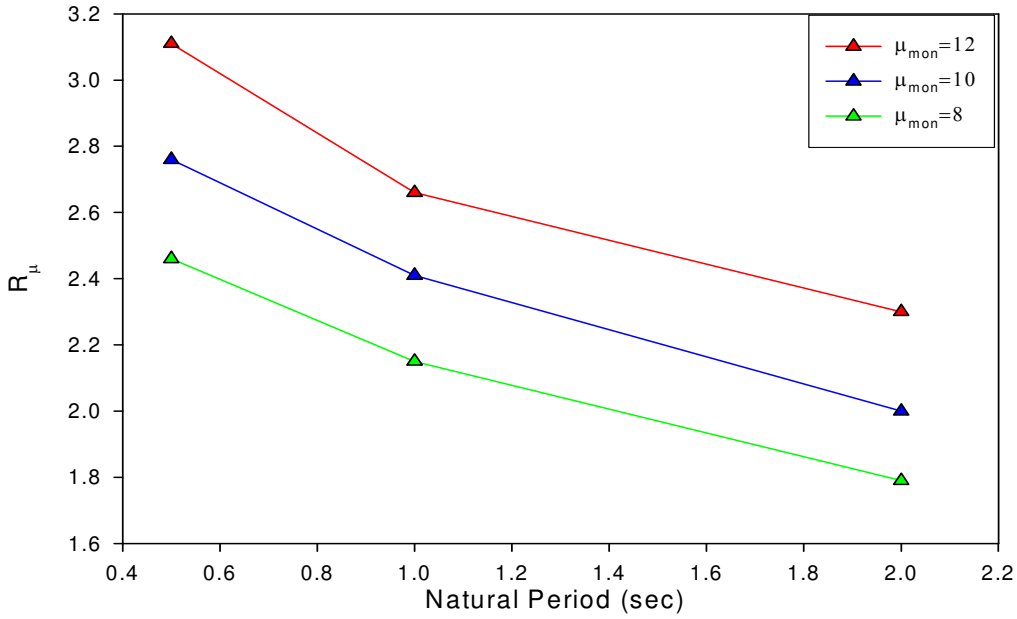


Figure 4.21 Sensitivity of $R_\mu$ to $\mu_{mon}$ for period of 0.5, 1, and 2sec.

If a sensitivity coefficient is defined for this particular case as the variation of $R_\mu$ divided by the variation of $\mu_{mon}$, its value will be in the order of 14% obtained by averaging over three periods of 0.5, 1, and 2sec.

## 4.15 CALIBRATION OF $R_\mu$ FOR OTHER SITES

Similar to the procedure applied to San Francisco site, the calibration of Response Modification factors for other sites in the USA can be performed to propose a rational set of $R_\mu$ that incorporates the seismic uncertainties based on available data for each particular site and the material uncertainties of bridge columns. In this study, hypothetical columns are considered for Los Angles, Seattle, Memphis, and New York with monotonic ductilities of 12, 7, 7, and 2 respectively. These values are proposed by the author and it can be adjusted to reflect the actual values used by engineers for each

location. The results for the damage limit state and collapse limit state are given in Tables 4.8, 4.9, 4.10, 4.11.

Table 4.8: Reliability index for damage beyond repair (D.B.R) and Collapse limit state for Los Angeles.

| **Period (sec)** | | **0.5** | | | | **1** | | | | **2** | | | |
|---|---|---|---|---|---|---|---|---|---|---|---|---|---|
| **$R_\mu$** | | **1.5** | **2** | **2.5** | **3** | **1.5** | **2** | **2.5** | **3** | **1.5** | **2** | **2.5** | **3** |
| | **D.B.R** | 4.58 | 4.15 | 3.87 | 3.63 | 4.24 | 3.86 | 3.6 | 3.42 | 3.87 | 3.65 | 3.45 | 3.31 |
| **1yr** | **Collapse** | 5.51 | 4.96 | 4.54 | 4.2 | 5.1 | 4.56 | 4.18 | 3.89 | 4.54 | 4.27 | 4 | 3.79 |
| | **D.B.R** | 3.92 | 3.42 | 3.08 | 2.78 | 3.53 | 3.07 | 2.74 | 2.51 | 3.08 | 2.81 | 2.56 | 2.38 |
| **20yrs** | **Collapse** | 4.97 | 4.36 | 3.88 | 3.49 | 4.52 | 3.9 | 3.46 | 3.11 | 3.88 | 3.57 | 3.24 | 2.99 |
| | **D.B.R** | 3.72 | 3.19 | 2.82 | 2.5 | 3.3 | 2.81 | 2.46 | 2.2 | 2.82 | 2.53 | 2.25 | 2.05 |
| **50yrs** | **Collapse** | 4.81 | 4.18 | 3.68 | 3.26 | 4.35 | 3.7 | 3.24 | 2.87 | 3.68 | 3.36 | 3.01 | 2.73 |
| | **D.B.R** | 3.63 | 3.09 | 2.71 | 2.38 | 3.2 | 2.7 | 2.33 | 2.07 | 2.71 | 2.41 | 2.12 | 1.91 |
| **75yrs** | **Collapse** | 4.75 | 4.11 | 3.6 | 3.17 | 4.28 | 3.62 | 3.15 | 2.76 | 3.6 | 3.26 | 2.91 | 2.63 |
| | **D.B.R** | 3.57 | 3.02 | 2.63 | 2.29 | 3.14 | 2.63 | 2.24 | 1.97 | 2.63 | 2.32 | 2.03 | 1.81 |
| **100yrs** | **Collapse** | 4.7 | 4.06 | 3.54 | 3.11 | 4.23 | 3.57 | 3.08 | 2.69 | 3.54 | 3.2 | 2.84 | 2.55 |

Table 4.9: Reliability index for damage beyond repair (D.B.R) and Collapse limit state for Seattle

| **Period (sec)** | | **0.5** | | | | **1** | | | | **2** | | | |
|---|---|---|---|---|---|---|---|---|---|---|---|---|---|
| **$R_\mu$** | | **1.5** | **2** | **2.5** | **3** | **1.5** | **2** | **2.5** | **3** | **1.5** | **2** | **2.5** | **3** |
| | **D.B.R** | 3.78 | 3.6 | 3.49 | 3.42 | 3.67 | 3.53 | 3.43 | 3.36 | 3.72 | 3.53 | 3.42 | 3.34 |
| **1yr** | **Collapse** | 4.3 | 4.02 | 3.77 | 3.6 | 4.15 | 3.88 | 3.7 | 3.6 | 3.98 | 3.77 | 3.64 | 3.56 |
| | **D.B.R** | 2.97 | 2.74 | 2.61 | 2.51 | 2.84 | 2.65 | 2.53 | 2.44 | 2.9 | 2.65 | 2.52 | 2.42 |
| **20yrs** | **Collapse** | 3.6 | 3.27 | 2.96 | 2.75 | 3.43 | 3.1 | 2.88 | 2.76 | 3.22 | 2.96 | 2.8 | 2.7 |
| | **D.B.R** | 2.7 | 2.46 | 2.31 | 2.2 | 2.56 | 2.36 | 2.22 | 2.12 | 2.63 | 2.36 | 2.21 | 2.09 |
| **50yrs** | **Collapse** | 3.39 | 3.04 | 2.71 | 2.48 | 3.2 | 2.85 | 2.61 | 2.49 | 2.99 | 2.71 | 2.53 | 2.42 |
| | **D.B.R** | 2.59 | 2.34 | 2.18 | 2.07 | 2.44 | 2.23 | 2.08 | 1.98 | 2.51 | 2.23 | 2.07 | 1.95 |
| **75yrs** | **Collapse** | 3.3 | 2.94 | 2.6 | 2.36 | 3.11 | 2.75 | 2.5 | 2.37 | 2.89 | 2.6 | 2.42 | 2.3 |
| | **D.B.R** | 2.51 | 2.25 | 2.09 | 1.97 | 2.35 | 2.14 | 1.98 | 1.88 | 2.43 | 2.14 | 1.97 | 1.85 |
| **100yrs** | **Collapse** | 3.24 | 2.87 | 2.52 | 2.28 | 3.04 | 2.68 | 2.42 | 2.29 | 2.82 | 2.52 | 2.34 | 2.22 |

Table 4.10: Reliability index for damage beyond repair (D.B.R) and Collapse limit state for Memphis

| **Period (sec)** | | **0.5** | | | | **1** | | | | **2** | | | |
|---|---|---|---|---|---|---|---|---|---|---|---|---|---|
| **$R_\mu$** | | **1.5** | **2** | **2.5** | **3** | **1.5** | **2** | **2.5** | **3** | **1.5** | **2** | **2.5** | **3** |
| | **D.B.R** | 3.85 | 3.6 | 3.46 | 3.34 | 4.15 | 3.91 | 3.73 | 3.56 | 4.56 | 4.24 | 4.01 | 3.8 |
| **1yr** | **Collapse** | 4.52 | 4.16 | 3.91 | 3.7 | 4.93 | 4.6 | 4.36 | 4.1 | 5.43 | 5.05 | 4.75 | 4.46 |
| | **D.B.R** | 3.05 | 2.75 | 2.56 | 2.41 | 3.42 | 3.14 | 2.91 | 2.7 | 3.9 | 3.53 | 3.26 | 3 |
| **20yrs** | **Collapse** | 3.86 | 3.43 | 3.12 | 2.87 | 4.32 | 3.95 | 3.67 | 3.36 | 4.88 | 4.45 | 4.12 | 3.78 |
| | **D.B.R** | 2.79 | 2.46 | 2.26 | 2.09 | 3.18 | 2.88 | 2.64 | 2.41 | 3.69 | 3.3 | 3.01 | 2.74 |
| **50yrs** | **Collapse** | 3.65 | 3.2 | 2.87 | 2.6 | 4.13 | 3.74 | 3.45 | 3.12 | 4.71 | 4.27 | 3.92 | 3.56 |
| | **D.B.R** | 2.68 | 2.33 | 2.12 | 1.94 | 3.08 | 2.77 | 2.52 | 2.28 | 3.6 | 3.2 | 3.91 | 2.62 |
| **75yrs** | **Collapse** | 3.56 | 3.1 | 2.76 | 2.48 | 4.05 | 3.66 | 3.35 | 3.02 | 4.64 | 4.19 | 3.84 | 3.47 |
| | **D.B.R** | 2.6 | 2.25 | 2.03 | 1.84 | 3.01 | 2.7 | 2.44 | 2.19 | 3.54 | 3.13 | 2.83 | 2.54 |
| **100yrs** | **Collapse** | 3.5 | 3.03 | 2.69 | 2.39 | 4 | 3.6 | 3.29 | 2.95 | 4.6 | 4.14 | 3.78 | 3.41 |

Table 4.11 : Reliability index for damage beyond repair (D.B.R) and Collapse limit state for New York

| Period (sec) | | 0.5 | | | | 1 | | | | 2 | | | |
|---|---|---|---|---|---|---|---|---|---|---|---|---|---|
| $R_\mu$ | | 1.5 | 2 | 2.5 | 3 | 1.5 | 2 | 2.5 | 3 | 1.5 | 2 | 2.5 | 3 |
| 1yr | D.B.R | 3.96 | 3.75 | 3.62 | 3.52 | 4.13 | 3.91 | 3.75 | 3.64 | 4.63 | 4.38 | 4.21 | 4.08 |
| | Collapse | 4.63 | 4.33 | 4.11 | 3.97 | 4.82 | 4.51 | 4.29 | 4.14 | 5.37 | 5.04 | 4.81 | 4.63 |
| 20yrs | D.B.R | 3.2 | 2.95 | 2.78 | 2.66 | 3.41 | 3.13 | 2.95 | 2.81 | 3.99 | 3.7 | 3.5 | 3.34 |
| | Collapse | 3.98 | 3.64 | 3.38 | 3.21 | 4.21 | 3.85 | 3.59 | 3.41 | 4.82 | 4.45 | 4.19 | 3.99 |
| 50yrs | D.B.R | 2.96 | 2.69 | 2.51 | 2.37 | 3.18 | 2.89 | 2.69 | 2.54 | 3.79 | 3.49 | 3.28 | 3.11 |
| | Collapse | 3.79 | 3.42 | 3.15 | 2.97 | 4.02 | 3.65 | 3.37 | 3.19 | 4.66 | 4.27 | 4 | 3.79 |
| 75yrs | D.B.R | 2.86 | 2.58 | 2.39 | 2.25 | 3.09 | 2.79 | 2.58 | 2.43 | 3.71 | 3.41 | 3.19 | 3.02 |
| | Collapse | 3.71 | 3.33 | 3.06 | 2.87 | 3.94 | 3.56 | 3.28 | 3.09 | 4.59 | 4.2 | 3.92 | 3.71 |
| 100yrs | D.B.R | 2.79 | 2.5 | 2.31 | 2.17 | 3.02 | 2.72 | 2.5 | 2.35 | 3.66 | 3.35 | 3.12 | 2.95 |
| | Collapse | 3.65 | 3.27 | 2.99 | 2.8 | 3.89 | 3.51 | 3.22 | 3.03 | 4.55 | 4.15 | 3.87 | 3.66 |

## 4.16 CONCLUSIONS AND RECOMMENDATIONS

This Chapter demonstrated how reliability analysis method can be used to enhance the seismic design of bridge columns. The model developed by the author provides a rational way to calibrate response modification factors for the seismic design of RC bridge columns that account for the large variabilites of the earthquake loadings, the material randomness inherent in RC bridge columns, and the uncertainties related to errors in the modeling of column response to seismic excitation. These uncertainties are estimated based on actual experimental data. For instance, the seismic uncertainties are extracted based on the seismic hazard analysis adopted by USGS and include the distribution of seismic threat by moment magnitude and epicentral distance. The material randomness and the modeling uncertainties are studied and identified based on previous studies (Park & Ang 1985) or based on cyclic test data on RC bridge columns assembled by the University of Washington (http://www.ce.washington.edu/~peera1). The developed model results in sets of Response Modification Factors rationally calibrated and ready to be used in seismic design of bridge columns to meet a preset reliability target. This model will

further be developed and extended in Chapter Five of this thesis to analyze a typical bridge with different possible modes of failure subjected to seismic loading.

# *Chapter5*

# *Structural Risk Assessment of Bridge System under Seismic Loading*

## 5.1 INTRODUCTION

The social and the economical activities of many major cities in the U.S depend to a large extent on the transportation network to exchange goods and services and transport people to their destinations. These activities would be impossible without the existence of bridges that connect different parts of the transportation network. Therefore, bridges form a crucial piece for a good and efficient functionality of the network. Because of their particular geometries, bridges are more vulnerable than the other elements of the transportation network to seismic damage. Past experiences from earthquakes have shown that entire region activities had come to a hold, cities were paralyzed, the lives of millions of people had been affected, and millions of dollars in losses had been recorded as a consequence of severe earthquake events. The negative effects of earthquake events lasted weeks and sometimes months because of closure of key bridges for damage investigation and repair. To reduce the time of traffic disruption in the aftermath of eventual seismic events, many agencies have developed preparedness plans and enhance

the structural capacities of bridges. The prediction of nonlinear seismic response and structural damage of bridges are important factors for determining the type and extent of retrofitting needs and in reducing the time of closure after earthquake occurences. However, structural damage to bridge elements cannot be determined based on a deterministic analysis because of the random nature of bridge member material properties, bridge support and boundary conditions, and the random nature of earthquake input. Hence, probabilistic methods that account for both the randomness in seismic input and material properties in addition to modeling errors must be used to provide rational measures of safety for all possible failure modes. Therefore, probabilistic models are necessary to develop a rational rehabilitation strategy to provide a uniform level of survival for bridge system failure modes.

Structural reliability, which is the level of damage to a bridge that can be tolerated by society, is commonly measured by a reliability index $\beta$ and set to match a reliability index target extracted from reviewing the response of other bridges that have shown a good degree of performance in past seismic events. The reliability index as explained in Chapter 2 gives the number of standard deviations that the mean value of the safety margin is away from the failure limit zone which corresponds to zero safety margin. Therefore, to provide a uniform survival level for members as well as for the bridge system consistent with the LRFD philosophy, this Chapter proposes a reliability based analysis procedure capable of quantifying the probability of failure of complex bridge systems as well as the contribution of each failure mode to system failure. The radial sampling method developed by the author and presented in Chapter 3 will be used for calculating the probability of failure of a typical highway bridge structure. To achieve the

aforementioned goal, this Chapter presents in a first stage the structural modeling of the bridge elements which include abutments, substructure, cap beams, girders, bearings, bridge piers, and foundations. The modeling of material uncertainties will also be discussed in addition to defining the modes of system failure. The seismic inputs as well as their uncertainties will be considered for a particular site located in the San Francisco area. Finally, the results of the seismic reliability analysis will be presented and analyzed. The chapter concludes by proposing a set of recommendations for implementing the proposed bridge reliability model to evaluate safety margin in existing and new bridges.

## 5.2 BRIDGE DESCRIPTION

The bridge considered in this example has similar geometry to that considered by Hwang & al (2001). The columns dimensions were modified to satisfy the seismic the seismic design criteria of San Francisco area. This bridge is a 235 ft long continuous span with two 45.5 ft end spans and two 75 ft interior spans supported by three concrete bents as shown in Figure 5.1. The bridge superstructure is 58 ft wide and 7 in thick, where the continuous cast-in-place concrete deck rested on 11 AASHTO TYPE III girders spaced at 5.25 ft as illustrated in the transverse view of the bridge in Figure 5.2. The section properties of the beams are provided in Figure 5.3. A 1 in thick Neoprene pad bearing separates each girder and the cap beam of the bents. The pad is tied by two A307 Swedge dowel bars. The girders are supported at the ends of the bridge by integral, open end abutments with U-shaped wing walls. The back wall is 6 ft 10 in high and 58 ft wide, and the wing wall is 6 ft 10 in high and 9 ft 6 in wide. Each abutment is supported by ten 14 in x 14 in precast concrete piles.

Each concrete column bent consists of a 3.25 ft x 4 ft rectangular cap beam and four 5 ft diameter and 15 ft high circular concrete columns. The concrete columns are reinforced with 20 # 14 grade 60 longitudinal bars and confined by # 6 grade 40 bars spaced at 3 in. The concrete cover is 2 in thick. Figure 5.4 shows the detailing of the concrete column. The column base is firmly secured to a rectangular mat of 9 ft width in each horizontal side, and 3.5 ft depth. The concrete mat is supported by eight 14 in by 14 in rectangular precast concrete piles embedded 12 in deep into the bottom of the concrete mat without any reinforcing bar ties.

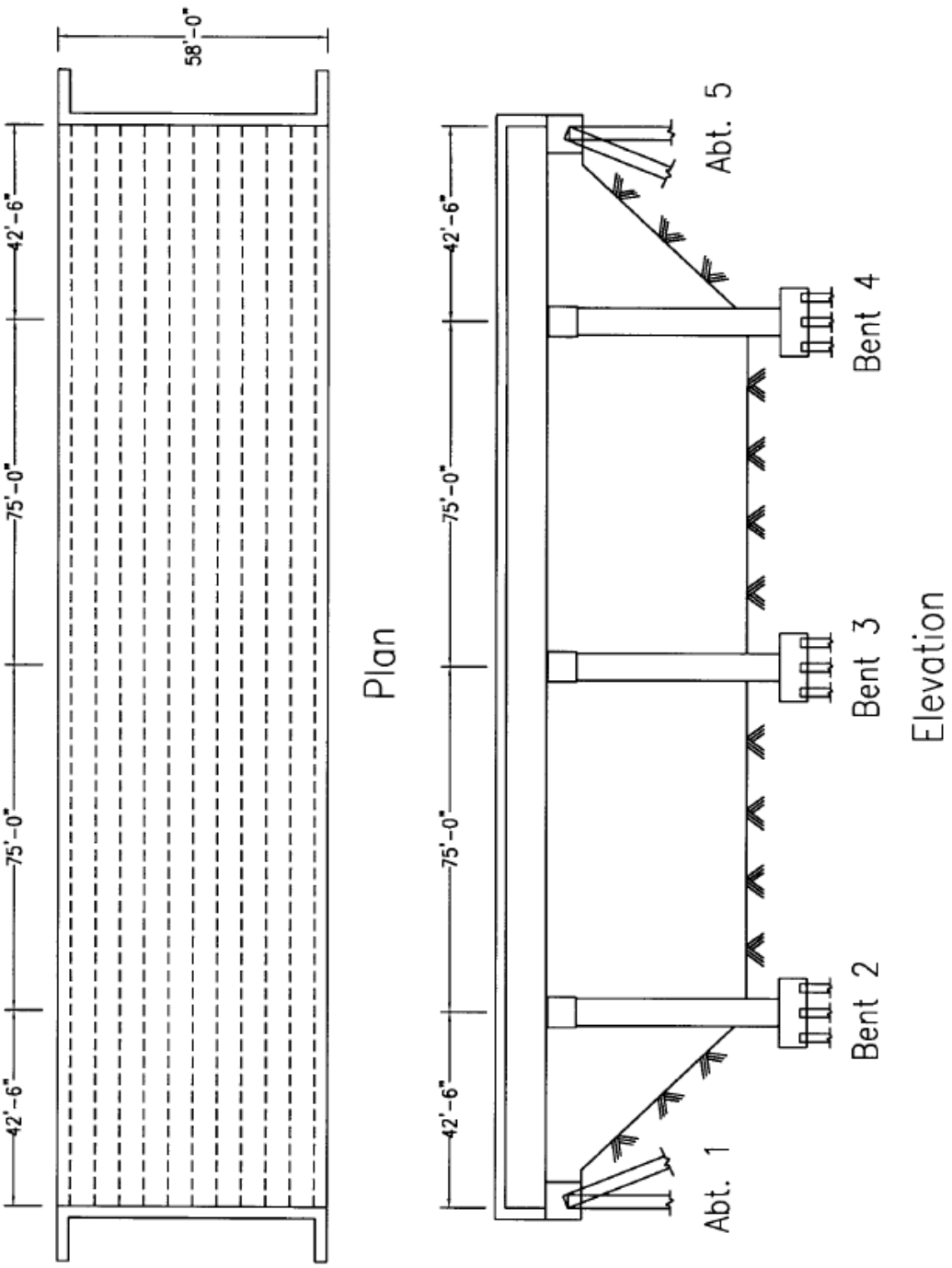


Figure 5.1 Plan and elevation view of the bridge.( After Hwang ;2001)

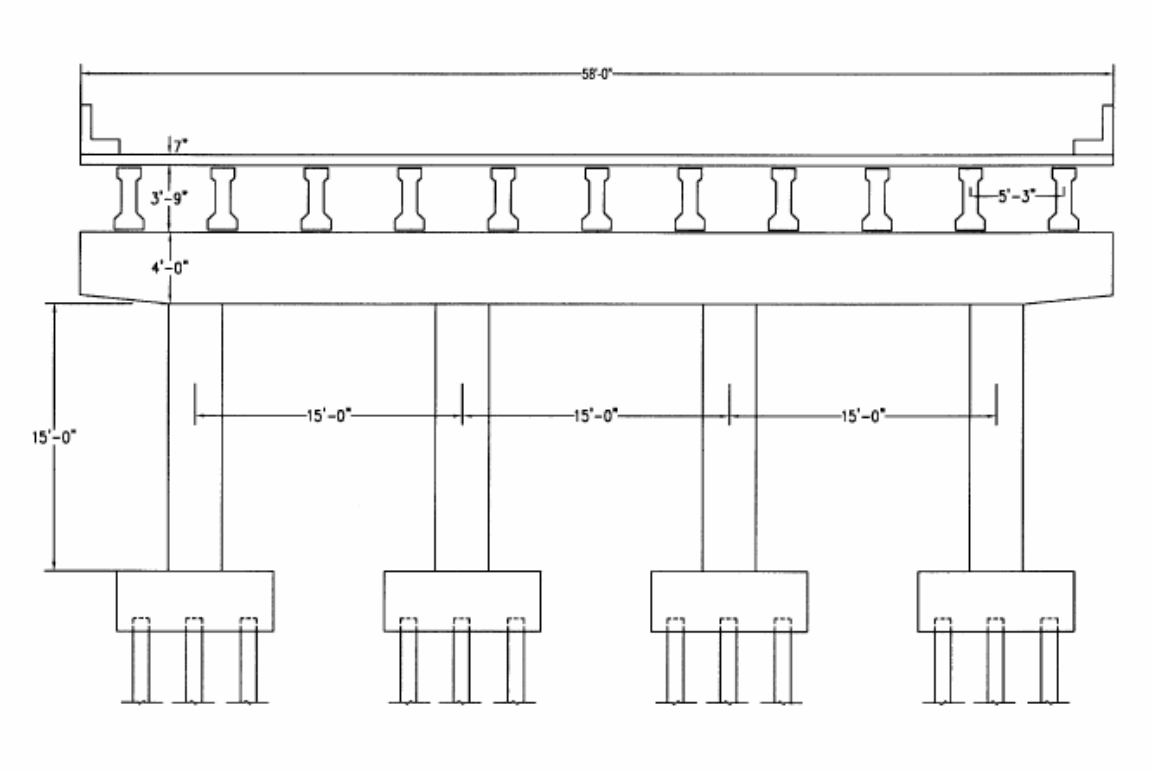


Figure 5.2 Transverse view showing cast in place concrete deck, girders, four columns bent, and column piles.(After Hwang; 2001)

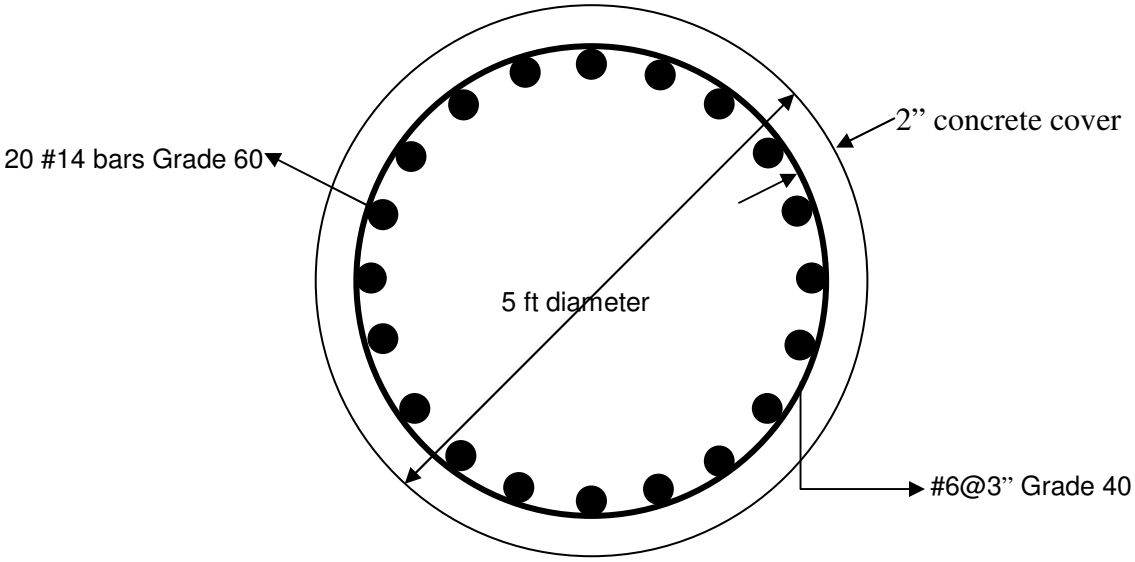


Figure 5.3 Detailing of cross sectional area of bridge column

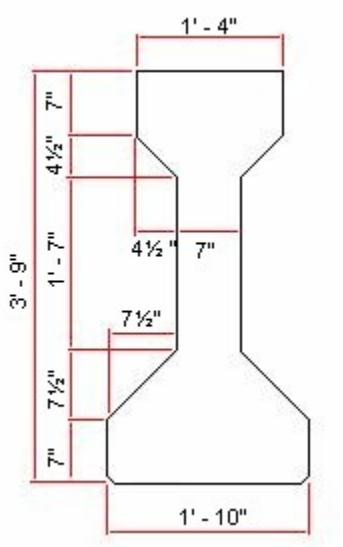


| Section Properties | | | | | | |
|---|---|---|---|---|---|---|
| Designation | A ($in^2$) | I ($in^4$) | $Y_b$ (in) | $Z_b$ ($in^3$) | $Z_t$ ($in^3$) | w (plf) |
| Type III | 560 | 125.39 | 20.27 | 6186 | 5070 | 583 |

Figure 5.4 AASHTO Type III concrete girder [AASHTO]

## 5.3 BRIDGE MODELING

The bridge components are modeled using SAP2000 finite elements computer program following the approach used by Hwang & al (2001). The structural response behavior of each component dictates the choice of the finite element available in SAP2000 that mimics as closely as possible the actual behavior of the bridge components. Following the analysis performed by Pan (2007), it was determined that only the bridge bearings and ends of the columns exhibit nonlinear behavior. Therefore, the bridge deck is represented by linear elastic quadrilateral shell elements that combine the behavior of plate bending element and membrane element with normal rotation (Wilson; 2004). Linear elastic beam elements are used to model the linear behavior of the girders, and linear segments of the columns and cap beams. The nonlinear behavior of the hinge zones of the columns and that of the bearings are modeled by nonlinear link elements. The pile-foundation behavior is modeled using linear springs.

The most critical step in the modeling of the bridge is the modeling of the hinge zone in the columns which requires the generation of the moment-curvature diagram. This was achieved using a monotonic analysis program developed by the author for reinforced concrete columns. The program uses the constitutional material laws for steel, confined concrete, and unconfined concrete. A linear distribution of strains is assumed along each column cross section to compute the moment for a given curvature that satisfies the equilibrium of axial forces. A full description of this procedure is included in Appendix A. The model and numerical inputs for the other components are presented in the coming sections of this chapter.

## 5.4 MOMENT CURVATURE ANALYSIS OF BRIDGE COLUMNS

The moment curvature diagram for the column cross section of the bridge is obtained for an axial force ratio of 0.10. The diagram provides valuable information about the envelope of the response to dynamic loads. The initial stiffness, and the yielding bending moment are extracted from the moment- curvature curve to be assigned to the nonlinear link elements that model the hinge zone in the bridge columns located at the top and the bottom of each column. The hinge length is calculated empirically based on the following equation (Priestley & al; 1996):

$$L_h = 6.35\sqrt{d_b} \qquad in \ \ inch \tag{5.1}$$

where $d_b$ is the longitudinal bar diameter in inch. The initial stiffness of the hinge zone is determined from moment $M_{yo}$ and curvature $\phi_{yo}$ that correspond to the first yielding of a longitudinal bar using the following equation:

$$K_o = \frac{M_{yo}}{\phi_{yo} L_h} \qquad 5.2$$

The yield moment $M_y$ is determined by approximating the moment curvature by a bilinear curve that represents the elastic and the plastic behavior as shown in Figure 5.5. The intersection of these two lines determines the yield moment $M_y$ which is different from $M_{yo}$.

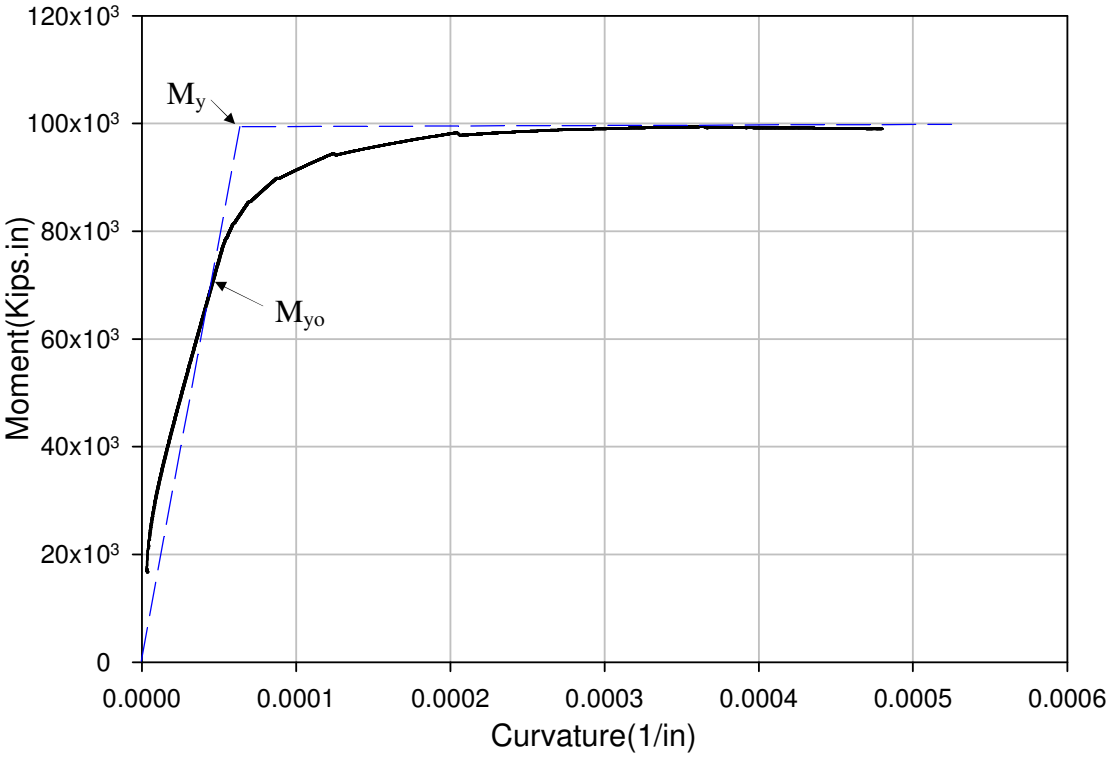


Figure 5.5 Moment Curvature diagram for the bridge column and its approximation by a bilinear curve

## 5.5 MODELING OF BRIDGE COLUMNS

Each bridge column is modeled by four beam elements assumed to be linear. Their stiffnesses are calculated using the cracked concrete cross section. The nonlinear behavior of the two hinge zones at the top and bottom of each column are modeled by nonlinear link elements with six springs. The axial and the torsion load-deformations of

linear elements can be determined knowing the hinge zone length given by Equation 5.1, the cross sectional area, Young modulus, and the shear modulus. The shear stiffnesses are also assumed linear and are given by the following equation (Mander; 1988):

$$K_{vh} = \left( \frac{A_g}{\frac{1}{E_s \rho_v} + \frac{4}{E_c}} \right) \frac{1}{L_h} \qquad 5.3$$

where $A_g$ is the gross sectional area of the column. $E_s$ and $E_c$ are the young modulus for steel and concrete respectively. $\rho_v$ is the transverse steel ratio.

The bending behavior in the transverse and longitudinal directions of the NLink elements are assumed nonlinear. The cyclic response of the moment-rotation curve is approximated by Bouc-Wen model (Baber & Wen; 1980) given by the following equation:

$$\dot{z} = A\dot{u} - \beta|\dot{u}||z|^{n-1} z - \gamma\dot{u}|z|^n \qquad 5.4$$

The variables z and u are respectively the applied moment normalized to the yielding moment and the angle of rotation normalized to the yielding rotation. The parameters β and γ define the general shape of the hysteretic loops as shown in Figure 5.6.

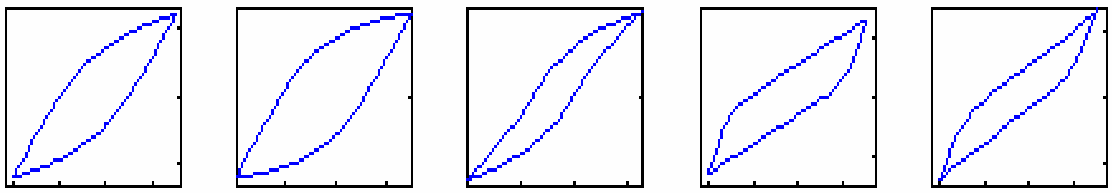


Figure 5.6 Possible hysteresis shapes for n=1 (Babar & Wen 1980)

The parameter n controls the smoothness of the curve in transition between elastic and plastic regions; a small value of n provides a very smooth transition while a large value provides a sharp transition to the plastic range. The ideal elastoplastic behavior is obtained as n approaches infinity as illustrated in Figure 5.7. The parameter A is the initial stiffness ratio of z which generally is taken as 1(Wen; 1985). The values of γ, β, and A are preset in SAP2000 program while n is taken equal to 10.

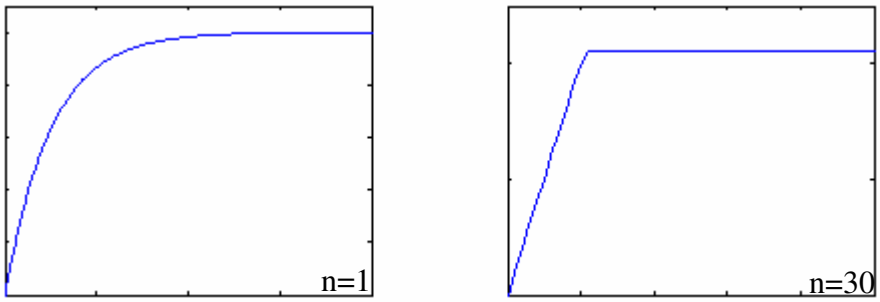


Figure 5.7. Smooth and sharp transition generated by Bouc-Wen Model

Figure 5.8 shows the column bent model composed by two nonlinear link elements at the top and the bottom linked by four linear elastic beam elements.

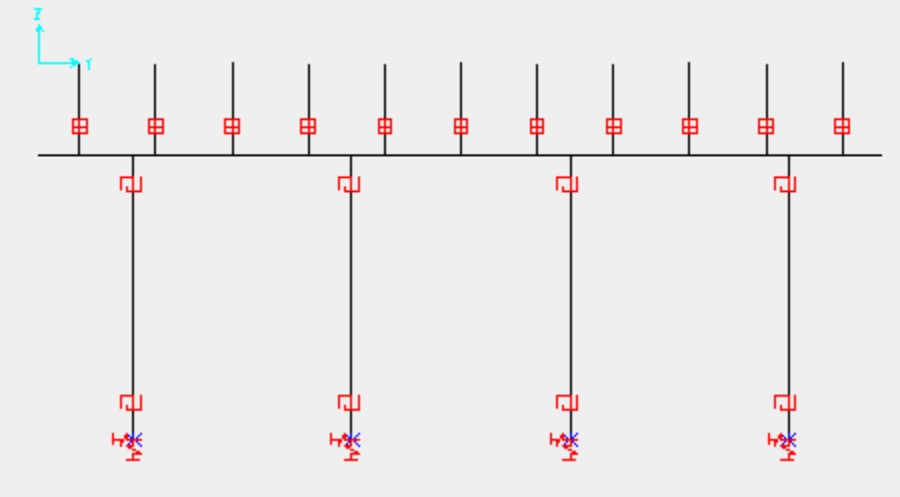

Figure 5.8 Transverse view of bridge FE model

## 5.6 MODELING OF BRIDGE BEARINGS

Figure 5.9 shows the detailing of the 1-in thick Neoprene pad bearing and Swedge dowel bars which connect each girder to the cap beam. The model used herein closely follows the one used by Hwang & al (2001). The shear deformation behavior of each bearing is modeled by a nonlinear link element whose behavior can be modeled by a bilinear hysteresis loop. The initial stiffness is calculated in terms of the dowel bar area $A_b$, its shear modulus $G_b$, and its height $h_b$ using the following equation:

$$K_{bv} = \frac{G_b \, A_b}{h_b} \tag{5.5}$$

The yield shear and the ultimate shear forces are calculated respectively by equations 5.6 and 5.7 in terms of the yielding stress $f_{by}$ and the ultimate stress $f_{bu}$ of the Swedge dowel bar.

$$V_{by} = f_{by} \, A_b \tag{5.6}$$

$$V_{bu} = f_{bu} \, A_b \tag{5.7}$$

The bearing is assumed infinitely rigid in the axial direction, and it can freely rotate in all three rotational degrees of freedom. The connections between top column-cap beam, cap beam-bearing, bearing-girder, and girder-bridge deck are assumed to be rigid and they are modeled using constraints available in SAP2000.

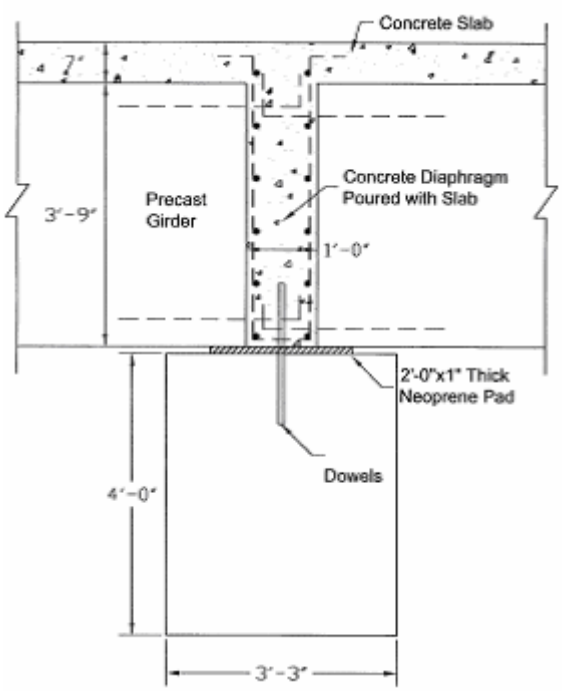


Figure 5.9 Detailing of connections between beam cap, bearing, and girder(After Hwang; 2001).

## 5.7 MODELING OF PILE FOUNDATION

The pile footings that support the bridge columns are modeled using linear springs. The degrees of freedom in the axial direction and two rotations about the horizontal axes are considered as restrained degrees of freedom. The soil at the bridge site is considered stiff. The lateral stiffness $k_p$ of an individual pile is taken equal to 40 kips/in. As Figure 5.10 shows, each column is supported by eight piles and therefore the horizontal stiffness of the model spring is calculated based on Equation 5.8 after neglecting the group effect of the pile foundation.

$$K = n_p \, k_p \tag{5.8}$$

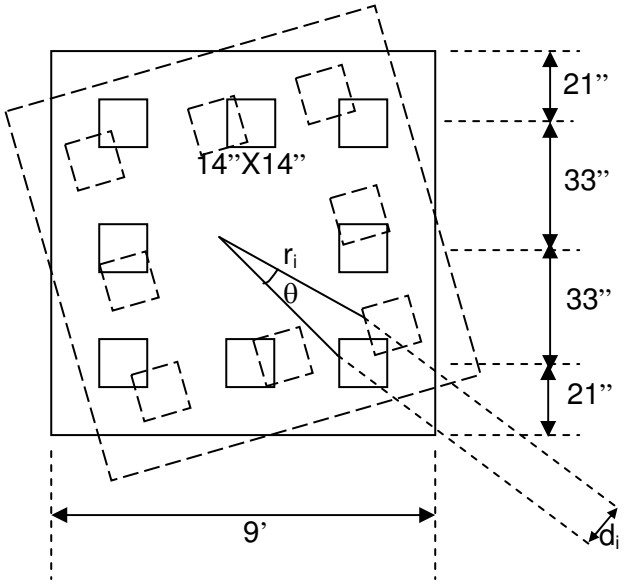


Figure 5.10 Plan view of the foundation supporting the bridge column

To determine the torsional stiffness of the pile foundation, let's assume that the pile foundation is rotated by an angle θ about the center point of the foundation. Given the distance $r_i$ from the center of pile i to the center point of the foundation, the displacement $d_i$ of this individual pile is related to θ by the following equation:

$$d_i = r_i \, \theta \tag{5.9}$$

The force $f_i$ that should be applied to pile i to displace it by a distance $d_i$ is given by the following equation knowing the pile stiffness $k_{pi}$ :

$$f_i = k_{pi} \, d_i \tag{5.10}$$

By replacing $d_i$ in Equation 5.10 by its expression given in Equation 5.9, and multiplying both sides of the equation by $r_i$, we obtain the following equation:

$$\theta \, k_i \, r_i^2 = f_i \, r_i \tag{5.11}$$

The summation of equation 5.11 over all the piles gives the resultant torque applied to column, $T = \sum_{i=1}^{n} f_i \; r_i$ , or:

$$\theta \sum_{i=1}^{n} k_i \; r_i^2 = T \qquad 5.12$$

Therefore, the torsional stiffness of the pile foundation is assigned a spring constant is calculated using the following equation:

$$K_{PT} = \sum_{i=1}^{n} k_i \; r_i^2 \qquad 5.13$$

The pile foundation is thus modeled by three linear springs; two in the horizontal shear directions and one torsional rotation as illustrated in Figure 5.11. The other degrees of freedom are restrained. In the pile foundation modeling process described in this section, the mat stiffness is neglected based on the recommendation of Priestley & al (1996) and therefore it is considered as a rigid link between the free end of foundation springs and the hinge zone at the bottom of the column.

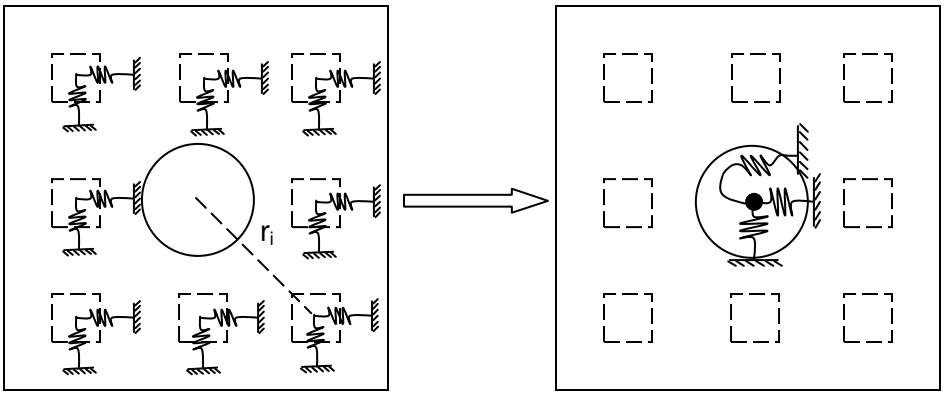


Figure 5.11. Transforming pile stiffnesses into bridge column fixity stiffness

## 5.8 MODELING OF ABUTMENTS

The abutment resistance to lateral and transverse loads are secured by the back wall and two side wings as shown in Figure 5.12. Their stiffnesses are modeled by 11 springs in each horizontal direction while the remaining of degrees of freedoms are restrained. These springs represent the effect of passive soil pressure on walls and piles.

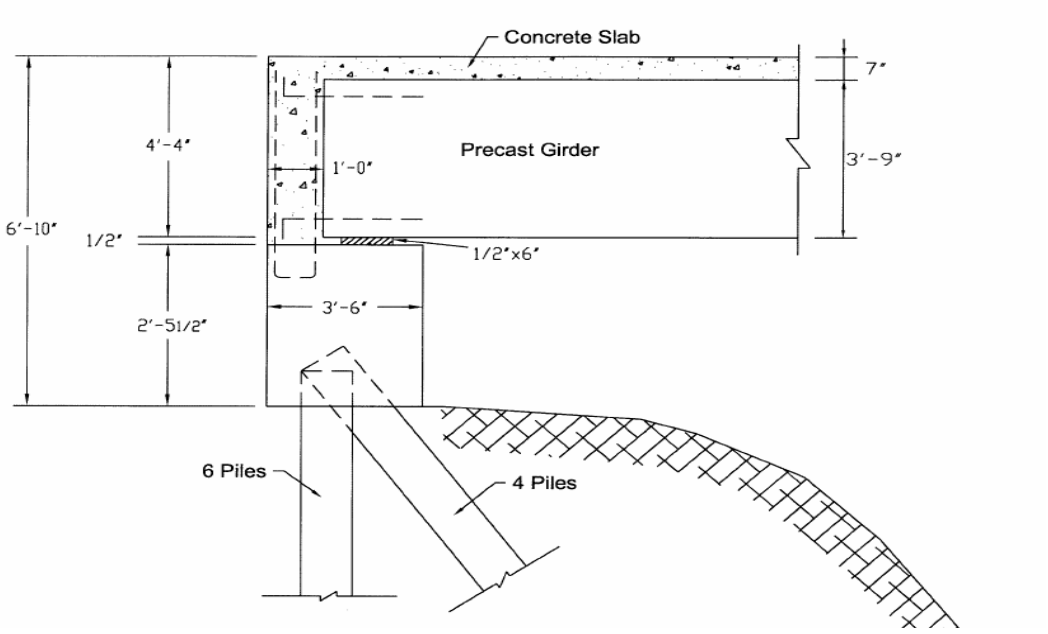


Figure 5.12 Bridge abutment supported by 10 piles, one back wall, and 2 side wing walls

Assuming the ultimate passive soil pressure on the back wall and the side wings is given by the following expression in term of the abutment height H in ft, based on ATC-32(1996) recommendation:

$$p = 7.7\left(\frac{H}{8}\right) \qquad 5.14$$

The contribution of 10 piles to the abutment stiffness is also considered given that the ultimate lateral capacity $f_p$ of a single pile is 60 kips. Assuming that the acceptable

displacement $\delta$ for the concrete pile is 2 in, and the structural response of the abutment system is linear, the transverse stiffness of each spring can be determined by the following equation:

$$k_L = \frac{\left(p\ A_w + n_p\ f_p\right)}{11\,\delta} \tag{5.15}$$

where $A_w$ is the projected side wing area. $n_p$ is the number of piles supporting the abutment foundation, and number 11 refers to the number of springs that model the effect of the abutment on the bridge structure. Similarly, the spring stiffness in the longitudinal direction can be calculated by the following expression:

$$k_T = \frac{\left(p\ A_b + n_p\ f_p\right)}{11\,\delta} \tag{5.16}$$

where $A_b$ is the projected longitudinal area of the abutment. Figure 5.13 is an illustration of abutment modeling by 11 springs in each direction in the horizontal plan. This figure also shows the modeling of bearings at the end of the bridge. The bridge deck, the bearing, the girder, and the cap beam are all connected by rigid elements.

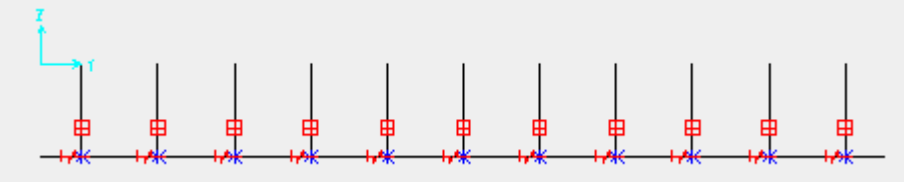

Figure 5.13 Illustration of the abutment modeling

Up to this point of this chapter, we described the modeling of the bridge structure that includes the bridge deck, girders, cap beams, concrete columns, abutments, and the piles foundation. The SAP2000 view of the bridge model is illustrated in Figure 5.14. The

numerical estimation of the model inputs which we will refer to from now on as design values, are based on material analysis as was the case for the hinge zone of the bridge column, or on code recommendations as was the case for the pile foundations. However, these values are highly susceptible to variations due to errors in modeling, uncertainties in the estimation of the controlling parameters, and epistemic uncertainties that are inherent to the model. These variations may reduce the chance of survival of the bridge system in an earthquake event. To address the issue of uncertainties and material and model randomness and evaluate the reliability of the bridge, this thesis will perform a reliability based analysis using the radial sampling method developed in chapter Three of this report. The input required to perform such a reliability analysis includes statistical models for all the pertinent random variables.

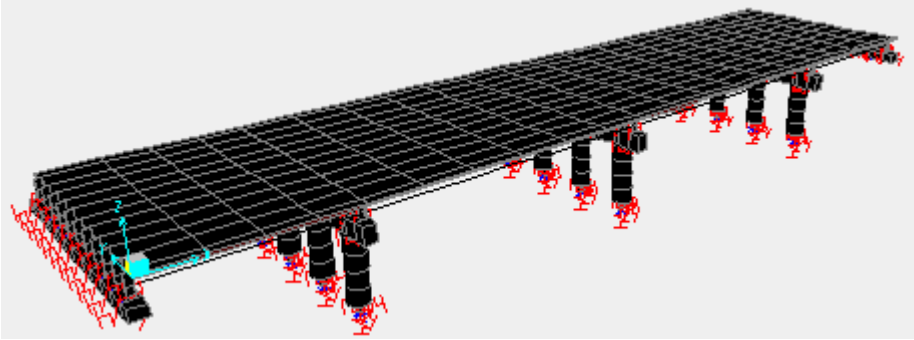

Figure 5.14 General view of bridge model considered in this study

## 5.9 MODELING UNCERTAINTIES IN BRIDGE ELEMENTS

The variations encountered in bridge modeling can be attributed to two types of uncertainties; epistemic uncertainties which are inherent in models due to natural randomness impossible to eliminate, and non epistemic uncertainties which include variability in the parameters that control the behavior of the bridge. In this study, the material and modeling random variables are assumed to follow normal distributions

because of the lack of sufficient data where the mean values are assumed equal to the design values determined in previous sections and the coefficients of variation listed in Table 5.1. The random variables include 110 variables representing the shear stiffness of 55 bearings in two horizontal directions, 55 variables that describe the yield shear strengths of the bearings, and 48 random variables that describe the flexural stiffness in two horizontal directions of hinge zones at the top and the bottom of twelve reinforced concrete columns supporting the bridge substructure. Uncertainties in the 55 shear capacities of the bearings, the 24 shear capacities, and 24 flexural capacities in column hinge zones are included in the analysis. The total adds up to 316 independent random variables for the bridge system.

## 5.10 MODELING OF MEMBER CAPACITIES

The mean value of the shear capacity of each bearing is taken equal to 220 kips which is about 21% higher than its yield strength with a coefficient of variation of 5%. The flexural capacity of column hinge zone is assumed to have a mean value of 100,000 kips extracted from moment curvature diagram illustrated in Figure 5.5 and a coefficient of variation of 11%. The mean value of column shear capacity is calculated based on ACI 318 that states that the shear strength of columns is carried by concrete shear resistance $V_c$, and transverse reinforcement steel resistance $V_s$:

$$V = V_c + V_s \tag{5.17}$$

The concrete shear strength is calculated in terms of concrete strength $f_c^{'}$ in psi, the column gross area $A_g$, and the concrete shear resistance factor k=3.5 using the following expression:

$$V_c = 0.8\, A_g\, k\, \sqrt{f_c^{'}} \qquad 5.18$$

Given a concrete strength equal to 4500psi and column diameter of 5 ft, Equation 5.18 yield concrete shear strength of 664 kips.

The transverse steel shear strength is given by:

$$V_s = \frac{\pi}{2} \frac{A_v\, f_{yh}\, D^{'}}{s} \cot\theta \qquad 5.19$$

Where $A_v$ is the area of a #6 transverse bar. $f_{yh}$ is the yield strength of grade 40 transverse steel bar. $D^{'}$ is diameter of core concrete measured from the hoop center. s=3" is the spacing of the hoops. The crack angle θ is assumed to be $30^o$ as recommended by Priestley et al (1996). Therefore, the transverse shear strength based on Equation 5.19 is 894 kips which will yield when combined with concrete strength a total shear resistance of 1558 kips assumed as the mean value for shear capacity of columns with a coefficient of variation of 12%.

The structural and modeling uncertainties considered in this and the previous sections are summarized in Table 5.1 that includes mean values and coefficients of variation for the assumed random variables. However, the bridge related uncertainties are not the only source of randomness that controls the system reliability. The uncertainties in the seismic input are also very critical for assessing the reliability of the bridge system.

Table 5.1.random variables considered for reliability analysis of the bridge

| Type of Random variables | Considered number of variables | Mean | C.O.V | Distribution |
|---|---|---|---|---|
| Bearing shear stiffness | 110 | 17511(kips/in) | 8% | Normal |
| Bearing yield strength | 55 | 190(kips) | 5% | Normal |
| Bearing shear capacity | 55 | 210(kips) | 5% | Normal |
| Column flexural stiffness | 48 | 13.29 $10^7$(kips/in) | 10% | Normal |
| Column flexural capacity | 24 | 100.000(kips.in) | 11% | Normal |
| Column shear capacity | 24 | 1558(kips) | 12% | Normal |

## 5.11 SEISMIC HAZARD UNCERTAINTIES

The approach for considering seismic uncertainties in the reliability analysis of the bridge system is similar to the approach developed in Chapter 3 for the reliability analysis of the Response Modification Factors of bridge columns. The seismic uncertainties are limited to the moment magnitude $M_w$, epicentral distance R, earthquake intensity, and the record to record randomness. The earthquake intensity contains two terms, a deterministic part dependent on the moment magnitude $M_w$ and the epicentral distance R, and a random part unrelated to $M_w$ and R that follows a lognormal distribution. The variability parameters of the earthquake intensity are determined from Boore model developed for Western U.S (see section 9 of Chapter 3).

## 5.12 DEFINING SYSTEM FAILURE MODES

In a typical structural system, different failure modes can be present where each mode is a combination of different failed structural elements arranged in parallel and series paths (Melchers; 1987). The determination of each path requires defining the structural behavior of the system after each element's failure. However, in practical application of reliability analysis of structural systems, system failure can be defined as the failure of a limited number of structural elements.

In this study, bridge system failure is assumed to occur when any one bearing fails in shear, or any one column hinge zone fails in flexure or in shear. The total number of failure modes is 103 failure modes arranged in series path, which means that any member failure will result in system failure. These failure modes represent those that will be likely to occur when the bridge is seismically loaded in the transverse direction. Specifically, the shear failure of a bearing or a column in the longitudinal direction and the flexural failure of columns about the transverse direction are ignored since these modes of failure are highly unlikely to occur compared to the other failure modes considered for the bridge system of this study.

The failure mode $g_i$ of a structural member i of the bridge occurs when the member response $R_i$ exceeds the member capacity $C_i$ as expressed by the following Equation:

$$g_i(X) = \frac{\left(C_i(X) - R_i(X)\right)}{C_i(X)} \qquad 5.20$$

where X is a vector whose elements are the structural, modeling, and seismic random variables.

Since the bridge system is assumed as a series system where the failure of one member results in system failure, the mathematical representation of the bridge's failure domain is given by:

$$F = \left\{ \min_{1 \le i \le N_F} \left( \left| g_i(X) \right| \right) \ge 0 \right\} \tag{5.21}$$

where | | refers to the absolute value and $F$ is the failure domain. Therefore the probability of system failure will be:

$$P_f = \Pr(F) \tag{5.22}$$

The assessment of the probability of failure given by Equation 5.22 requires the use of an efficient structural reliability method combined with nonlinear dynamic structural analysis to search for the failure surface given implicitly by combining $N_F$ failure surfaces ($g_i$). The Radial Sampling method developed by the author in Chapter 3 of this thesis can be efficiently used for the reliability analysis of the bridge system considered as a multivariate random system where the system failure surface is defined implicitly by different possible modes of failure.

## 5.13 IMPLEMENTATION OF RADIAL SAMPLING METHOD

The mathematical expression for the form of probability of failure can be formulated as:

$$P_f = \int_F P(X).dX \tag{5.23}$$

where $P$ is the probability density of the random vector X composed of material and seismic variables. F is the system failure domain defined by Equation 5.21. Let us define

the structural variables as $X_B$, the seismic variables as $X_S$, and the earthquake intensity variable as $I_n$ so that $X=[X_B, X_S, I_n]$. The expression of Equation 5.23 becomes:

$$P_f = \int_F \left\{ P_{X_S}(X_S) \left[ \int P_{X_B}(X_{M_B}).P_{I_n}(I_n).d(X_B, I_n) \right] \right\} dX_S \qquad 5.24$$

Where $P_{Xs}$ ,$P_{XB}$ , and $P_{In}$ are the probability density functions for the random variables in the vectors $X_S$, $X_B$, and $I_n$ respectively.

The Seismic variables $X_S$ include the moment magnitude $M_w$, and the epicentral distance R, as well as the inherent randomness within the earthquake itself given $M_w$ and R. The probability distributions of $M_w$ and R can be determined using the seismic deaggregation technique available on the USGS web site for any site in the U.S using the altitude and longitude coordinates for the site and a suitable level of hazard limit. The deaggregation provides $(M_{wj},R_j)_{j=1..Ns}$ pairs that are discretely distributed such that their probability densities $(w_j)_{j=1..Ns}$ are given by the percentage contribution of every $M_w$-R pair to the total hazard. Therefore, Equation 5.24 can be written as:

$$P_f = \sum_{j=1}^{N_s} w_j \left[ \int_F W(X).P_{X_B}(X_{M_B}).P_{I_n}(I_{nj}).d(X_B, I_{nj}) \right] \qquad 5.25$$

The subscript j is purposely added to the variable $I_n$ to show that it is a function of the pair $(M_{wj},R_j)$. Thus, the term inside the bracket of Equation 5.25 depends on pair $(M_{wj},R_j)$ and will be designated as $Pf_j$. Equation 5.25 becomes:

$$P_f = \sum_{j=1}^{N_s} w_j \; P_{fj} \qquad 5.26$$

Equation 5.26 suggests that each term $P_{fj}$ can be determined separately for a given set $(M_{wj},R_j)$ using the Radial Sampling method. The application of the Radial Sampling method requires the designation of an important sampling direction in the vector space composed of the material variables $X_B$ and the earthquake intensity $I_n$. In this analysis, the important direction is chosen to be that of the variable $I_n$ which represents the intensity of the earthquake expressed in terms of PGA. Thus, the material variables, $X_B$, represent the subspace perpendicular to the important direction, $I_n$. The subspace will be used to generate unit directional vectors and radial samples while the important direction guides the search for the system's failure surface. The search for the failure point for each set of $X_B$ is carried out by an iterative process illustrated in Figure 5.15. Trials and adjustments of $I_n$ are performed until convergence to a point on the system failure surface that separates the failure domain from the survival domain. This process is repeated for a number of $X_B$ samples $N_s$. Each of the $N_s$ samples provides one value for $I_n$ that lies on the failure surface. This failure point will be designated as $I_n^*$. The value of $I_n$ that fall above $I_n^*$ belongs to the failure zone while the values below $I_n^*$ fall within the safe zone.

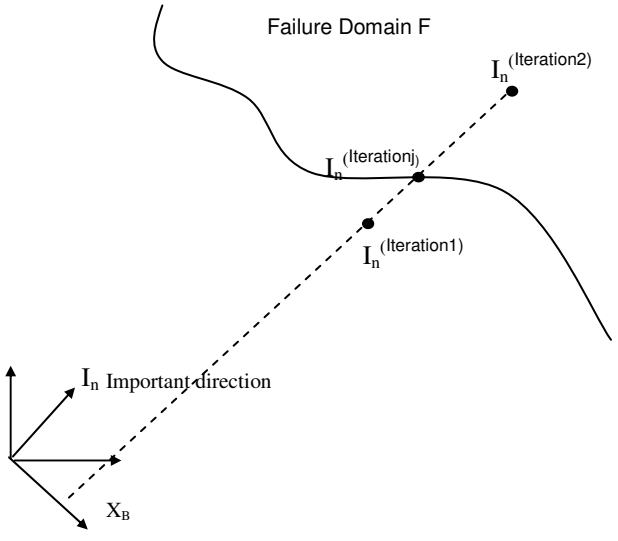


Figure 5.15 Illustration of iterative process guided by $I_n$ direction to search for failure surface.

Recalling from the deaggregation procedure performed in Chapter 4, the earthquake modes selected are those that produce a seismic intensity $I_n$ exceeding a limit hazard value $I_{lim}$. Since $I_n$ follows a lognormal distribution, its unconditional distribution should be scaled to account the imposed condition using the following formula:

$$P_{In} = \frac{\phi(\log(I_n))}{\Phi(\log(I_{\lim}))} \tag{5.27}$$

where $\phi$ and $\Phi$ are the probability density and the cumulative probability of the normal distribution. The logarithmic mean and standard deviation of the earthquake intensity are provided by the attenuation model for a specified bridge site.

If we subdivide the subspace into a total of m $H_k$ zones as described in the Radial Sampling method of Chapter 3, the probability of failure $P_{fj}$ for a given earthquake set $(M_{wj},R_j)$ can be estimated by:

$$P_{fj} \cong \tilde{P}_{fj} = \sum_{k=1}^{m} \tilde{P}_f^k . \Pr(H_k) \tag{5.28}$$

The evaluation of $\Pr(H_j)$ can be executed directly from the cumulative function of the Radial distribution using Equation 4.32. $\tilde{P}_f^k$ is the probability of failure given the subspace samples that belong to zone $H_k$.

$$\tilde{P}_f^k = \frac{1}{N_s} \sum_{i=1}^{N_s} C(I_n) \tag{5.29}$$

where C is the complementary function of the cumulative probability distribution corresponding to the density function given by Equation 5.27. $N_s$ is the number of samples drawn from the subspace of material random variables.

The procedure followed in this study to estimate the probability of failure consists of the following steps:

1- Initiate the process at j=1 for the first earthquake set ($M_{wj}$,$R_j$)

2- Generate 100 normalized earthquake records for ($M_{wj}$,$R_j$), The records are normalized so that the Peak Ground Acceleration is scaled to 1. This step is specifically performed to account for record to record variation for the given set of moment magnitude $M_{wj}$, and epicentral distance $R_j$.

3- Initiate k at 1 for the subspace zone $H_k$ assuming m subspace zones ($H_1$,..,$H_m$).

4- Generate $N_s$ directional vectors in the subspace of the structural random variables.

5- Generate $N_s$ radius samples using Markov Chain algorithm detailed in Chapter 3 of this thesis.

6- By multiplying the directional vectors by the radius samples generated in step 4 and 5, a population of size $N_s$ is created in the region limited by $H_k$.

7- Initiate a loop at i=1 to search for the failure surface in the direction corresponding to earthquake intensity $I_n$.

8- Randomly select an earthquake from the bin created in step 1.

9- Using trial and adjustment, search for the $I_n^*$ value that lies on the failure surface. The search involves performing the structural dynamic analysis in Sap2000 program, and scaling the earthquake peak ground acceleration until the process converges to a value $In_i^*$.

10- Increment i by 1 by setting i=i+1. If i is less than or equal to $N_s$, go to step 8.

11- Calculate the probability of system failure $\tilde{P}_f^k$ given the subspace samples belonging to $H_k$ using Equation 5.29.

12- Increment k by 1 by setting k=k+1.

13- If k is less or equal m go to step 4, otherwise, calculate the probability of system failure associated with earthquake set j.

14- increment j by 1 by setting j=j+1

15- If j is less than or equal the number of $M_w$ and R sets then go to step 2.

16- Using Equation 5.28, calculate the conditional probability of system failure given that an earthquake has occurred.

## 5.14 MODAL ANALYSIS OF BRIDGE SYSTEMS

The modal analysis of a bridge system provides a good insight on the general response of the system which is a combination of all the modal responses. The first 30 fundamental modes are considered for the bridge response analysis. The dominant first mode for deterministic system at the mean values of the random variables is estimated at $T_1$=0.33sec and corresponds to the motion of the integral bridge structure in the longitudinal direction. The second mode is estimated at $T_2$=0.30sec and involves the vertical mid spans motion in unsynchronized manner. The third mode captures the rocking motion of the mid spans at a period of $T_3$=0.29sec. The transverse motion of the integral structure is captured by the fourth mode at a period of $T_4$=0.27sec while the fifth mode provokes the vertical response of the mid spans in a synchronized manner at period $T_5$=0.246sec. The periods of these first five modes are in a range for which the design spectral acceleration of the selected San Francisco site is maximum. These modes are estimated for the mean values of material properties and modeling random variables and are illustrated in Figure 5.16 to 5.21.

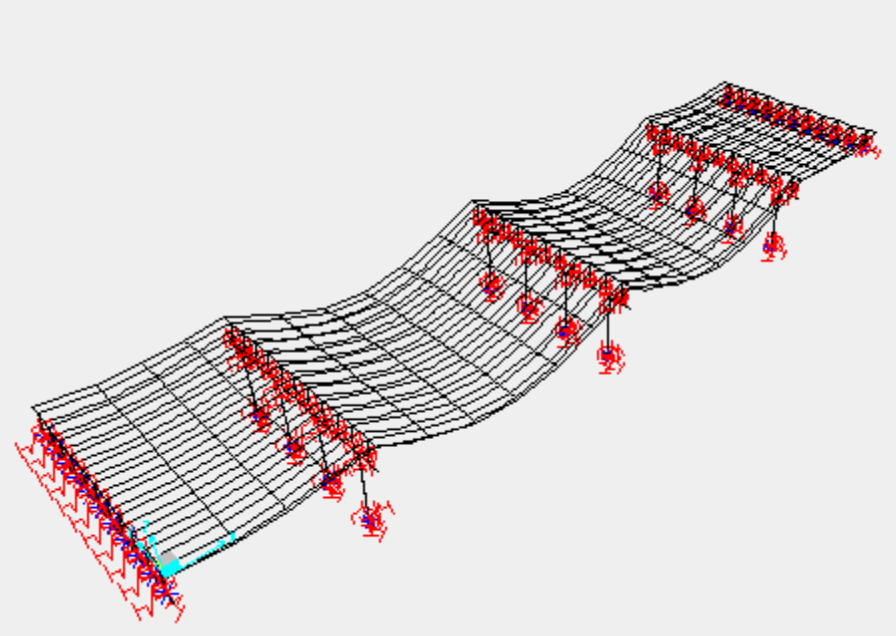

Figure 5.16 Deformed shape of bridge structure at mean values of bridge random variables from combined modes.

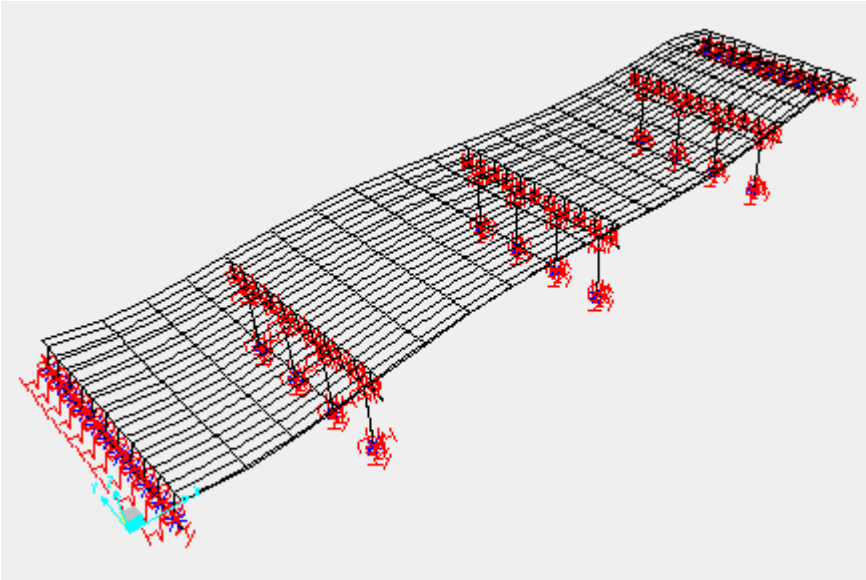

Figure 5.17 First mode at $T_1$ =0.33sec that affects bridge motion in longitudinal direction

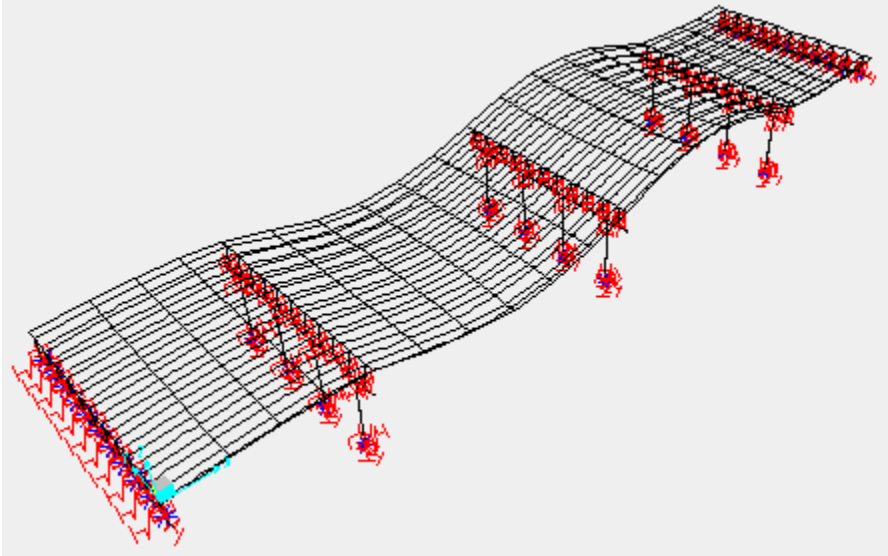

Figure 5.18 Second mode at $T_2$=0.30sec involving the response of the superstructure response in unsynchronized motion of the mid spans

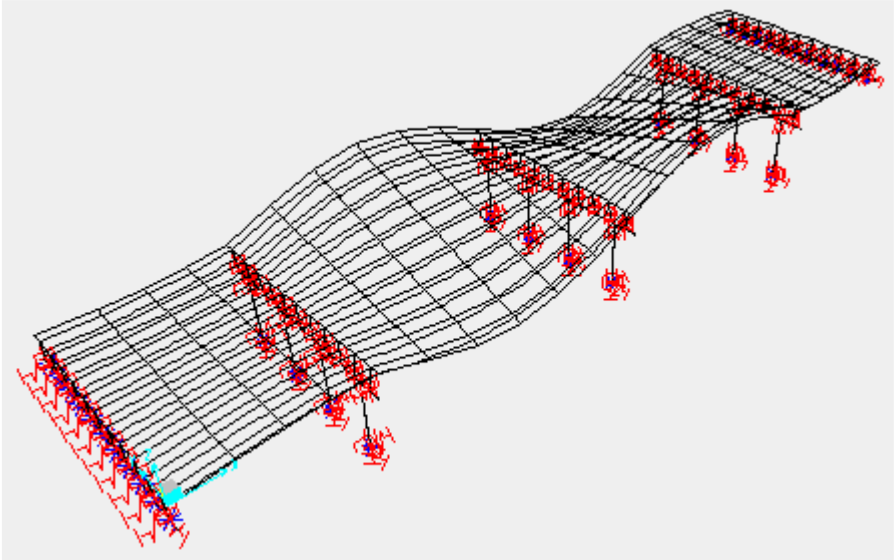

Figure 5.19 Third mode at $T_3$=0.29sec that affects the rocking motion of superstructure

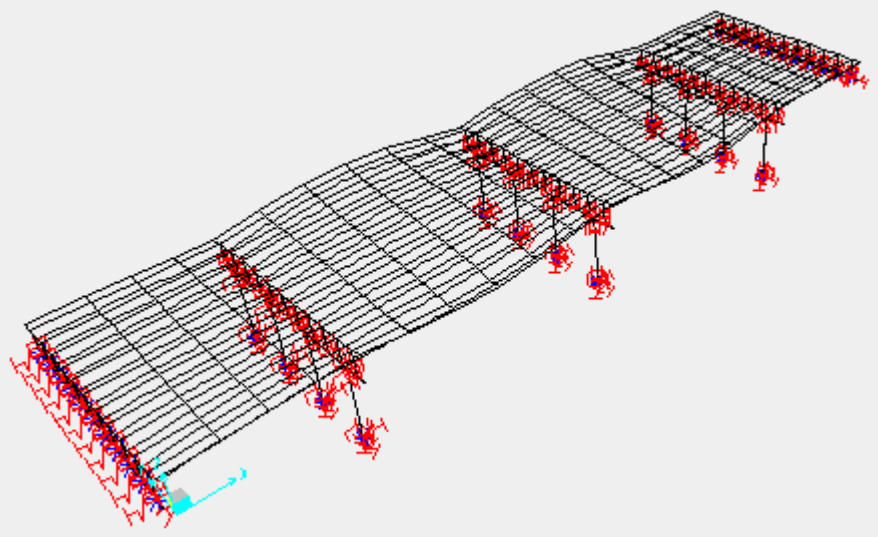

Figure 5.20 Fourth mode at $T_4$=0.27sec which affects the transverse response

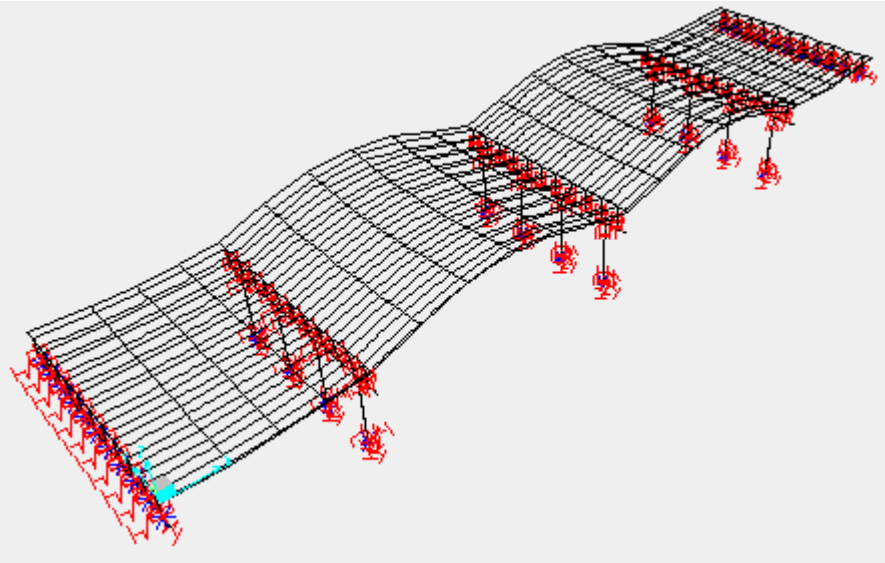

Figure 5.21 Fifth mode at $T_5$=0.246sec which affects the superstructure response in a synchronized motion of the mid spans

## 5.15 SEISMIC HAZARD ANALYSIS FOR SAN FRANCISCO SITE

The Probabilistic Seismic Hazard Analysis (PSHA) is performed to generate earthquake records that have spectral accelerations with a 20% probability of exceedence in 50years. This high percentage is intended to cover all earthquake magnitudes that are

likely to produce significant structural damage. Samples of the ($M_W$, R) pairs for these earthquakes are listed in Table 5.2 along with their percentage contributions to the total hazard. Figure 5.22 provides a histogram of the earthquake mode frequencies.

One hundred synthetic earthquake records are generated for each mode using the program SMSIM-version 2.3 developed by Boore (2002) and the input parameters of a single-corner frequency coastal California model from the file WR032496.datavailable on the USGS web site (Frankel & al 1996)) to represent rock sites.

Table 5.2: Summary of earthquake deaggregation at 20% PE in 50 years for San Francisco (damping ratio=5%)

| Modal Earthquakes | Distance (km) | Magnitude ($M_w$) | Contribution to total Hazard(%) |
|---|---|---|---|
| Mode # 1 | 3.4 | 7.84 | 32.883 |
| Mode # 2 | 3.2 | 7.98 | 15.13 |
| Mode # 3 | 3.3 | 7.44 | 12.167 |
| Mode # 4 | 3.3 | 7.26 | 7.742 |
| Mode # 5 | 3.7 | 7.05 | 4.852 |
| Mode # 6 | 3.3 | 7.69 | 4.232 |
| Mode #7 | 4.3 | 6.65 | 4.162 |
| Mode #8 | 4.5 | 6.84 | 2.704 |
| Mode #9 | 5 | 6.44 | 2.516 |
| Mode #10 | 17.6 | 7.26 | 1.44 |
| Mode#11 | 17.6 | 7.44 | 1.42 |
| Mode#12 | 6.6 | 6.2 | 0.945 |
| Mode#13 | 8.3 | 5.2 | 0.848 |
| Mode#14 | 13.8 | 6.61 | 0.838 |
| Mode#15 | 8.3 | 5.4 | 0.833 |
| Mode#16 | 7.6 | 6.01 | 0.821 |
| Mode#17 | 8.3 | 5.6 | 0.815 |
| | | | Total Contribution 94.35% |

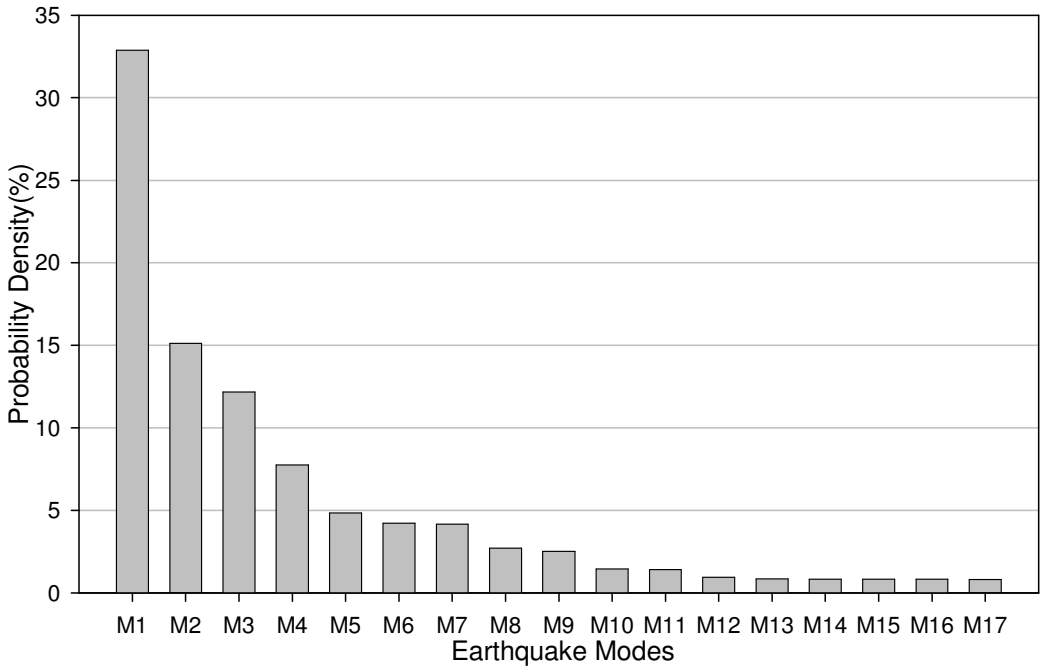


Figure 5.22 Modal Earthquake distribution.

## 5.16 DETERMINISTIC SEISMIC ANALYSIS OF BRIDGE SYSTEM

In order to get quick understanding of the behavior of the bridge and identify the weakest structural elements, in this section, the bridge material properties are assumed to be deterministic taken equal to their mean values. The seismic input corresponds to the first mode earthquake having a peak ground acceleration of 1g that approximately represents a 100-year earthquake. Analysis of the results illustrated in Figure 5.23 shows the safety reserve ratios in bridge structure for all the modes of failure. The safety reserve is calculated as the difference between capacity and demand divided by capacity. The results indicate that the bridge system has a safety margin that varies between 40% and 90% for all possible failure modes which suggests that if a deterministic seismic analysis is considered, the bridge has a considerable safety margin to sustain a 100 year intensity earthquake in the San Francisco area. However, this analysis which duplicates common

practice in seismic engineering has its shortcomings in many aspects. The limitation of the number of earthquakes to less than 10 in engineering practice cannot represent the variation in moment magnitude, epicentral distances as well as earthquake intensities and therefore results in unreliable estimation of the level of reliability of the bridge. The material properties are not deterministic parameters as has been shown in Chapter 3 of this thesis for bridge columns. Ignoring these uncertainties can be critical and may lead to underestimation of bridge safety. The reliability based analysis is certainly a better approach that is rational and consistent with the LRFD philosophy and provides the probability of failure as a measure of the risk that the bridge structure faces in an eventual earthquake event.

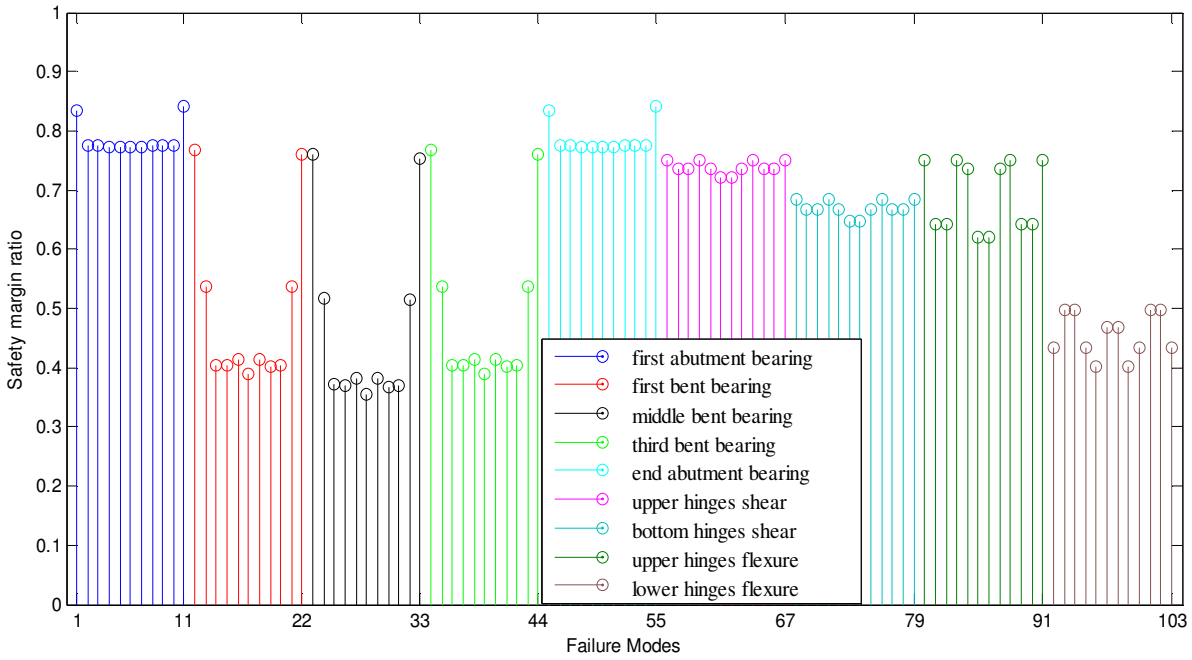


Figure 5.23 Safety margin ratios at the mean point of bridge random variables

## 5.17 PROBABILITY OF FAILURE OF EARTHQUAKE MODES

The destructibility of a bridge due to a particular earthquake mode can be established by calculating the probability of the bridge's failure when subjected to earthquake

excitations generated for that mode. This probability of failure takes into account the probability density for the earthquake mode shown in Figure 5.22. The histogram of Figure 5.24 illustrates the probability of failure of each mode and shows that more than 80% of the bridge system failure is attributed to the first two modes which have relatively high moment magnitudes and shorter distance to the seismic source, and have high probability density compared to the rest of the earthquake modes listed in Table 2. This result can be exploited when seismically analyzing similar bridge structures in the San Francisco area by considering the first three or four most destructive earthquake modes and ignoring the other modes since they don't significantly contribute to the overall probability of failure.

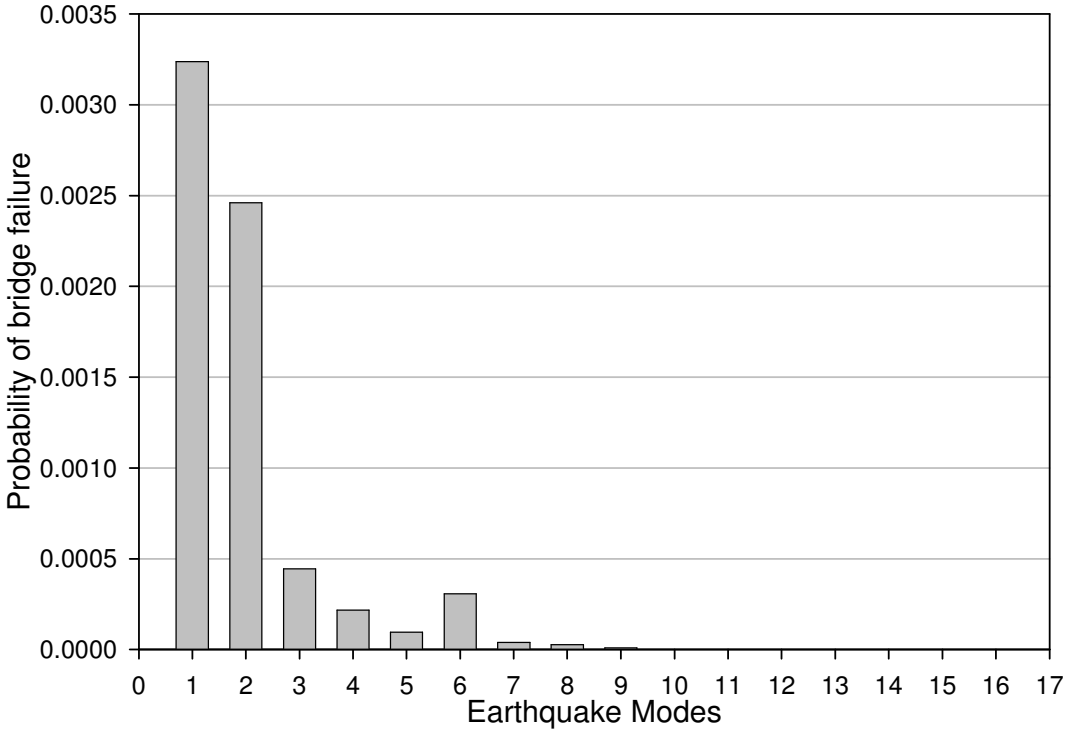


Figure 5.24 Probability of failure for each earthquake mode

## 5.18 PROBABILITY OF FAILURE FOR DIFFERENT FAILURE MODES

The results of the reliability analysis of the bridge system shows clearly that failure due to the formation of flexural hinges at the bottom of the columns are predominant compared to other failure modes including flexural hinges in the upper parts of the columns, and bearing shear failures. Figure 5.25 indicates that the bearings at the abutments don't cause any system failure while the bearings in the external bents contribute with a small percentage to system failure. Bearings of the middle bent contribute more than the other bearings to the probability of failure but their contributions are still negligible compared to the other dominant modes and can be estimated to contribute about 3 to 4% of the total probability of failure. Failure of the columns in shear is practically non-existent while the upper column flexural hinge failures contribute less than 1% to the total probability of failure. Therefore, more than 90% of the probability of failure is due to flexural hinge failures in the lower parts of the columns. The external columns appear to be more vulnerable to earthquake destruction compared to internal columns and contribute almost three times more than the internal columns to the overall probability of failure. This can be explained by the fact that the internal columns are braced at the top from both sides by the girder systems. The results also show that the internal bent columns flexural failure produces double the amount of probability of failure of the external bent columns. The results also reflect on the average the symmetry of the bridge system in both transverse and longitudinal directions since the probability of failure of the two external columns are practically the same.

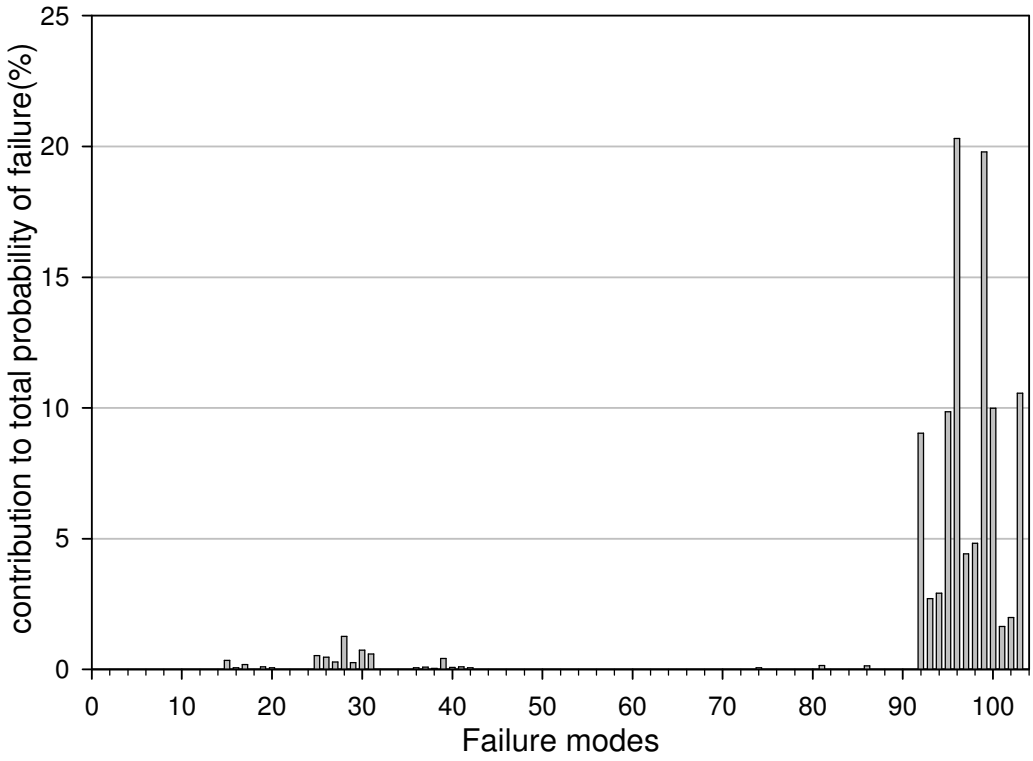


Figure 5.25 Percentage contributions of failure modes to total probability of failure

## 5.19 ESTIMATION OF STRUCTURAL RISK OF THE BRIDGE SYSTEM

The conditional probability of failure for the bridge is estimated at $6.84.10^{-2}$. This value is obtained by summing over all the modal probabilities of failure assuming the occurrence of the earthquake. This probability of failure value can be interpreted as indicating that if an earthquake hits at the bridge location; there is 93.16% chance that the bridge will survive. However, the interpretation doesn't include the probability of occurrence of an earthquake event.

The earthquake modal distribution assumes a rate of occurrence of 1 event in 250 years return period which corresponds to 20% Probability of exceedence in 50 years. Using a Poisson distribution model for earthquake occurrences as explained in Chapter 4 of this report, the probability of occurrence of an earthquake is calculated for different

life time periods of the bridge structure as illustrated in Table 5.3. The reliability index β is calculated such that $P_f = \Phi^{-1}(-\beta)$, where $\Phi^{-1}$ is the inverse of the cumulative normal probability distribution.

Table 5.3**:** Probability of failure and reliability index for various time exposure

| **Time of exposure** | **Pr(EQ)** | **$P_f$** | **Reliability index, β** |
|---|---|---|---|
| **1 year** | 0.004388 | $3.10^{-4}$ | 3.43 |
| **20 years** | 0.083258 | $5.7\ 10^{-3}$ | 2.53 |
| **50 years** | 0.192293 | $1.32\ 10^{-2}$ | 2.22 |
| **75 years** | 0.270884 | $1.185\ 10^{-2}$ | 2.08 |
| **100 years** | 0.340101 | $2.33\ 10^{-2}$ | 1.99 |

From Table 5.3, the bridge has a reliability index β=3.43 for one year exposure, 2.53 for a 20 year exposure, 2.22 for a 50 year exposure, 2.08 for a 75 year exposure, and 1.99 for a 100 year exposure. These values can be enhanced to increase the chance of survival and meet the life time criteria of the bridge structure by rehabilitating the failure modes that contribute most to bridge failure. The information produced by the reliability analysis can play a critical role in developing a rational approach to rehabilitate the bridge by targeting the most vulnerable parts of the bridge.

## 5.20 SENSITIVITY OF BRIDGE RESPONSE TO FOUNDATION STIFFNESS

Due to the fact that the foundations are impossible to inspect, bridge codes such as the AASHTO code recommend that the foundation should remain elastic for all types of loading including earthquakes. This elastic design makes the bridge foundation highly unlikely to fail in an earthquake loading as confirmed by field observations.

To better understand the effect of the foundation modeling on this bridge's responses, the foundation stiffnesses are varied around the nominal value by $\pm 25\%$. When the stiffnesse are increased by 25%, the three dominant natural periods of the bridge decreased from 0.33 sec, 0.3 sec, and 0.29 sec to 0.3 sec, 0.27 sec and 0.26 sec for the first three modes respectively. Similarly when the stiffnesses are decreased by 25%, the natural periods of the bridge increased to 0.37 sec, 0.33 sec, and 0.32 sec for the first three modes. These results show negligible effect of the variations in the foundation stiffnesses on the bridge natural modes.

To investigate the effect of the foundation of failure modes in the bridge system, the bridge is subjected to one typical earthquake record after varying the foundation stiffnesses by $\pm 25\%$. The differences in the responses of critical members due to the higher and lower stiffnesses are divided by the member capacities in order to obtain a normalized sensitivity measures. Figure 5.26 illustrates the effect of the foundation stiffnesses on the response of the critical members which define the dominant failure modes. The figure shows the maximum change in the response/capacity ratio is on the order of 5% for the 50% variation in the stiffnesses. The results show that the foundation effect is minimal and the uncertainties in foundation stiffness do not affect the probability of failure of the bridge critical members.small. However, its variations can be incorporated as uncertainties in additional random variables if enough data is available to realistically interpolate its statistical parameters.

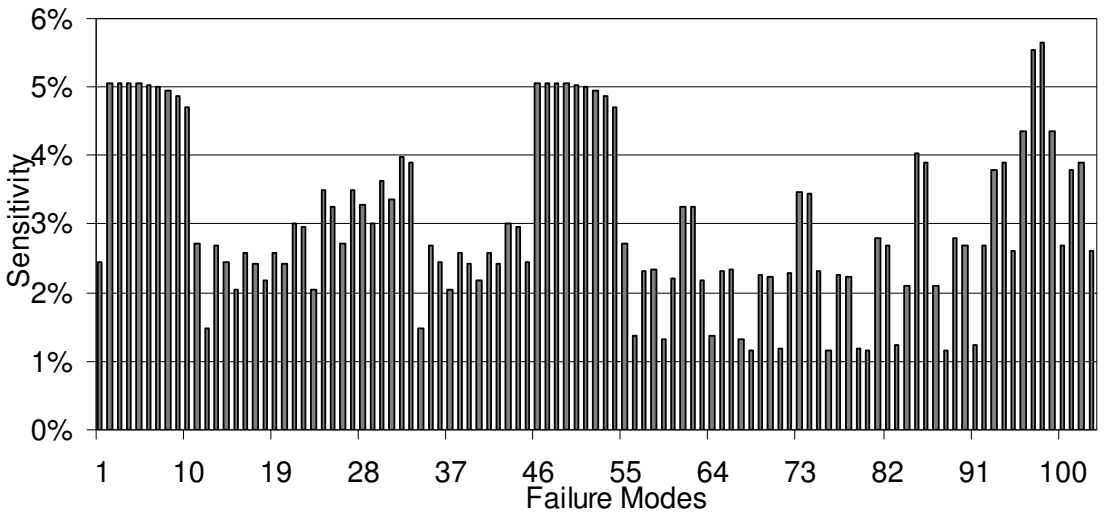


Figure 5.26 Sensitivity of failure modes responses to the foundation stiffnesses

## 5.21 CONCLUSION

In this Chapter, we demonstrated how the Radial Sampling method can be applied to a bridge structural system subjected to earthquake loading. The model developed herein takes into account the seismic variabilities, and material randomness in a similar manner to that developed for the reliability analysis of the bridge columns described in Chapter 4. The Radial Sampling method used in this process was able to provide valuable information on each failure mode as well as its contribution to the overall probability of failure. For the hypothetical bridge considered in this study, it was found that if an earthquake hits the San Francisco area, the bridge is likely to fail due to plastic hinges at the bottom of the columns. However, that may not be the case for other bridges in the vicinity of this site or for other bridge configurations. The detailing of bridges may reveal different dominant modes of failures. The results hence provided by the Radial Sampling method can be exploited to develop a rational rehabilitation plan to enhance the chances of survivability of bridges by targeting the bridge members responsible for the dominant

failure modes. The results can also be used to set a preparedness plan that identifies the critical bridge members in case of a seismic event. Alternatively, the model can be used to focus bridge inspections on critical members in order to expedite the repair process after a seismic event and quickly reopen the stricken bridge to traffic.

# *Chapter 6*

# *CONCLUSIONS AND RECOMMENDATIONS*

## THESIS SUMMARY

This thesis developed the Radial Sampling method to estimate the probability of failure of structural systems with high numbers of random variables. The study showed that the proposed method significantly improves the convergence rate of the Monte Carlo Simulation when estimating small probabilities of failure. The proposed method also is considerably more accurate than the FORM algorithm and the Response Surface Methods particularly when solving structural system reliability problems with multiple failure modes.

The application of the Radial Sampling method to a multi-dimensional stochastic example revealed that the proposed method is most efficient when the probability of failure is in the range of $10^{-1}$ to $10^{-4}$. Another advantage of the Radial Sampling method when compared to the Stepwise methods is in the considerable reduction in the effort required during the Markov Chain sampling process. The one-dimensional Markov Chain sampling employed in the proposed method reduces the correlation between successive

samples compared to the multidirectional Markov Chain sampling used in the Subset and the Stepwise methods.

The proposed method was applied to perform the reliability analysis of nonlinear dynamic problems. The results of the analysis are used to recommend rational values for the Response Modification Factors normally used for the force based seismic design of simple structures. Previous studies have shown that the Response Modification factors for bridge columns are related to column ductility and recommendations have been made to select the appropriate factor based on the period of the system as well as the ductility of the member. However, these recommendations were based on average values and ignored the large variability of this factor, which is due to the random nature of seismic input as well as the material uncertainties and modeling errors. In order to recommend rational values for the Response Modification Factors of bridge columns, this study proceeded to study the material variabilities inherent in R C bridge columns and the modeling errors introduced by normally employed hysteretic analysis models. Based on experimental data from available R C columns tests, the uncertainties in estimating column stiffness and strength were studied and their mean values, standard deviations, as well as their distributions were identified. The test data were also used to identify the modeling errors introduced by Takeda model for cyclic loading. The damage uncertainties in Park & Ang model were extracted based on their studies conducted on a large number of test data.

The response modification factors recommended by the proposed reliability analysis are calibrated to meet a target reliability index. Thus, the calibration approach is

consistent with the concepts of LRFD, which form the bases of modern structural design codes.

Finally, the Radial Sampling method was applied to study the reliability of a typical bridge system subjected to earthquake loadings. The reliability analysis took into consideration the seismic variabilities as well as material randomness. The presence of multiple modes of failure in the bridge systems is successfully handled by the Radial Sampling method which led to the extraction of valuable information about the reliability of the bridge system as a whole and the reliability of individual members as well.

## THESIS CONTRIBUTIONS

The development of the Radial Sampling method proved its efficiency when applied to the seismic risk analysis of R C bridge columns. This method is found to reduce the computational effort during the Markov Chain process and it considerably improves the efficiency of obtaining the probability of failure of structural systems as compared to the more classical methods such as Monte Carlo and First Order Reliability Methods.

Furthermore, the new approach is found to be successful in estimating the modal probabilities of failure. The issue of finding individual modes of failure was not addressed in recently developed methods such as stepwise method and subset method.

This thesis also developed a rational approach that leads to appropriate selection of response modification factors for the force based design methodology. The proposed approach is consistent with the LRFD philosophy which is the basis of modern design codes.

During the process of developing the proposed approach, material uncertainties inherent in reinforced concrete columns are extracted based on actual data. The probability densities that describe the uncertainties in column stiffness, column yield strength, and the Damage Index as well as hysteretic analysis parameters are determined and incorporated along with the seismic uncertainties into the reliability analysis.

In order to analyze the seismic risk to bridge systems, this study developed a reliability model based on the Radial Sampling method. The proposed approach is able to identify a bridge system's weaknesses by providing individual probabilities of failure for each mode of failure as well as an overall assessment of the system's seismic risk.

This rational method overcomes the inconsistencies of the deterministic analysis approach as it identifies and provides accurate seismic risk assessments of the weakest members which can be targeted for rehabilitation in order to enhance the chances of bridge survivability in case of seismic event and uniformly distribute the structural seismic risk over the bridge members.

## RECOMMENDED FUTURE RESEARCH

Although this thesis has achieved its objective in developing a new reliability model that is applicable for the nonlinear dynamic analysis of structural systems subjected to seismic input, more research can be devoted to the following topics:

1) The radial sampling method developed in this study was applied to two different actual structural reliability problems, namely the calibration of response modification factor and the structural risk assessment of bridge systems. However, this method is based on subdividing the subspace normal to the important direction into different zones

within preset boundaries. Future studies can be devoted to investigate the optimal subdivision of the domain in order to improve the efficiency of the method.

2) The reliability based calibration approach of the response modification factor developed in this study can be used to develop a set of response modification factors for the different seismic zones within the USA. This information will provide a uniform seismic risk to bridge columns throughout the United States.

3) The response modification factors determined in this study for San Francisco, Seattle, New York, Memphis, and Los Angeles are based on rock conditions. The AASHTO design code suggests the use of adjustment factors to account for the soil conditions at bridge sites. These soil factors can be investigated and calibrated with the approach used for the response modification factor proposed by this study.

4) The structural risk assessment analysis of the bridge system under seismic loading developed in this study is proven to be a rational method to analyze the safety of bridge members as well as the bridge system. However, the uncertainties used in this model are assumed values that should be further refined to reflect as close as possible the actual uncertainties that exist in bridge systems.

# *Appendix A*

# *Monotonic Analysis Of R-C Bridge Columns*

## A.1 INTRODUCTION

The reliability-based approach that is developed in this study to calibrate the response modification factor for appropriate force based design method is performed based on the Park and Ang damage index (Park & Ang; (1985). On the other hand, the moment ductility analysis of RC columns subjected to combined flexure and axial load can provide an assessment of their capacity to sustain damage when subjected to seismic motions. For seismically active sites, the displacement based design methodology requires an estimation of the member monotonic ductility to ensure that the ductility capacity exceeds demand. One way traditionally used to check this capacity is by studying the monotonic moment curvature relationship in the nonlinear stage until failure. For bridge structures where columns carry very high axial loads, the effect of the axial force must also be included in the analysis. This Appendix reviews methods to obtain the moment curvature relationships of concrete bridge columns using realistic constitutive laws that accurately trace the stress-strain paths of the reinforcing steel, and plain or

confined concrete. The analysis is further extended to obtain the force deformation relationship. Considering different failure limit states such as the fracture of the first longitudinal steel bar, or reaching the ultimate compressive strain in concrete, the ductility capacity of a designed column can be deduced. This information can be used on its own to obtain nominal estimates of member capacity or can be incorporated into more advanced probabilistic models to assess the reliability of bridge columns subjected to EQ motions.

## A.2 STRESS-STRAIN MODEL FOR REINFORCING STEEL

A stress-strain model for reinforcing Steel has been proposed by Mander (1984) for mild steel. The form of the monotonic stress-strain curve is symmetric for tension and compression and is expressed in three piecewise functions as follows.

**a)** Elastic branch $\left(0 \le \varepsilon_s \le \varepsilon_y\right)$

The stress-strain relationship prior to yielding is given by:

$$f_s = E_s \varepsilon_s \qquad \text{A.1}$$

Where $E_s$ is the elastic young modulus.

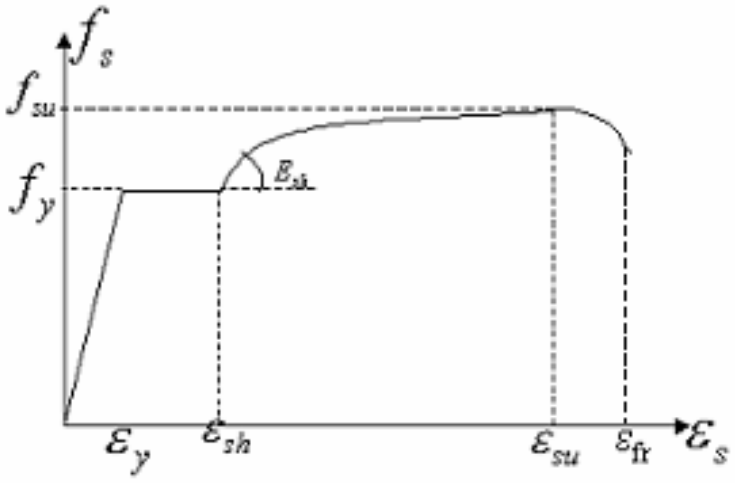


Figure A.1 Monotonic stress-strain curve for mild steel

**b)** Yield plateau $\left(\varepsilon_y \le \varepsilon_s \le \varepsilon_{sh}\right)$

In this range starting from the yield point to the beginning of the strain hardening phase when $\varepsilon_s = \varepsilon_{sh}$. The stress remains constant equal to the yield stress:

$$f_s = f_y \tag{A.2}$$

**c)** Strain hardened branch $\left(\varepsilon_{sh} \le \varepsilon_s \le \varepsilon_{su}\right)$

The strain-hardened branch commences when the strain increases above $\varepsilon_{sh}$ and extends to the ultimate strain $\varepsilon_{su}$. The ultimate strain is defined as the strain at which the ultimate stress occurs. After this point, the stress decreases while the strain increases until the fracture of the steel occurs at $\varepsilon_{sf}$. Mander (1984) proposed an equation for the strain hardened curve between the points $\left(\varepsilon_{sh}, f_y\right)$ and $\left(\varepsilon_{su}, f_{su}\right)$, based on the interpolation polynomial function, the stress-strain relation is of the form:

$$f_s = f_{su} + \left(f_y - f_{su}\right)\left|\frac{\varepsilon_{su} - \varepsilon_s}{\varepsilon_{su} - \varepsilon_{sh}}\right|^p \tag{A.3}$$

where p is the strain-hardening power and is calculated by differentiating Equation A.3 to get the tangent modulus $E_{sh}$ at the initial point $\left(\varepsilon_{sh}, f_y\right)$:

$$E_{sh} = p\left(\frac{f_{su} - f_y}{\varepsilon_{su} - \varepsilon_{sh}}\right) \tag{A.4}$$

Therefore, $p$ is expressed as:

$$p = E_{sh}\left(\frac{\varepsilon_{su} - \varepsilon_{sh}}{f_{su} - f_y}\right) \tag{A.5}$$

The stress-strain behavior of steel bars is illustrated in Figure A.1.

## A-3 STRESS-STRAIN MODEL FOR CONCRETE

Many studies proposed different models describing the monotonic behavior of concrete. Kent & Park(1971), Sheikh & Uzumeri(1979), Shah & al (1982), Mander & el(1983), have proposed models to describe the effects of confinement on concrete strength. These models showed good agreements with experimental results. The monotonic analysis of RC columns in this study uses Mander model (1984) which is detailed in what follows.

The stress-strain compression curve for both confined and unconfined concrete is illustrated in Figure A.2 and follows the equation suggested by Popovics(1973):

$$f_c = \frac{f'_{cc} x r}{r - 1 + x^r} \qquad \text{A.6}$$

In which:

$$x = \frac{\varepsilon_c}{\varepsilon_{cc}} \qquad \text{A.7}$$

$$r = \frac{E_c}{E_c - E_{\sec}} \qquad \text{A.8}$$

$$E_c = 5000\sqrt{f'_{co}} \qquad f'_{co} \text{ in Mpa} \qquad \text{A.9}$$

$$E_{\sec} = \frac{f'_{cc}}{\varepsilon_{cc}} \qquad \text{A.10}$$

where $f'_{cc}$ is the maximum longitudinal compressive stress of the stress-strain curve for confined concrete. $\varepsilon_{cc}$ is the strain at peak concrete stress. $E_c$ is the initial elastic modulus of concrete. $f'_{co}$ is the unconfined compressive strength of concrete. $f_c$ and $\varepsilon_c$ are respectively the concrete compressive stress and strain. Mander et al (1984) proposed

equations that estimate the strength of confined concrete $f_{cc}^{'}$ and the corresponding strain $\varepsilon_{cc}$. These parameters depend on the mechanical properties of transverse hoops and amount and type of confinement as follows.

$$f'_{cc} = f'_{co}\left(-1.254 + 2.254\sqrt{1 + 7.94\frac{f'_l}{f'_{co}}} - \frac{2f'_l}{f'_{co}}\right) \quad \text{A.11}$$

$$\varepsilon_{cc} = \varepsilon_{co}\left(1 + 5\left(\frac{f'cc}{f'_{co}} - 1\right)\right) \quad \text{A.12}$$

where $f'_l$ is the effective lateral confining stress given by:

$$f'_l = k_e \frac{(2+\sqrt{2})A_{sb} f_{yh}}{s_h h''} \quad \text{A.13}$$

where $f_{yh}$ is the yield strength of transverse reinforcing steel, $A_{sb}$ is the hoop bar cross section area, $s_h$ is center to center spacing of hoop sets and $k_e$ is the confinement effectiveness coefficient and is determined from:

For circular cross sections with circular hoops: $k_e = \frac{(1-0.5\,s'/d_c)^2}{1-\rho_{cc}}$ A.14-a

For circular cross sections with circular spirals: $k_e = \frac{1-0.5\,s'/d_c}{1-\rho_{cc}}$ A.14-b

For rectangular cross sections: $k_e = \frac{(1-0.5\,s'/b_c)(1-0.5\,s'/h_c)\left(1-\sum_{i=1}^{n}\frac{w_i'^2}{6b_c h_c}\right)}{1-\rho_{cc}}$ A.14-c

in which $s'$ and $w'_i$ are respectively the clear spacing between hoop sets and longitudinal reinforcing bars that are supported by the corner of a hoop or by a cross-tie. $d_c$ is the core

diameter of a section confined with a circular hoop or spiral. $b_c$ and $h_c$ are the core side dimensions of a rectangular cross section.

Mander & al (1984) found that the effect of confinement on concrete strength and the overall performance of concrete is significant. Figure A.2 shows the gain in strength and the enhancement in performance for confined concrete compared to plain concrete. The transverse reinforcement that provides the confinement to the concrete also increases the shear resistance of the column to the horizontal forces applied at the top of the bridge column.

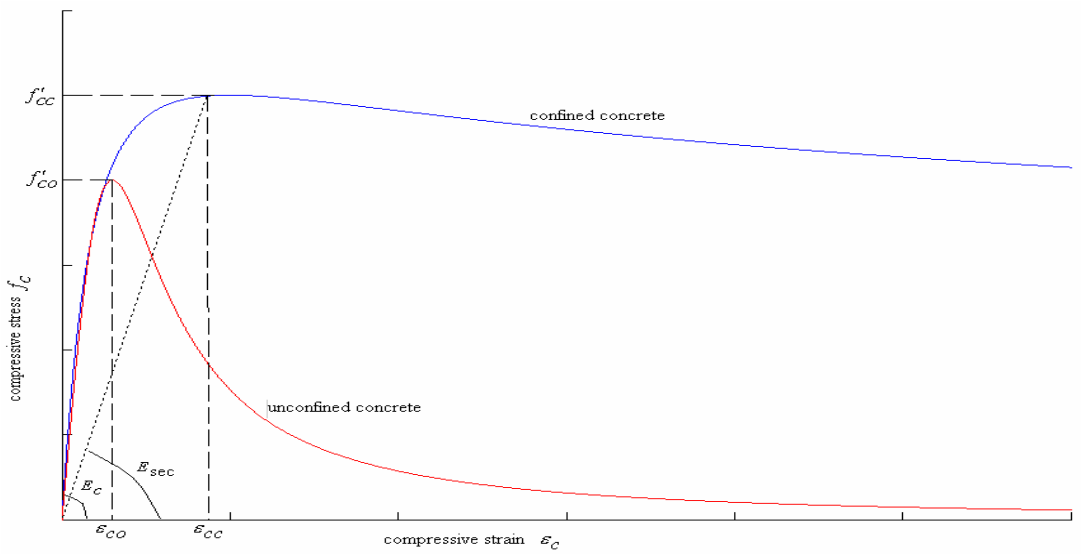


Figure A.2 Typical stress-strain curves of plain and confined concretes

## A-4 INELASTIC BUCKLING OF LONGITUDINAL REINFORCING BARS

The effect of inelastic buckling on the monotonic and cyclic behavior of reinforcing steel has been extensively studied by Monti and Nuti (1992). They conducted series of monotonic and cyclic tests on steel bars for different ratios of bar length *L* and diameter *D*. from those experiments, it was observed that for *L/D* ratio less than or equal to 5, the

bars showed no sign of inelastic buckling and the stress-strain curve for these bars practically coincides with the tensile monotonic curve. For ratios of *L/D* from 5 up to 8, only a short portion of the stress-strain curve after yielding coincides with the tensile monotonic curve. This curve generally deviates from the monotonic curve toward lower values. The stress-strain curve for the bars with ratio *L/D*=11 produces lower stress values compared to the tensile curve as soon as yielding is reached. Monti and Nuti (1992) proposed the following empirical relation for $5 < \frac{L}{D} \le 11$:

$$\gamma_s = \frac{11 - \frac{L}{D}}{e^{c(L/D)} - 1} \qquad \text{A.15}$$

where $\gamma_s$ is the strain range where the difference between the stress-strain curve and tensile curve is less than 5%, i.e $\gamma_s = \varepsilon_{5\%} - \varepsilon_y$.

when the ratio L/D is greater than the critical value $(L/D)_{cr}$=5, inelastic buckling is observed and a softening branch appears after yielding with slope $b^-$ proposed by Monti and Nuti (1992) to be:

$$b^- = a\left[\left(\frac{L}{D}\right)_{cr} - \frac{L}{D}\right] \qquad \text{A.16}$$

Where a is the secant slope ratio and found to be a=0.006.

## A-5 LOW CYCLE FATIGUE OF LONGITUDINAL REINFORCING BARS

Under seismic motion, the longitudinal reinforcing bars of concrete columns undergo repeated tension and compression strain reversals of various amplitudes. As a result, low cycle fatigue can provoke the fracture of the bars and therefore the failure of the

structure. Mander (1993) conducted experimental fatigue tests of steel bars with different strain amplitudes for seismic applications in medium and high-seismic-risk zones. These tests show common phenomena for small amplitude tests as described in the following paragraphs.

The strength of steel drops in the beginning due to cyclic softening or hardening until a saturation state is reached. During this stage the maximum strength remains at a constant level for repeated cycles until a fatigue crack forms. Then, a rapid drop in maximum stress is observed followed by a complete fracture of the bar. The number of cycles at fracture referred to as $N_f$ is found to be large for small amplitude tests ($\varepsilon_a < 0.02$). For large strain amplitude tests where $\varepsilon_a > 0.02$, the drop in the maximum stress of the specimen was observed to be continuous and no stabilized behavior is exhibited. The corresponding number of cycles at fracture is found to be low.

The fatigue life of steel material, in term of number of cycles, can be related to the strain amplitude $\varepsilon_a$ by the Coffin-Manson relationship Monti and Nuti (1992):

$$\varepsilon_a = \frac{\sigma_f^{'}}{E}(2N_f)^b + \varepsilon_f^{'}(2N_f)^c \qquad \text{A.17}$$

The first term in Equation A.17 is the contribution of the elastic strain component to the fatigue strain amplitude $\varepsilon_a$, while the second term is the contribution of the plastic strain component to $\varepsilon_a$. The values of material fatigue constants as reported by Mander (1993) are $\frac{\sigma_f^{'}}{E}$=0.008, b=-0.14, $\varepsilon_f^{'}$=0.08 and c=-0.5.

## A-6 MONOTONIC MOMENT-CURVATURE RELATIONSHIP

The stress-strain relationships of steel and concrete described in sections 2 & 3 of this Appendix are used to derive the theoretical moment-curvature diagram for concrete columns subjected to both flexure and axial loads. The basic assumption in this analysis is that plane sections before bending remain plane after bending. This assumption implies that the distribution of the strain over the cross section remains linear as shown in Figure A.3. Therefore, the strain distribution can be obtained using the material constitutive models.

In this study, a computer program is developed to provide monotonic moment curvature diagrams for typical circular or rectangular bridge columns as described in this section. The strain at depth y from the extreme compressive fiber is written in terms of $\varepsilon_{comp}$ and depth of neutral axis c as:

$$\varepsilon_c = \frac{c - y}{c} \varepsilon_{comp} \qquad \text{A.18}$$

The strain at distance y from the top of the cross section, which is given by Equation A.18 is plugged into the constitutive laws given by Equation A.6 for concrete, and Equations A.1, A.2, and A.3 for steel. The resulting internal force is then calculated by integrating stresses over the cross section Using Simpson's rule. This step is repeated with the adjustment of the neutral axis location c until the resulting force is within a tolerance error with the applied axial force (force equilibrium principle). Once the location of the neutral axis is found, the moment resultant in the cross section is computed using Simpson's rule again by integrating:

$$M = \int y.\sigma.dA \qquad \text{A.19}$$

where $\sigma$ and $dA$ are respectively the stress and the infinitesimal area at a distance y from the top of the cross section. The corresponding curvature is calculated using the following formula:

$$\phi = \frac{\varepsilon_{comp}}{c} \qquad \text{A.20}$$

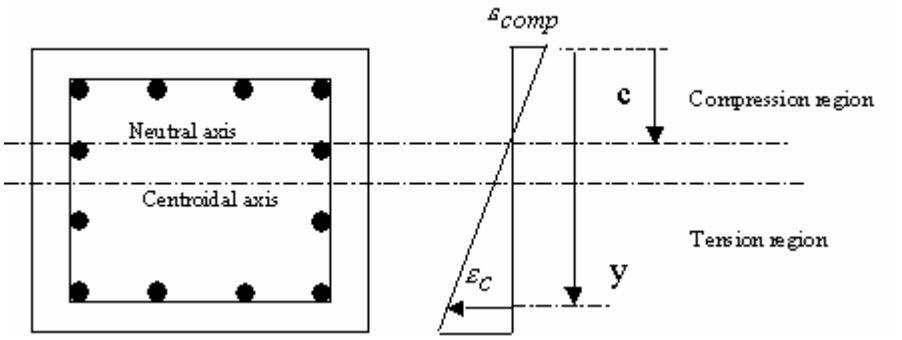


Figure A.3 Linear strain distribution assumption for rectangular cross section

## A-7 YIELDING AND FAILURE DISPLACEMENT

The yielding point is simply defined as the point where the first yield occurs in a longitudinal reinforcing bar. At this point and under the assumption that the column is considered as fixed-free as shown in Figure A.4, the yielding displacement can be expressed as follows:

$$\Delta_y = \frac{\phi_y L^2}{6} \qquad \text{A.21}$$

where $\phi_y$ is the curvature at yielding. L is the length of the column.

The failure of the column is defined as the point where the moment falls back and the moment is 80% of the maximum moment reached at the ultimate point. Although this definition has been commonly used, in reality experimental investigations conducted by

Mander (1984), and Lehman & Moehle (2000) proved that column failure is difficult to predict because it can occur in different modes due to:

-Stirrup fracture.

-Longitudinal bar fracture.

-Concrete crushing.

-Failure due to gradual loss of strength.

-Buckling failure of longitudinal bar.

Many studies have shown that two major zones develop along the column length (Mander; 1984), (Zahn; 1986), (Soesianawati; 1986), (Lehman&Moehle; 2000). The first zone is the hinge region, which develops near the base of the column; The second zone extends from the hinge limit to the top of the column.

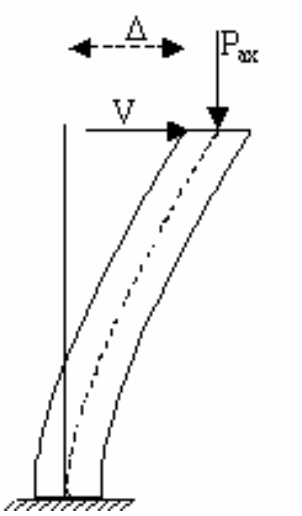


Figure A.4 Bridge column under axial force and uniaxial loading

For a typical concrete column fixed at the bottom, subjected to experimental reversal loading, the damage generally started with cracking of the concrete cover above the footing-column interface (Lehman&Moehle 2000, Kunnath et al 1997). The length of the cracked region increases and spreads followed by the yielding of the first longitudinal

bar. Then, spalling of the unconfined concrete initiates and develops over the hinge length $L_p$ until the maximum moment is reached. At this stage, the hinge is completely formed allowing a partial rotation of the column, and the moment drops down until complete failure occurs caused by any of the failure modes previously listed.

## A-8 FORCE DEFORMATION ANALYSIS

In the previous section, we developed the moment curvature relationship for uniaxial bending under axial load. In this section, we will present a methodology developed by Mander (1994) for deformation assessment based on the moment curvature relationship. It consists of expressing the total deformation in terms of the elastic flexural deformation, $\Delta_e$, the plastic flexural deformation, $\Delta_p$, the elastic shear deformation, $\Delta_{se}$, and the plastic shear deformation, $\Delta_{sp}$, as shown in the following equation:

$$\Delta = \Delta_e + \Delta_p + \Delta_{se} + \Delta_{sp} \qquad \text{A.22}$$

Each of those components is described in detail in what follows for a cantilever column.

### A.8.1 Elastic Flexural Deformation

The flexural deformation at the top of the column is found by taking the first moment of the curvature:

$$\Delta = \int_0^L x.\phi(x).dx \qquad \text{A.23}$$

The moment at any distance from the bottom is found to be:

$$M_x = \frac{M_o}{L} x \qquad \text{A.24}$$

where L is the length of the column, $M_o$ is the moment at the bottom of the column, which equals VL, where V is shear force as shown in Figure A.5. By substituting the variables, the relationship given in Equation A.23 can be expressed in terms of the moment M as:

$$\Delta = \frac{L^2}{M_o^2} \int_0^{M_o} M.\phi(M).dM \qquad \text{A.25}$$

The above integral can be evaluated numerically using Simpson's rule or any other numerical method. The discrete points method used in this study leads to the following:

$$\Delta = \frac{L^2}{6M_o^2} \sum_{j=1}^{n} (M_j - M_{j-1}).[\phi_j.(2M_j + M_{j-1}) + \phi_{j-1}.(M_j + 2M_{j-1})] \qquad \text{A.26}$$

where n is number of discrete points up to moment $M_o$.

Beyond the elastic behavior, the inelastic deformation includes two components: the elastic and plastic deformations. The elastic component is obtained by dividing the moment by the effective elastic stiffness:

$$\Delta_e = \frac{M_o}{K_{eff}} \qquad \text{A.27}$$

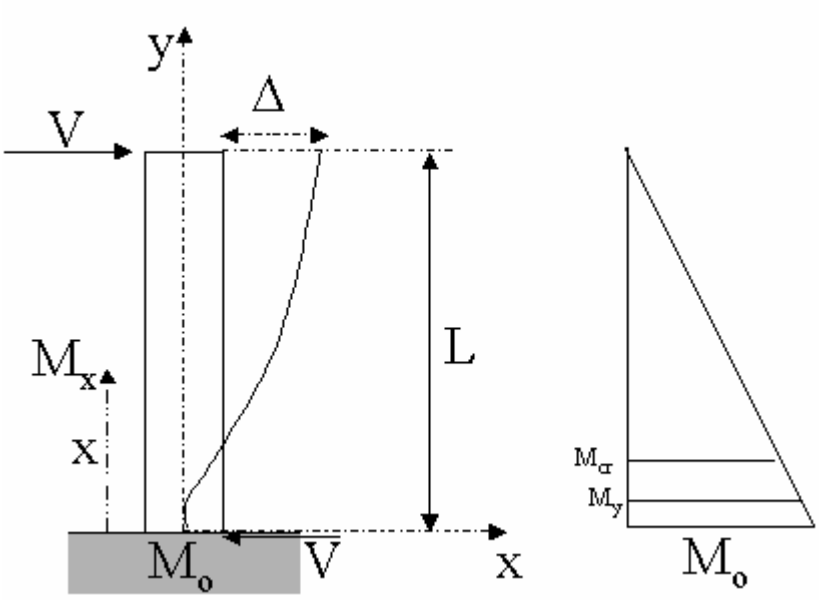


Figure A.5 Moment distribution over column length

The effective stiffness is calculated at first yielding, which is found to be:

$$K_{eff} = \frac{M_y}{\Delta_y} = \frac{3EI_{eff}}{L^2} \qquad \text{A.28}$$

where $\Delta_y$ is the yield displacement calculated from Equation A.20 when the moment at critical cross section causes the first longitudinal bar to yield, i.e when $M_o = M_y$.

### A.8.2 Plastic Flexural Deformation

Mander et al (1984) conducted an experimental study to assess the distribution of curvature along the column. They proposed a parabolic distribution of plastic curvature. This finding is adopted to evaluate the plastic deformation from of the following procedure:

a) Evaluate the magnitude of the plastic curvature, $\phi_p$, at the critical section given by:

$$\phi_p = \phi - \phi_e \qquad \text{A.29}$$

where the elastic curvature $\phi_e = \frac{3}{L^2}.\Delta_e$ and $\phi$ is the total curvature at the critical cross section.

b) Evaluate the length of the plastic curvature distribution, $L_{pc}$, from:

$$L_{pc} = L - L\left|\frac{M_y}{M_{\max}}\right| \qquad \text{A.30}$$

where $M_{max}$ is the maximum moment, $M_y$ is the moment at first yield and L is the cantilevered length of the column.

c) The additional plastic curvature resulting from penetration of the yielding of the longitudinal reinforcement is accounted for by defining an empirical length of yield penetration as:

$$L_{py} = 6.35\sqrt{d_b} \quad \text{(in)}$$
$$L_{py} = 32\sqrt{d_b} \quad \text{(mm)} \qquad \text{A.31}$$

Where $d_b$ is the longitudinal bar diameter.

d) The total plastic rotation, $\theta_p$, of the column is then calculated as:

$$\theta_p = \phi_p\left(\frac{L_{pc}}{3} + L_{py}\right) \qquad \text{A.32}$$

e) Thus, the plastic deformation is given by:

$$\Delta_p = \theta_p\left(L - \frac{L_{pc}}{4}\right) \qquad \text{A.33}$$

### A.8.3 Elastic Shear Deformation before the occurrence of first yielding

In addition to the flexural deformations, the shearing deformations are especially important in bridge columns. The elastic shear deformation for the elastic and cracked stages when the member has not yielded can be calculated based on the procedure outlined by Park and Paulay (1975) and explained in what follows:

a) Prior to cracking the shear deformation can be computed as:

$$\Delta_{se} = \frac{V}{K_{ve}} L \qquad \text{A.34}$$

where V is the applied shear and $K_{ve}$ is the shear stiffness given by:

$$K_{ve} = \frac{0.4 E_c A_q}{f} \qquad \text{A.35}$$

In which the factor 0.4 assumes that the Poisson ratio for concrete is $\nu = 0.25$. Therefore, the shear modulus is $G=0.4E_c$ where $E_c$ is the modulus of elasticity of concrete. $A_q$ is the area that contributes to shear stiffness, and f is the shear form factor. For rectangular cross sections f=1.2, and for T, I and hollow sections f=1.

b) As cracking propagates over a length smaller than the hinge zone and before first yielding occurs, the elastic shear deformation can be expressed as:

$$\Delta_{se} = V\left[\frac{1}{K_{ve}} L_{uncr} + \frac{1}{K_{vh}} (L - L_{uncr})\right] \qquad \text{A.36}$$

where $L_{uncr}$ is the length of the uncracked zone given by: $L_{uncr} = L\frac{M_{cr}}{M_o}$, $M_{cr}$ is the cracking moment and $K_{vh}$ is the post-cracking shear stiffness within the plastic hinge

region. Park and Paulay (1975) showed that $K_{vh}$ is related to the inclination of cracks and is calculated from the following expression:

$$K_{vh} = \frac{\rho_v \sin^4\theta \sin^4\beta\left(\cot\theta + \cot\beta\right)}{\sin^4\theta + n\rho_v \sin^4\beta} E_s b_w d \qquad \text{A.38}$$

where $\theta$ is the angle of inclination of the cracks with respect to the longitudinal axis, $\beta$ is the angle of inclination of the stirrups, normally $\beta = 90^o$. $E_s$ is the modulus of elasticity of the hoop reinforcement, $n = E_s / E_c$ is the modular ratio, $E_c$ is the modulus of elasticity of concrete, and $\rho_v$ is the volumetric ratio of hoop reinforcement calculated by:

$$\rho_v = \frac{A_v}{sb_w} \qquad \text{A.39}$$

in which $A_v$ is the total area of hoop steel, $b_w$ is the width of the concrete web, and s is the hoop spacing.

For transverse reinforcement with $\beta = 90^o$, Equation 2.38 can be simplified to:

$$K_{vh} = \frac{b_w d \cot\theta}{\frac{1}{E_s\rho_v} + \frac{1}{E_c \sin^4\theta}} \qquad \text{A.40}$$

c) When cracking extends beyond the hinge region, then the shear deformation is given by:

$$\Delta_{se} = V\left[\frac{1}{K_{ve}} L_{uncr} + \frac{1}{K_{vh}} L_h + \frac{1}{K_{vc}}\left(L - L_{uncr} - L_h\right)\right] \qquad \text{A.41}$$

where $K_{vh}$ is the shear stiffness within the hinge region with length Lh calculated using Equation A.41 for hoop spacing sh within the hinge region, while $K_{vc}$ is the shear stiffness outside the hinge region calculated for a hoop spacing su. Figure A.6 illustrates

the distribution of uncracked zone, cracked zone outside the hinge region, and cracked zone within the hinge zone over the length of the fixed free column.

### A.8.4 Elastic shear deformation after the occurrence of first yielding

After first yielding, an inelastic zone appears of length $L_{pc}$ within the hinge zone. The inelastic shear deformation resulting from this zone is generally very small for long columns and may be important for squat columns. In the present study, we neglect this shear component. Thus, only the elastic uncracked zone and elastic cracked zone are assumed to contribute to shear deformation and therefore can be calculated using the following equation:

$$\Delta_{se} = V\left(\frac{L_e}{K_{ve}} + \frac{L_{crc}}{K_{vc}} + \frac{L_{crh}}{K_{vh}}\right) \qquad \text{A.42}$$

This formula divides the cracked zone into two zones, the first one is within the hinge region with length $L_{crh} = L_h - L_{pc}$ if the cracked area has extended beyond the hinge region, otherwise $L_{crc} = L_{cr}$ which means the cracked zone is within the hinge region when there is no inelastic zone. The shear stiffness $K_{vh}$ associated with the cracked hinge zone is calculated using Equation A.40 as a function of hoop spacing $s_h$.

The second zone appears when the cracks have propagated beyond the hinge region with length $L_{crc} = L_{cr} - L_h$. The associated shear stiffness, $K_{vc}$, is assessed using again Equation A.40 for the hoop spacing $s_u$ outside the hinge region.

The first term in Equation A.42 reflects the uncracked elastic zone contribution to shear deformation. Its length is proportional to the total length and can easily be estimated by the following equation:

$$L_e = L\left|\frac{M_{cr}}{M_{\max}}\right| \qquad \text{A.43}$$

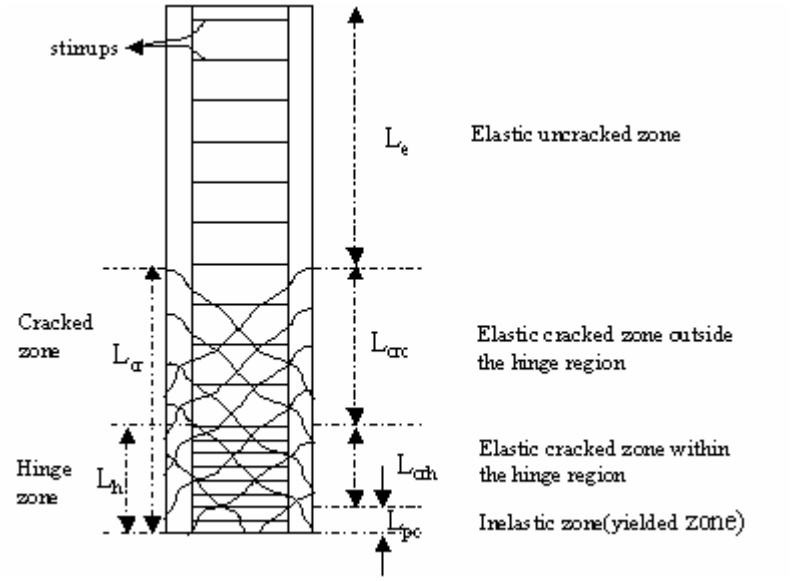


Figure A.6 Distribution of cracked zone,uncracked zone and inelastic zone along the column length

## A-9 CONCLUSION

This appendix detailed the procedure for developing moment-curvature as well as the moment displacement curves. These curves are exploited to extract mechanical properties of RC bridge columns necessary for the column modeling used in this study.

# *SELECTED PUBLICATIONS AND CONFERENCE PROCEEDINGS*

**Journal Publication**

Mechakhchekh. A, Ghosn. M, "Reliability-based Procedure for Developing LRFD Seismic Bridge Design Specification" in Press, Transportation Research Board(TRB), 2008.

**Conference Proceedings**

Mechakhchekh. A, Ghosn. M, "A Rational Method for Calibrating Appropriate Response Modification Factors for Seismic Design of Bridge Columns" Fifth National Seismic Conference on Bridges and Highways, San Francisco, September 2006.

Mechakhchekh. A, Ghosn. M, "Effect of Variability in Response Modification Factors on Seismic Damage of R-C Bridge Columns." IABMAS'06, Third International Conference on Bridge Maintenance, Safety and Management, Porto-Portugal, July 2006.

Mechakhchekh. A, Ghosn. M, "Determination of Response Modification Factor for Seismic Design" New York City Bridge Conference, September 2005.

Mechakhchekh. A, Ghosn. M, "Evaluation of the Adequacy of the Response Modification Factor for Seismic Design of R-C Columns" ICOSSAR 2005, 9th International Conference on Structural Safety and Reliability, Rome, Italy, June 2005.

# *REFERENCES*

AASHTO, 2002, ”Standard specifications for Highway Bridges” American Association of State Highway and Transportation Officials.

Abrahamson. N. A, Silva. W. J, 1997, “Empirical response spectral attenuation relations for shallow crustal earthquakes”, Seismological Research Letters, Vol. 68, No1, Jan/Feb 1997.

Ang, A.H. and Tang, W. H. 1975, “ Probability Concepts in Engineering Planning and Design”, Vol.I,Probability and Statistics, John-Wiley, 1975.

ATC-32, (1996) “Improved seismic design criteria for California bridges: provisional recommendations” Applied Technology Council, Redwood City, CA.

Au. S. K, Beck. J. L, 2001, “Estimation of small failure probabilities in high dimensions by subset simulation”, Probabilistic Engineering Mechanics, 16, (2001), 263-277.

Au. S. K, Beck. J. L, 2003, “Subset simulation and its application to seismic risk based dynamic analysis” Journal of Engineering Mechanics, 16, (August 2003), 901-917.

Au. S. K, 2004, “Probabilistic failure analysis by importance sampling markov chain simulation”, Journal of Engineering Mechanics, (March 2004), pp 303-11.

Bazzurro. P, Cornell. C. A, 1999, “Disaggregation of seismic hazard”, *Bull. Seism. Soc. Am.* **89,** 501–520

Benjamin, J. R., and Cornell, C. A. 1970. “Probability, Statistics, and Decision for Civil Engineers”, McGraw-Hill, Book Co., New York.

References

Boore, D.M. Joyner, W.B. and Fumal, T.E. 'Estimation of Response Spectra and Peak Accelerations from Western North American Earthquakes: An Interim Report', *Open File Report 93-509*, US Geological Survey, 1993.

Boore, D. M. and Joyner, W. B. " Prediction of Ground Motion in North America", ATC-35-1,1994, pp.6-1to 6-41.

Boore. D. M, 2002, "SMSIM-Fortran Programs for Simulating Ground Motions from Earthquakes: Version 2.3" A revision of OFR 96-80-A.

Campbell, K. W. and Y. Bozorgnia (1994). "Empirical analysis of strong ground motion from the 1992 Landers, California, earthquake" , Bull. *Seism. Sot. Am.* 84, no. 3, 573-588.

Chang. G.A, Mander. J.B, (1994) "Seismic energy based fatigue damage analysis of bridge columns" Technical Report, NCEER-94-0006.

Choek. G. S, Stone. W. C, 1986, "Behavior of 1/6 scale model bridge columns subjected to cycle inelastic loading", NBSIR 86-3494, Center for building Technology, National Engineering Laboratory, National Institute of Standards and Technology, Gaithersburg, Maryland, 20899, November 1986, 291 pages.

Chopra, A. K. 1967. "Earthquake response of earth dams", *J. of Soil Mechanics and Foundation Division* 93: SM2. ASCE.

Cooper. J. D, Friedland. I. M, Buckle. I. G, Ninis. R. B, McMullin Bobb. N, 1994 " The Northridge Earthquake: progress made, lessons learned in seismic resistant bridge design".

Cornell. C.A, 1968, "Engineering seismic risk analysis", *Bull. Seismol. Soc.Am.,58*, 1583–1606.

Cornell. C. A, 1971,"Probabilistic analysis of damage to structures under seismic loads", in Dynamic Waves in Civil Engineering, edited by D.A.Howells et al., 473– 493,Wiley-Interscience, Hoboken,N. J.

References

Cosenza. E, Manfredi. G, Ramasco. R, 1993, " The use of damage fuctionals in earthquake engineering: a comparaison between different methods" Earthquake Engineering and Structural Dynamics, vol. 22, 1993, pp 855-868.

Crouse, C. B., B. Hushmand, and G. R. Martin. 1987. Dynamic soil-structure interaction of single-span bridge. In *Earthquake Engineering and Soil Dynamics,* Vol. 15, pp. 711–29.

Dakoulas, P., and G. Gazetas. 1985. "A class of inhomogeneous shear models for seismic response of dams and embankments". *Soil Dynamics and Earthquake Engineering* 4(4): 166–82.

Dakoulas, P., and G. Gazetas. 1986. "Seismic shear strains and seismic coefficients in dams and embankments". *Soil Dynamics and Earthquake Engineering* 5(2): 75–83.

Deng. L, Ghosn. M, Shao. S, (2000),"Development of a shredding genetic algorithm for structural reliability" Structural Safety, Volume 27, Issue 2, April 2005, pages 113-131.

Douglas. J, 2001," A comprehensive worldwide summary of strong-motion attenuation relationships for peak ground acceleration and spectral ordinates (1969 to 2000)" ESEE Report No. 01-1 January 2001.

Engelund. S, Rackwitz. R, 1992, "Experiences with experimental design schemes for failure surface estimation and reliability", In Y.K. Lin, ed., ASCE Specialty Conference on Probabilistic Mechanics and Structural and Geotechnical Reliability, 244 – 247, Proceedings, 6th ASCE, New York, USA.

FEMA 273, 1996, "NEHRP guidelines for the seismic rehabilitation of building", Building Seismic Safety Council, Washington, DC.

Frankel. A, Mueller. C, Barnhard. T, Perkins. D, Leyendecker. E, Dickman. N, Hanson. S, Hopper. M, 1996, "National seismic hazard maps: Documentation", June 1996. U.S. Geol. Surv. Open-File Rept. 96-532, 69pp.

References

Friedland. I, et al. (2001) "Comprehensive Specification for the Seismic Design of Bridges, Revised LRFD Design Specifications", NCHRP 12-49, Washington DC

Goel, R. K., and A. K. Chopra. 1997. "Evaluation of bridge abutment capacity and stiffness during earthquakes", *Earthquake Spectra*. 13(1): 1–23.

Gazetas, G. 1987. "Seismic response of earth dams: some recent developments". *Soil Dynamics and Earthquake Engineering* 6(1): 2–47.

*Gibbs. J. F, . Boore. D. M, Joyner. W. B, Fumal. T. E. 1994* "The attenuation of seismic shear waves in Quaternary alluvium in Santa Clara Valley, California" *Bulletin of the Seismological Society of America*; February 1994; v. 84; no. 1; p. 76-90.

Gutenberg, R. and Richter, C. F. (1944), "*Frequency of earthquakes in California"*, Bull. Seism. Soc. Am. **34**, 185-188.

Halldorsson. B, Dong. G, Mavroeidis. G, Zhang. F, Papageorgiou. A, 2004, "Simulation of Earthquake Strong Ground Motion Using the Specific Barrier Model" American Geophysical Union, Fall Meeting 2004.

Hardin, B. O. 1965. "The nature of damping in sand". *J. of Soil Mechanics & Foundation Engineering* 91:63–97. New York.

Hastings. W. K, 1970, "Monte Carlo sampling methods using Markov chains and their applications" Biometrika, 57, 97-109.

Iwasaki, T., F. Tatsuoka, and Y. Takagi. 1978. "Shear moduli of sands under cyclic torsional shear loading". *Soils and Foundations* 18(1): 39–56.

Kameda. H, and Ishikawa. Y, 1988, "Extension of Seismic Hazard Analysis in Terms of Hazard consistent Magnitude and Epicentral Distance", Journal of JSCE, 392:I-9 395-402.

Kameda. H, and Ishikawa. Y, (1993). Hazard-consistent magnitude and distance for extended seismic risk Analysis, *ICOSSAR'93*, 2139-2146.

References

Kaynia, A. M., and E. Kausel. 1982. "*Dynamic stiffness and seismic response of sleeved piles''*.Report No. R80-12. Cambridge, Mass.: Massachusetts Institute of Technology.

Koutsourelakis. P. S, Pradlwarter. H. J, Schueller. G. I, 2004, "Reliability of structures in high dimensions, part I: algorithms and applications", Probabilistic Engineering Mechanics 19 (2004) 409-417.

Kowalsky. M.J, 2000, "Deformation limit states for circular reinforced concrete bridge columns", J. Struct. Eng-ASCE, August 2000.

Kunnath. S. K, El-Bahy. A, Taylor. A. W, Stone. W. C, 1997,"Cumulative seismic damage of reinforced concrete bridge piers" National Institute of Standards and Technology, October 1997.

Lehman. D. E, Moehle. J. P, 1998, " Seismic performance of well-confined concrete bridge columns", Pacific Earthquake Engineering Research Center, PEER 1998/01, Dec. 2000.

Makris, N., D. Badoni, E. Delis, and G. Gazetas. 1994. Prediction of observed bridge response with soil-pile-structure interaction. *J. of Structural Engineering* 120(10): 2992–3011.

Makris, N., and G. Gazetas. 1992. Dynamic pile-soil-pile interaction Part II: Lateral and seismic response. *Earthquake Engineering and Structural Dynamics* 21(2): 145–62.

Makris, N., and G. Gazetas. 1993. Displacement phase differences in a harmonically oscillating pile. *Geotechnique* 43(1): 135–50.

Maragakis, E. A. 1985. A *model for the rigid body motion of skew bridges.* Report No. EERL 85-02. Pasadena, Calif.: California Institute of Technology.

McCallen, D. B., and K. M. Romstad. 1994. Analysis of a skewed short-span, box-girder overpass. *Earthquake Spectra* 10(4): 729–55.

McGuire. R, and Shedlock. K.M, (1981). Statistical Uncertainty in Seismic Hazard Evaluations in the United States, *BSSA*, **71** 1287-1308

References

McGuire R. K., Arabasz, W. J. (1990), “An Introduction to Probabilistic Seismic Hazard Analysis. In S. H. Ward ed”. Geotechnical and Environmental Geophysics, Vol. I, Review and Tutorial, SEG. pp. 333-352.

McGuire. R.K, 1995, ”Probabilistic seismic hazard and design earthquakes: closing the loop”, *Bull. Seism. Soc. Am.*, 85, 5, 1275-1284.

Mechakhchekh. A, Ghosn. M, 2005, “Reliability-Based Calibration of Response Modification Factors for Seismic Design of Bridge Columns”, Master thesis in Civil Engineering, The City College of the City University of New York, January 2005.

Mechakhchekh. A, Ghosn. M, 2005,”Evaluation of the Adequacy of the Response Modification Factor for Seismic Design of Bridge Columns”, ICOSSAR’2005, Rome Italy.

Metropolis. N, and Ulam. S, 1949, ” The Monte Carlo method”, Journal of the American Statistical Association 44:335-341

Metropolis. N, Rosenbluth. A. W, Rosenbluth. M. N, Teller. A. H, (1953), ”Equations of state calculations by fast computing machines”, Journal of Chem. Phys, 21(6), 1087-1092.

.Miranda. E, Bertero. V. V, 1994, “Evaluation of strength Reduction Factors for Earthquake-Resistant Design”, Earthquake Spectra, Vol. 10, No.2, 357-379.

Nassar A.A, and Krawinkler. H, (1991) “Seismic demands for SDOF and MDOF systems,” Report No. 95, The John A. Blume Earthquake Engineering Center, Stanford University, California, USA.

Newmark. N.M, and Hall. W.J, (1973) “Seismic design criteria for nuclear reactor facilities” Report No. 46, Building Practices for Disaster Mitigation, National Bureau of Standards, U.S, Department of Commerce, 209-236

References

Park. Y.J, Ang. A.H-S, 1985, "Mechanistic Seismic Damage Model for Reinforced Concrete", J. Struct.Engr ASCE, Vol. 111, No.4, 722-739.

Poulos, H. G. 1968. Analysis of the settlement of pile groups. *Geotechnique* 18(4): 449–71.

Priestley, M. J. N, Seible. F, Calvi. G. M, 1996, "Seismic design and retrofit of bridge structures", Wiley, New York.

Rajashekhar. M. R, Ellingwod. B. R, 1993, "A new look at the response surface approach for reliability analysis", Structural Safety, vol. 12, no. 1 edn.

Roesset, J. M. 1984. Dynamic stiffness of pile groups. In *Pile Foundations.* New York: ASCE.

Romstad, K. M., B. Kutter, B. Maroney, E. Vanderbilt, M. Griggs, Y. H. Chai. 1995. *Experimental measurements of bridge abutment behavior.* Report No. UCD-STR-95-1. Davis, Calif.: University of California.

Sanchez-Salinero, I. 1983. *Dynamic stiffness of pile groups: approximate solutions*. Geotech.Engrg. Report No. GR83-5. Austin, Texas: University of Texas.

Seed, H. B., and I. M. Idriss. 1969. Influence of soil conditions on ground motions during earthquakes. *J. of Soil Mechanics and Foundations* 95(V SM1): 99–137. ASCE.

Seed, H. B., and I. M. Idriss. 1970. *Soil moduli and damping factors for dynamic response analysis.* Report No. EERC 70-10. Berkeley, Calif.: University of California.

Shome. N, Cornell. C.A, Bazzurro. P, and Carballo. J.E, (1997) "Earthquakes, Records, and Nonlinear Responses", Report No. RMS-29, Reliability of Marine structures, Dept. of Civil Eng, Stanford University, Stanford, CA.

Siddharthan, R., M. El-Gamal, and E. A. Maragakis. 1997. "Stiffnesses of abutments on spread footings with cohesionless backfill". *Canadian Geotechnical J.* 34(5): 686–97.

Takeda. T, Sozen. M.A, Nielsen. N. N, 1970, "Reinforced Concrete Response to Simulated Earth-quakes", J.Struct. Engrg. Div., ASCE, Vol. 96, No. 12pp.2557-2573.

References

Tatsuoka, F., T. Iwasaki, Y. Takagi, 1978. “Hysteretic damping of sands and cyclic loading and its relation to shear modulus”. *Soils and Foundations* 18(2): 25–40.

Tierney. L, 1994, ” Markov chain for exploring posterior distributions (with discussion)”, Annals of Statistics, 22,pp.1701-1762.

Tseng, W.-S., and J. Penzien. 2000. Soil-foundation-structure interaction. In *Bridge Engineering Handbook,* chapter 42, eds. W.-F. Chen, and L. Duan. Boca Raton, Fla.: CRC Press.

Vucetic, M., and R. Dobry. 1991. Effect of soil plasticity on cyclic response. *J. of Geotechnical Engineering* 117(1): 89–107. ASCE.

Wang. J, Ghosn. M, (2003),”Hybrid Data Mining / Genetic Shredding Algorithm for reliability Assessment of Structural systems” Wang. J, Ghosn. M, Journal of Structural Systems, Issue 9, pp:1451-1460, September 2006

.Wen. Y. K, Wu. C. L, 2001, “Uniform hazard ground motions for Mid-America Cities.”, Earthquake spectra 17(2): 359-384.

Wen. Y. K,. Ellingwood. B. R, Veneziano. D, Bracci. J, 2003, ”Uncertainty Modeling in Earthquake Engineering” , MAE Center Project FD-2 Report, February 12, 2003.

Werner, S. D, 1994, “Study of Caltrans’ seismic evaluation procedure for short bridges”. In *Proc.3rd Annual Seismic Research Workshop*. Sacramento, Calif.: California Department of Transportation.

Wilson, J. C., and B. S. Tan. 1990a. “Bridge abutments: formulation of simple model for earthquake response analysis”, *Journal of Engineering Mechanics* 116(8): 1828–37.

Wilson, J. C., and B. S. Tan. 1990b, ”Bridge abutments: accessing their influence on earthquake response of Meloland Road Overpass”, *Journal of Engineering Mechanics* 116(8): 1838–56.

References

Working Group on California Earthquake Probabilities, “Seismic hazards in southern California; probable earthquakes, 1994 to 2024”, *Bulletin Seismological Society of America*, Vol. 85, 1995 pp. 379-439.

Zahn. F. A, Park.R, Priesley. M. J. N, 1986, “Design of reinforced concrete bridge columns for strength and ductility” Departmenet of Civil Engineering, University of Canterbury, Report 86-7, March 1986.

Zhang. J, and Makris. N, 2000, “Time-domain viscoelastic analysis of earth structures”. E*arthquake Engineering and Structural Dynamics* 29: 745–68.

Zhang. J, and Makris. N, March 2001, “Seismic Response Analysis of Highway Overcrossings Including Soil-Structure Interaction”, PEER Report 2001/02, College of Engineering, University of California, Berkeley.